SYNTHESIS AND CHARACTERIZATIONS OF WATER DISPERSIBLE HYBRID NANOPARTICLES BASED ON SPIONs AND CONJUGATED POLYMERS FOR DUAL IMAGING APPLICATIONS

A THESIS SUBMITTED TO
THE GRADUATE SCHOOL OF ENGINEERING AND SCIENCE
OF BILKENT UNIVERSITY
IN PARTIAL FULFILLMENT OF THE REQUIREMENTS FOR
THE DEGREE OF
MASTER OF SCIENCE
IN
CHEMISTRY

By
Sinem Gürbüz
July, 2015

SYNTHESIS AND CHARACTERIZATIONS OF WATER DISPERSIBLE HYBRID NANOPARTICLES BASED ON SPIONs AND CONJUGATED POLYMERS FOR DUAL IMAGING APPLICATIONS

By Sinem Gürbüz

July, 2015

We certify that we have read this thesis and that in our opinion it is fully adequate, in scope and in quality, as a thesis for the degree of Master of Science.

_____
Assoc. Prof. Dönüş Tuncel

_____
Prof. Dr. Engin Umut Akkaya

_____
Assist. Prof. İrem Erel-Göktepe

Approved for the Graduate School of Engineering and Science:

_____
Prof. Dr. Levent Onural
Director of the Graduate School

ABSTRACT

SYNTHESIS AND CHARACTERIZATIONS OF WATER DISPERSIBLE HYBRID NANOPARTICLES BASED ON SPIONs AND CONJUGATED POLYMERS FOR DUAL IMAGING APPLICATIONS

Sinem Gürbüz

M.S. in Chemistry

Supervisor: Assoc. Prof. Dr. Dönüş Tuncel

July, 2015

This study focuses on the synthesis and characterizations of conjugated polymer coated super-paramagnetic iron oxide nanoparticles for their potential uses *in vivo* and *in vitro* imaging. Water dispersible, stable super-paramagnetic iron oxide (SPIO) hybridized conjugated polymer nanoparticles are synthesized with three different types of conjugated polymers emitting in the region of blue, green and red. SPION, which is a T_2 contrast agent due to its magnetic susceptibility, is taken into consideration because of its unique uptake mechanism by the Kupffer cells in the liver, spleen or bone marrow.[1] The core iron oxide nanoparticles are coated to increase blood circulation time, reduce the agglomeration of them and improve pharmacokinetic effect.[2]

Conjugated polymers utilized in this work were modified with allyl pendant groups in order to obtain cross linkable moieties. Polymer chains were cross-linked via [2+2] cycloaddition of ethylene units under UV light to confer stability .Cross-linking would not only confer stability to these hybrid nanoparticles but it can also help preventing the early leakage of SPIONs from the polymer matrix in the biological media.

For this purpose, three polymers used in this study, which were poly[(9,9-bis{3-dihexyl}flourenyl-2,7-diyl)-co-(9,9-bis{3-diallyl}fluorenyl-2,7-diyl)] (PB), Poly[(9,9-bis ({3-diallyl}flourenyl-2,7-diyl)-co-(benzothiodiazole)] (PG) and

poly[3-{(allyloxy)ethyl} (thiophene 2,5-diyl)-co-(5,5'-{2,2'}-bithiophene)] (P2). Nanoparticles of these polymers with and without SPIONs were synthesized. Optical and morphological characterizations were investigated via DLS, SEM, TEM, UV-Vis and Fluorescence spectroscopy.

Keywords: Conjugated polymers, SPIONs, hybrid nanoparticles, [2+2] cycloaddition reaction.

ÖZET

SPION ve KONJUGE POLİMERLERİN KULLANIMINA DAYANAN SUYA KARIŞABİLEN HİBRİT NANOPARÇACIKLARIN İKİ YÖNLÜ GÖRÜNTÜLEME UYGULAMLARI İÇİN SENTEZİ VE KARAKTERİZASYONU

Sinem Gürbüz
Kimya, Yüksek Lisans
Tez Danışmanı: Doç. Dr. Dönüş Tuncel
Temmuz 2015

Bu çalışma polimerlerle kaplanmış demir oksit nanoparçacıklarının potansiyel *in vivo* ve *in vitro* görüntüleme yöntemlerinde kullanılmasını amaçlar. Konjuge polimerle hibritleştirilerek sentezlenen suya karışabilen, stabil süper-paramanyetik demir oksit nanoparçacıklarının (SPIONs) sentezi üç ayrı bölgede ışıyan mavi, yeşil ve kırmızı polimerlerle yapıldı. Manyetik duyarlılığından dolayı T_2 tipi kontrast malzemesi olan SPION'ların bir diğer özelliği karaciğer, kemik iliği ve dalaktaki kuppfer hücreleri tarafından özel içeri alınış biçimidir. Demir oksit nanoparçacıklarının çekirdek olarak kullanılması ve kaplanması kandaki dolaşım süresini arttırmak, kanda topaklanmasını azaltmak ve farmokokinetik etkisini geliştirmek üzere yapılmıştır.

Bu çalışmada kullanılan konjuge polimerler çapraz bağlanabilir fonksiyonel gruplar elde etmek amacıyla alil ilave gruplarıyla modifiye edildi. Polimer zincirlerinin kararlılık kazanması için etilin grupları UV ışığı altında [2+2] siklo katılım reaksiyonuyla çarpa bağlandı. Çapraz bağlanma sadece kararlılık sunmakla kalmayıp, aynı zamanda SPION'ların polimer matrisinden biyolojik medyaya erken kaçışını da önleyebilecek.

Bu amaçla kullanılan üç polimer şunlardı, poli[(9,9-dihekzil fulorenil-2,7-diyil)-co-(9,9-bis {3-dialil}fulorenil-2,7-diyil)] (PB), poli[(9,9-bis ({3-dialil}fulorenil-2,7-diyil)-co-(benzotiyadiyazol)] (PG) and poli[3-{(aliloksi)etil} (tiyofen 2,5-

diyil)-co-(5,5'-{2,2'}-bitiyofen)] (P2). Bu polimerlerin SPIONs içeren ve içermeyen nanoparçacıkları sentezlendi. Optik ve Morfolojik karakterizasyonları ise sırasıyla Dinamik Işık Saçılımı (DLS) ölçümleri, Taramalı Elektron Mikroskobu (SEM), Geçirimli Elektron Mikroskobu (TEM), UV-Vis ve Flüoresans Spektroskopi yöntemleriyle incelenmiştir.

Anahtar Kelimeler: Konjuge polimerler, SPIONs, hibrit nanoparçacıklar, [2+2] siklo katılım tepkimesi.

Acknowledgement

First of all, I would like to thank to my supervisor Assoc. Prof. Dönüş Tuncel for her encouragement, enthusiasm, motivation and understanding throughout my master period. Her patience and trust helped me to overcome all obstacles during my research project and academic plans as well. I own her all my academic progress and motivation during my studies.

I would like to express my appreciation to our collaborators, Assist. Prof. Funda Acar Yağcı and her co-workers Dr. Rouhollah Khodadust and Yasemin Yar from Koç Üniversity. Moreover, I would like to thank to Assist. Prof. Emine Ülkü Saritas and her master student Mustafa Ütkür from UMRAM due to the relaxivity assays part of my thesis. Zeynep Erdoğan and Mustafa Güler provide contribution for Mass spactra and TEM images of my thesis.

Lab members, Dr. Josheed PK., Esra Deniz Soner, Hamidou Keita, Muazzam İdris, Alp Özgün, Dr. Rehan Khan, Obadah Albahra, Emre Köken, Ahmet Koç and Dr. Masi Bazaar provided their endless help and friendship.

I would like to extand my special thanks to my friends Gözde Deniz Sağlam, Gözde Uzunallı, Kerem Emre Ercan, Maral Emrahlı and Tuğçe Deniz for their support and motivated conversations during my all master progress.

I would like to express my thankfulness to my family members, Nedret Gürbüz, Enver Gürbüz, Didem Gürbüz and Ahmet Şenol for their love and understanding.

We thank TUBITAK (project no: 112T704) for the financial support.

Contents

List of Figures

List of Schemes

List of Tables

List of Abbreviations

^{1}H-NMR	Proton-Nuclear Magnetic Resonance spectroscopy
^{13}C-NMR	Carbon-Nuclear Magnetic Resonance spectroscopy
FTIR	Fourier Transform Infrared spectroscopy
LC-MS/TOF	Liquid Chromatography Mass Spectrum Time of Flight
UV-Vis	Ultraviolet-Visible spectroscopy
PL	Fluorescence spectroscopy
DLS	Dynamic Light Scattering
SEM	Scanning Electron Microscope
TEM	Transmission Electron Microscope
$CDCl_3$	Deuterated Chloroform
DMSO	Dimethyl sulfoxide
THF	Tetrahydrofuran
TBAI	Tetrabutylammonium Iodide
NPs	Nanoparticles
CPNs	Conjugated Polymer Nanoparticles
SPIONs	Super-paramagnetic Iron Oxide Nanoparticles
P1	poly[2-{ethyl acetate}(thiophene-2,5-diyl)-co-(5,5'-{2,2'}- bithiophene)]
P2	ploy[3-{(allyloxy)ethyl}(thiophene 2,5-diyl)-co-(5,5'-{2,2'}-bithiophene)]
P3	Poly[2-{ethanol}(thiophene-2,5-diyl)-co-(5,5'-{2,2'}-bithiophene)]
M1	2-(2,5-dibromothiophen-3-yl)ethanol

M2 2-(2,5-dibromothiophen-3-yl)ethyl acetate

M3 3-(2-(allyloxy)ethyl)-2,5-dibromothiophene

PB Poly[(9,9-dihexylflourene)-co-alt-(9,9-bis (3-diallylflourene)]

PG Poly[(9,9-bis ({3-diallyl}flourene)-co-(benzothiodiazole)]

SPB Hybrid Nanoparticles of Poly[(9,9-dihexylflourene)-co-alt-(9,9-bis (3-diallylflourene)] PB and SPIONs

SPG Hybrid Nanoparticles of Poly[(9,9-bis ({3-diallyl}flourene)-co-(benzothiodiazole)] PG and SPIONs

SP2 Hybrid Nanoparticles of Poly[3-{(allyloxy)ethyl}(thiophene 2,5-diyl)-co-(5,5'-{2,2'}-bithiophene)] (P2) and SPIONs (SP2)

Chapter 1

Introduction

1.1. Conjugated Polymers

The idea of charge transfer on organic materials emerges with the conductivity studies on poly(acetylene) by doping it with halogens which creates charge transfer between halogen and poly(acetylene).[3, 4] In 2000, Alan J. Heeger, Alan G. MacDiarmid and Hideki Shirakawa were awarded with Nobel Prize due to the conductivity on plastics. Conjugated structures include sp^2 hybridized carbon backbone with partially filled set of p orbital. Conjugated Polymers consist of electron delocalization through their π conjugated backbone which gives them applicability in the area of electronics and photonics.[1] π-π^* electronic transition, in other words, electron excitation from highest occupied molecular orbital (HOMO) to lowest unoccupied molecular orbital (LUMO) creates exciton.[6, 34] Relaxation of this electron to fill the hole back in the π backbone implies the luminescence (Figure 1.1). [6] Engineering on the band gap between HOMO and LUMO level of π- conjugated systems makes them promising to design devices such as organic light emitting diodes (LEDs), solar cells and field effect transistors.[2] These approaches are reviewed by Roncali extensively and summarized as bond length alteration, aromaticity, planarity of the backbone and substituent on the pendant group of the polymer chains.[2]

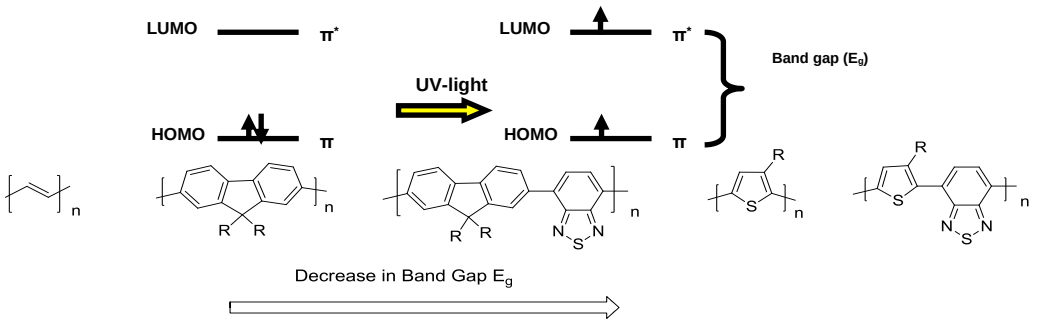

Figure 1.1: Representation of HOMO-LUMO electron transition and common conjugated polymers

Synthesis of conjugated polymers

Synthesis of polyacetylene can be discussed as the starting point of the conjugated polymer generation with the contribution of Ziegler and Natta by discovering polymerization of olefins in the presence of alkyl aluminum and Ti-based catalyst.[10, 11] Alkyl aluminum chloride works as a co-catalyst which activates Cl-Ti-alkene complex by polarizing Ti-Cl bond and let the migration of alkene and relieves polymers behind.[12] Even though the motivation of this work is to produce plastics and artificial rubbers for military purposes, it guided to the new field of conductive polymers by the synthesis of polyacetylene. Conjugated polymer synthesis technology continue with the synthesis of aromatic systems such as polyaniline,[17] polythiophene,[13,14a] polyflourene [14b] and their derivatives. [14c] Yamamoto synthesis route for polythiophene synthesis, including Grignard adduct and Ni (0) catalyst with aryl halide developed by other groups using different solvents or monomer type in order to increase the yield.[13,14a-c] Oxidative and electro polymerization are introduced as an easy methods of polymers synthesis. [14-16]

The synthesis of conjugated polymers through Palladium catalyzed cross-coupling reactions is one of the efficient methods in terms of high yield and earned Nobel Prize in 2010 to Richard Heck, Ei-Ichi Negishi and Akira Suzuki.[9a, 9b] Catalytic cycle starts with oxidative addition of aryl halide to Pd(0) and continue with the transmetalation. Finally, reductive elimination occurs to yield carbon-carbon bond of the polymer chains indicated in Figure 1.2 as general steps of cross coupling reactions.[9a] In Heck coupling reactions, π-complex occurs after oxidative addition of aryl halide to Pd(0). Migratory insertion leads to target carbon-carbon bond between alkene and aryl followed by β-hydride elimination to yield new generated alkene molecule. The role of the base is to activate the catalyst by reductive elimination from Pd(2) to Pd (0). Another role of the base is to quench the acid produced at the end of the reaction.

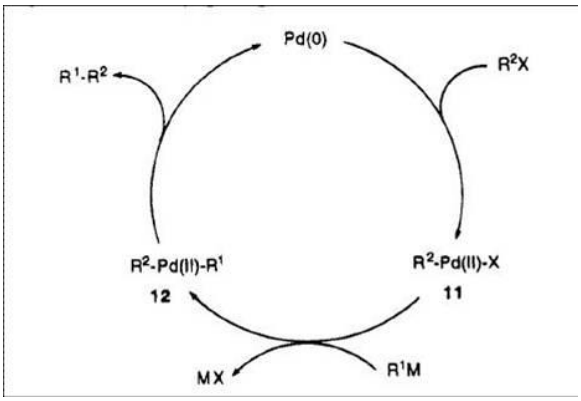

Figure 1.2: Pd catalyzed cross-coupling reaction general mechanism. (Reprinted with permission from ref. 9a. Copyright 1995 American Chemical Society.) [9a]

Suzuki cross coupling reactions defines the formation of the carbon-carbon bond between organoboronic acid or esters and aryl halides in the presence of a base with Pd(0) catalyst.[9b] The difference in Suzuki cross coupling reactions is the role of the base which activates the boronic compound by increasing the nucleophilic character of boron and leads to transmetalation between Pd and Boron. Reductive elimination releases carbon-carbon bond and Pd(0) catalyst in the cycle. [9a-c]

Stille cross coupling reactions follows general mechanism of Pd catalyzed coupling reactions [9d] indicated as in Figure 1.3. R represents alkyl or aryl halide undergoing oxidative addition. R$^{'}$ is the aryl or allyl group of the organostannanes and $SnR_3^{''}$ defines the Tin moiety with three alkyl substituent. Typically, transmetalation and reductive elimination is the key step of the carbon-carbon bond.[9d]

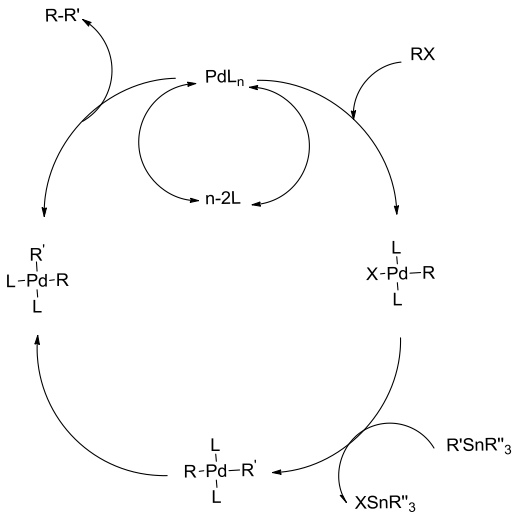

Figure 1.3: Stille coupling Pd catalyzed cross coupling reaction cycle. [9d]

1.1.1. Conjugated Polymer Nanoparticles

Conjugated polymers are good fluorescent probes for biological applications due to their high quantum yield, low toxicity and photostability.[5] One of the obstacles is that most of them are not water soluble. In order to make them water soluble or dispersible, their functional groups are changed with the solubilizing pendant groups or they are made water dispersible by preparing conjugated polymer nanoparticles (CPN).

Preparation of these nanoparticles can be done with three methods; reprecipitation, miniemulsion and self assemblies.[1,5] In reprecipitation method (Figure 1.4), polymer is dissolved in a water miscible solvent such as THF, acetone or methanol and the resulting solution is added into a certain amount of water. After ultrasonication, organic solvent is evaporated and water dispersible conjugated polymer nanoparticles are obtained. Reprecipitation method allows generating nanoparticles less than 100 nm by optimizing polymer concentration in the organic solvent or the amount of water added.[6] In miniemulsion method, size is reported as varying in a wide range such as between 40 nm to 500 nm.[6] This difference can be explained by their preparation methods. Miniemulsion technique involves the use of water immiscible solvents and surfactant in water layer to obtain nanoparticles. Instead of using hydrophobic effect of polymer nanoparticles in reprecipitation method, miniemulsion uses surfactants or additives as a driving force in the nanoparticles occurrence. Another advantage of

the reprecipitation method is to provide straightforward optimization on the size of the CPNs by adjusting the concentration of the polymer solution injected into the water.[1,5]

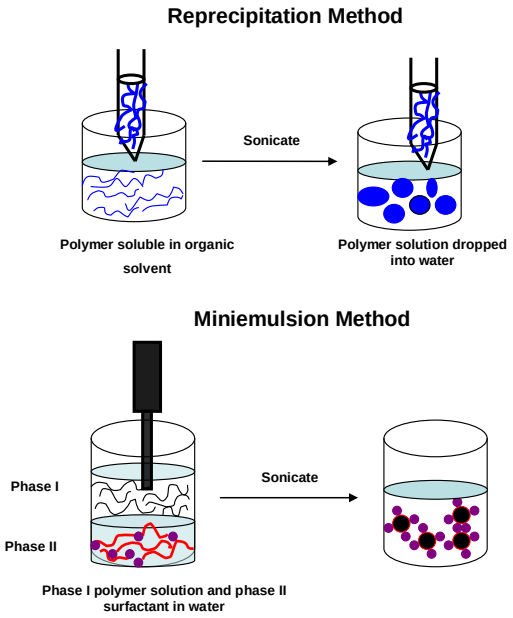

Figure 1.4: Schematic representation of nanoparticles preparation methods

Easy surface modification of these conjugated polymer nanoparticles allow them to be used as bioimaging, biosensors, energy transfer studies and other biomedical applications (Figure 1.5).[5] McNeil *et al.* introduced conjugated polymer nanoparticles coated with silica in order to functionalize surface with amine groups to show biosensor ability of these nanoparticles in the presence of metals. Amine groups are reported as good agents to bind on the surface of the gold nanoparticles.[7] Due to the resonance energy transfer between gold nanoparticles and conjugated polymer nanoparticles coated with active groups, quenching of these nanoparticles are observed. Another sensing example is Mercury ion detection with thiocarbonyl quinacridone based polyfluorene.[21] As it is known Hg^{2+} pollution is one of the most serious environmental concerns due to its extreme toxicity. Quinacridone functionalized polyfluorene backbone is preferred instead of utilizing quinacridone itself with substitution of water soluble moieties due to the higher yield synthesis of hydrophobic polyfluorene and easy preparation of its nanoparticles.[21]

PLGA (Poly-lactide-co-glycolide) modified conjugated polymer nanoparticles are examples that show increase in biocompatibility and enhanced cellular uptake [8]. Controlled release, targeting and pharmokinetic effect can be regarded as the main concerns of the biomedical applications. Poly(ethylene glycol) PEG is one of the key step for functionalization of CPNs. Its hydrophilicity is requirement for the amphiphilic character of CPNs and it is quite biocompatible.[1] Peptide labeling of the red emitting polymer nanoparticles is performed by Chui *et al.* in order to achieve targeting by using the (1-ethyl-3-(3-dimethylaminopropyl)-carbodiimide) (EDC) coupling reaction between carboxylate functionalized PEG on the surface of the CPNs and amine moiety of the specific peptide sequence.[26] These novel designed CPNs exhibit targeting for malignant brain tumors proven by biophotonic imaging and histological assays.[26] Tomczak and co-workers illustrate similar approach in nanoparticles design by targeting colon cancer cells integrated peptide sequence to the poly(9,9-dihexylfluorene-alt-2,1,3-benzoxadiazole) (PFBD) polymer nanoparticles.[36] Poly[(9,9-dioctylfluorenyl-2,7-diyl)-co- (1,4-benzo-{2,1',3}-thiadiazole)] (PFBT), a red emitting polymer nanoparticles surface, which is covered with azide substituted PEG moiety, can be altered covalently by using click chemistry between azide and alkyl on the protein.[37]

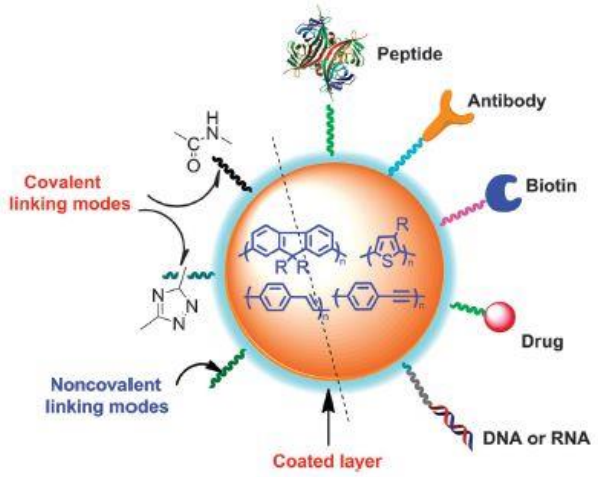

Figure 1.5: Surface modified CPNs representation. (Reprinted with permission from ref. 1. Copyright 2013 American Chemical Society.)

1.1.2 Conjugated Polymer Nanoparticles for Theranostic Applications

Theranostic implies the combination of 'therapy' and 'diagnostic' approach of the nanoparticles design in the field of nanomedicine. Diagnostic part is the bioimaging applications of the conjugated polymers owing to their inherent light emitting properties. Therapy can be explained with the drug loading, modifications of these nanoparticles with biomolecules or gene delivery studies.[1, 22-25, 35] Comparing to the same class of therapeutic agents for bioimaging such as quantum dots (Qdots) or dyes, CPNs exhibit lower toxicity, efficient cellular uptake and long blood circulation time.[30-33] Another advantage is their high photostability and higher quantum yield comparing to the water dispersible dyes or Qdots.[36, 38] McNeil and co-workers designed highly fluorescent CPNs with wide range of π-conjugated polymers (Figure 1.6) and illustrate their bioimaging studies with macrophage cells. [38]

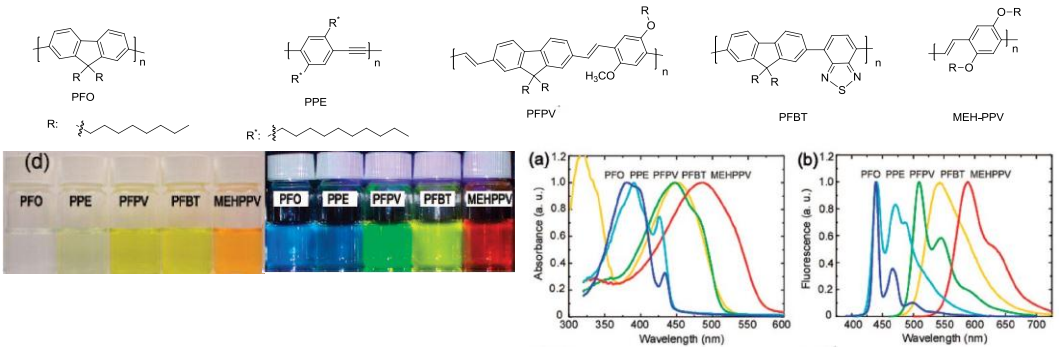

Figure 1.6: First line is the structures of the polymers. a) Absorbance of the polymers b) fluorescence of the polymers d) first photo is the CPNs under day light, second photo is the CPNs under UV-light. (Reprinted with permission from ref. 38. Copyright 2008 American Chemical Society.)

Designation of the conjugated polymers with covalently attached functional pendant groups such as cancer drug Cisplatin and folate groups are introduced in order to achieve targeting for the overexpressed folate receptor cancer cells or lipid and amino groups.[18-20] Since post functionalization of the polymer chains with bulky groups require tedious procedures, functionalization of the nanoparticles itself become more practical way for theranostic applications.

The other route is the encapsulation of the drug molecules inside of CPNPs or electrostatic complexation of them with CPNPs without covalent bonding of functional moieties with them.[22-25] PNPs carries dual functionalities in drug loading assays: one is to make water dispersible cancer drug and the other is cell imaging due to their intrinsic fluorescence.

Wang and coworkers demonstrate electrostatic assembly of cationic conjugated polymer with anionic Doxorubicin[65]-poly (L-glutamic acid) complex (Dox complex) (Figure 1.8).[22] As a result of electron transfer from positively charged conjugated polymer to negatively charged Dox complex, 'turn off state' and quenching of the system occur. After endocytosis of the complex, poly(L-glutamic acid) is hydrolyzed and electrostatic complex is destroyed. The release of the drug can be monitored by the strong blue emission of the conjugated polymer defined with the 'turn on state'.[22]

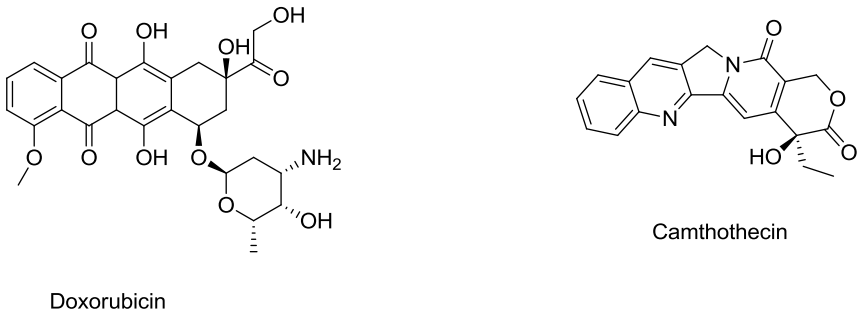

Figure 1.7: Cancer therapy drugs Doxorubicin (Dox)[65] and camptothecin.[66]

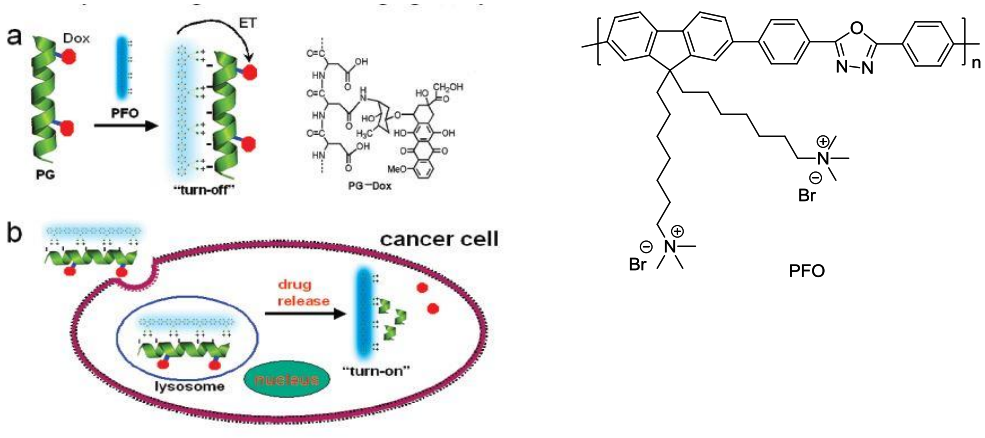

Figure 1.8: Cellular uptake triggered drug release and imaging with conjugated polymer. (Reprinted with permission from ref. 22. Copyright 2010 American Chemical Society.)

Green emitting conjugated polymer poly[(9,9-bis{propeny}fluorenyl-2,7-diyl)-co-(1,4-benzo-{2,1,3}-thiodiazole (PPFBT) nanoparticles can be loaded efficiently with the cancer drug- camptothecin[66] (Figure 1.7) because of the hydrophobicity of the highly aromatic character of camptothecin and polymer itself.[25] Encapsulation of the nanoparticles loaded with drug can be visualized with the help of green emitting conjugated nanoparticles under fluorescence microscopy.[25]

The effective use of the conjugated polymer nanoparticles in the field of nanomedicine requires obtaining far-red/ near-infrared emission in order to prevent interference with biological auto-fluorescence and tissue damage owing to the excitation with high energy.[1] Challenges of the designation of these nanoparticles are their low quantum yield and brightness in water.[26] Fluorescence quantum yields of the conjugated polymers are typically determined as ~%80 in organic solvents which decreases to ~% 10 in water in the form of nanoparticles, since polymer chains are packed within the nanoparticles formation leading to the more π-π stacking and quenching comparing to the same polymer in organic solvent.[6, 7, 27] Chui et al. introduced energy transfer from the donor (green emitting polymer) to the acceptor (deep red emitting polymer) resulting to emission at 650 nm and quantum yield of %56 (Figure 1.9).[26] Wang *et al.* illustrate more complex energy transfer system having different band gap conjugated polymers for cell imaging.[28] Varying cationic groups are introduced to the polymer chains in order to obtain different emission maxima due to the electrostatic interactions making more planar backbone in the polymers.[29] Their self-assembly with the bacteria E.Coli creates multicolor cell imaging by gaining shifting in emission spectra applying different excitation wavelength to the same complex media (Figure 1.9b).[28] Recently, multifunctional (pH sensitive) near-IR emitting conjugated polymer nanoparticles loaded with camptothecin was prepared indicating high drug loading efficiency and stability in water by serving both imaging and controlled release properties to nanoparticles design technology.[24] P1 is green emitting cationic polymer and P2 is the red emitting one indicated in Figure 1.9A, respectively. Imaging studies in Figure 1.9B, reveals

the energy transfer between P1 and P2 with the observation of yellow, orange and orange-red color in their different molar ratio prepared nanoparticles of green and red polymers. First image is the overlay of the Hoechest dye 33258 and P1 only which exhibit only green color around cell lines.[28]

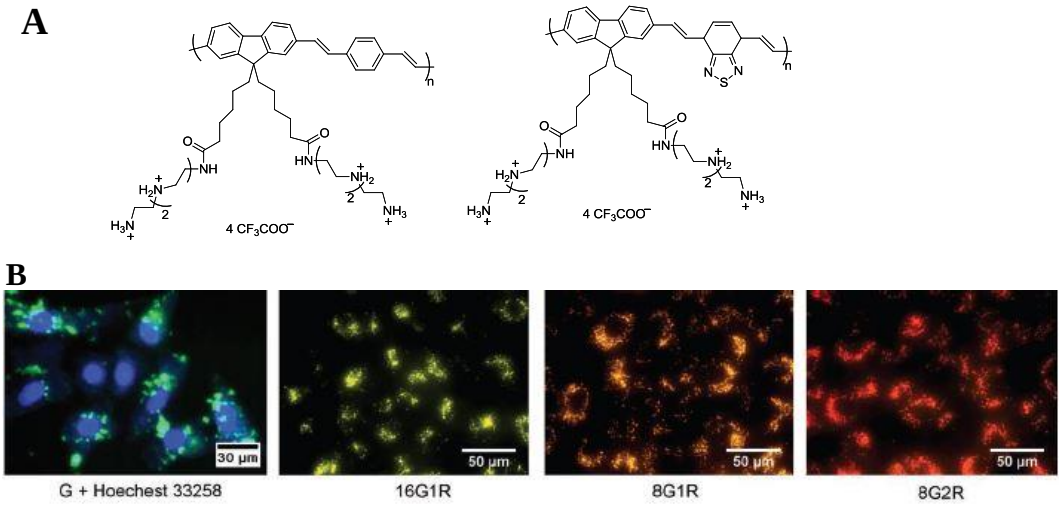

Figure 1.9: A) is the structure of the P1 and P2 respectively. B) First image is the overlay of the A549 cells treated with P1 and Hoechest dye 33258 second, third and fourth are the different ratios of the P1, P2 polymer complexes loaded A549 cells. (Reprinted with permission from ref. 28. Copyright 2011 Wiley-VCH Verlag GmbH & Co. KGaA.)

Gene delivery using green emitting PPE-NH_2 (poly(phenylene ethynylene)) is performed with the assistance of the attraction between positively charged amine carrying polymer and siRNA interaction in nanoparticles formation (Figure 1.10).[35] In order to increase the siRNA content of the nanoparticles formation, loose aggregation of the polymer chains are achieved by doing optimizations on the concentration of the polymer solution. Delivery of the siRNA in vitro studies is illustrated in Figure 1.10 owing to the luminescence of CPNs- siRNA complexation. Image A indicates only siRNA loading cell media and their emission due to the encapsulation. B is only CPNs loaded media and C is the merge image of the CPN-siRNA cell culture. Orange emission is attributable with the energy transfer between green emitting CPNs and red emitting siRNA complex.[35]

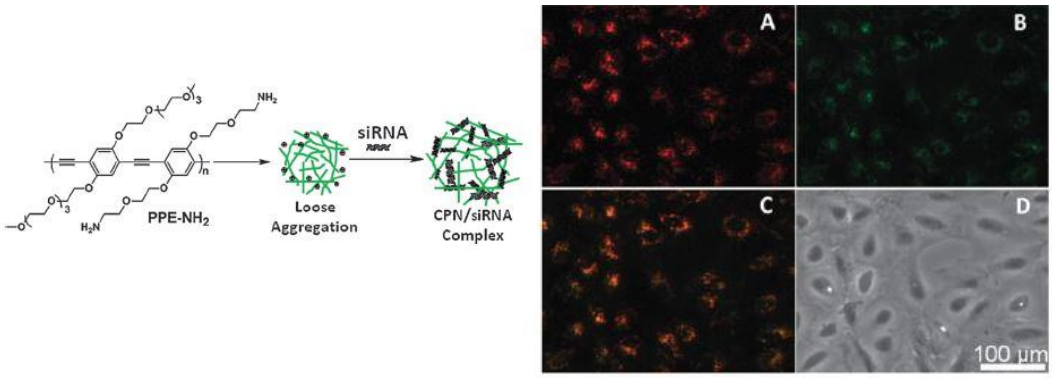

Figure 1.10: siRNA complexation with conjugated polymer schematic representation and confocal images. A) siRNA labeled with red emitting fluorescent dye. B) conjugated polymer nanoparticles C) merged image of the CPNs and siRNA-dye D) cells incubated with CPNs and siRNA-dye. (Reprinted with permission from ref. 35. Copyright 2011 Royal Society of Chemistry.)

1.2. Magnetic Resonance Imaging (MRI)

Magnetic resonance imaging (MRI) technique benefits the resonance of the hydrogen atoms included within the body due to the applied magnetic field externally.[39] After the alignment of the all protons within the tissues, radio wave is applied in order to observe the resonance of these protons with this additional energy in the form of frequency.[39] The relaxation of these protons results with a signal and radio wave emission which gives the visualization of the tissues on software.[39] Different tissues within the body is expected to have different relaxation time, therefore abnormalities such as tumors can be detected in that way. This relaxation is investigated in two pathways: one is spin-lattice relaxation time T_1 and the other is spin-spin relaxation time T_2.[40] Magnetized nuclei alignments (parallel or antiparallel) undergo oscillation with a specific frequency in their trajectory which is known as 'Larmor frequency' (Figure 1.11).[40] Changes on its z component due to relaxation are called T_1. T_1 can be explained as the energy transfer of the excited spin after applying radio frequency (RF) pulse.[40] It is called longitudinal or spin lattice relaxation. T_2 includes x-y

direction relaxation of the protons additional to z axis after turn on-off state of the RF. It can be defined as spin-spin relaxation or transverse relaxation.[40] Imaging with magnetic resonance needs contrast agents to differentiate normal and abnormal tissues by using effect of them on T_1 and T_2 relaxation times. Changes on relaxation times require performing paramagnetic species which consist of unpaired electron in their configurations. Gadolinium (Gd^{+3}) and super-paramagnetic iron oxide (SPIO, Fe_3O_4 or γ-Fe_2O_3) are the most widely used compounds as contrast reagents.[41, 42] MRI is one of the non-invasive and high resolution methods in cancer diagnosis due to its efficient in vivo imaging within soft tissues, brain and nervous system.

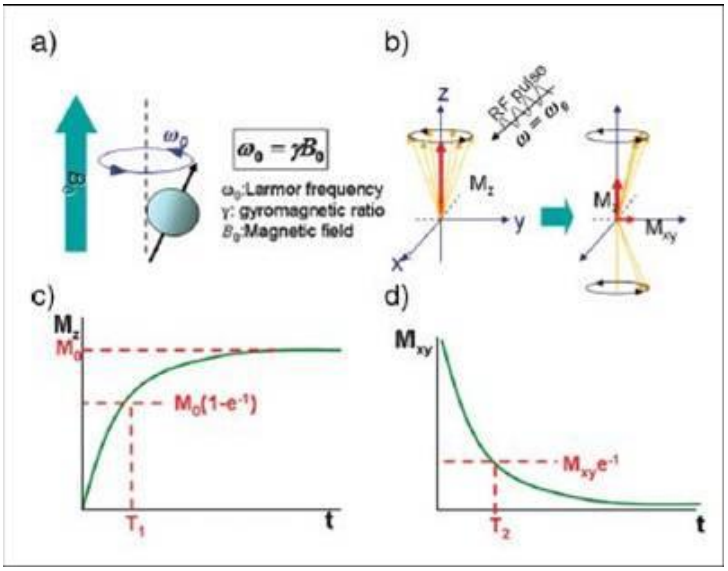

Figure 1.11: Principle of MRI a) Spins align paralel or antiparallel to the magnetic field and precess under Larmor frequency (w). b) After induction of RF pulse, magnetization of spins changes. Excited spins take relaxation process of c) T_1 relaxation and d) T_2 relaxation. (Reprinted with permission from ref. 40. Copyright 1999, American Chemical Society.)

1.2.1. Gadolinium based MRI Contrast Agents

Gd^{+3} based MRI contrast agents are studied extensively owing to its positive imaging as T_1 contrast agent which means it generates bright signals during the imaging.[43] In contrast to T_2 contrast agents (SPIO), T_1 contrast agents magnetic

susceptibility are less which results in better resolution.[43, 44] Gadolinium ions itself are toxic due to the accumulation of them as heavy metal within the cells, also, there is no biochemical pathway for their metabolism.[40, 41] Gd (III) based contrast agents occurs in the complex form of the chelating ligands to reduce this toxic effects.[41] Another point to utilize this chelate form of Gd (III) is to enhance the relaxivity of these contrast agents by allowing water exchange between contrast agent and surrounding protons.[45] Micelles, liposome, polymer nanocapsules, protein encapsulation are some techniques that are considered as useful for enhance relaxation and reduced toxicity.[45-49] Magnevist ®, MultiHance®, Omniscan ®, OptiMARK® and ProHance ® are Food and Drug Administration U.S. approved drugs as Gadolinium based contrast agents, even if patient, who is taken these drugs, can suffer from severe kidney failure or nephrogenic systemic fibrosis (NSF) are reported.[50]

1.2.2 Spions in MRI imaging

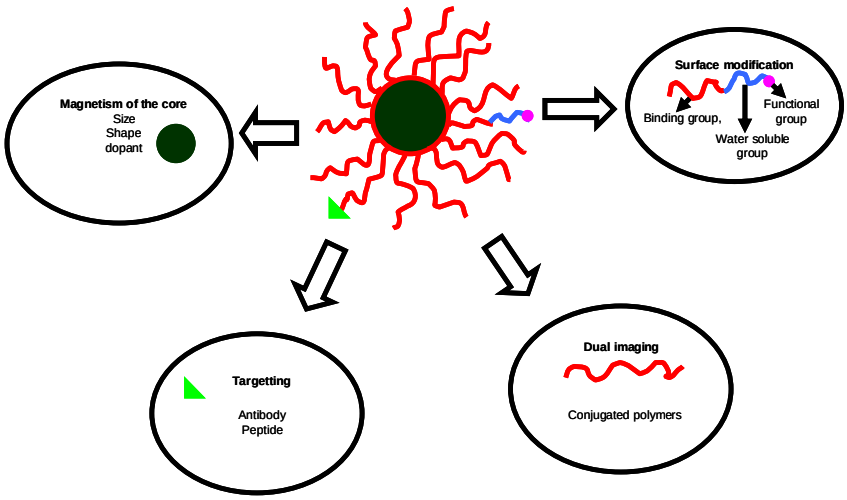

Figure 1.12: General scheme on functionalized SPIONs surface.

Super-paramagnetic iron oxide (SPIO), which are T_2 contrast agent due to its magnetic susceptibility, is taken into consideration because of its unique uptake mechanism by the Kupffer cells in the liver, spleen or bone marrow.[51] SPIO encapsulated by the cells of reticuloendotherial system (RES) shorten the T_2 relaxation time while, the liver cells, which are destroyed by tumor tissues or hepatic diseases, maintain the same relaxation time due to the lack of Kupffer

cells.[51] Nanotechnology (Figure 1.12) in this field provides coating of the core iron oxide to increase blood circulation time, reduce the agglomeration of them and improve pharmokinetic effect.[53] Another advantage of iron oxide nanoparticles is their metabolism within the body by biochemical pathway of the iron metabolism.[44] Food Drug Administration (FDA) approved super-paramagnetic iron oxide nanoparticles (SPION) drugs consist of dextran coated nanoparticles in order to increase its biocompatibility and to introduce easy surface modification by changing ligands of the dextran.[52] Dextran is a polysaccharide which is formed by linear backbone of the α-linked D-glucopyranosyl repeating units. Feridex ®, Resovist ®, Combidex ® and Feraheme ® are trademark drugs available since 1996 which is composed of dextran coated SPIONs or ultra-small SPIONs (USPION) means size is smaller than 50 nm.[44-52] Dougles *et al.* illustrate water soluble dendrimer assisted iron oxide nanoparticles formation with high T_1 and T_2 relaxivity.[54, 55] Micelles formation is introduced as another method of generating water dispersible SPIONS by using amphiphilic block co-polymers that it can enhance pharmokinetic effect as well.[56-57] New approaches on SPIONs are based on targeting, specific cellular uptake, enhanced relaxivity studies such as labeling them with peptides, antibodies or receptor specific residues.[53]

Magnetism effect of the core

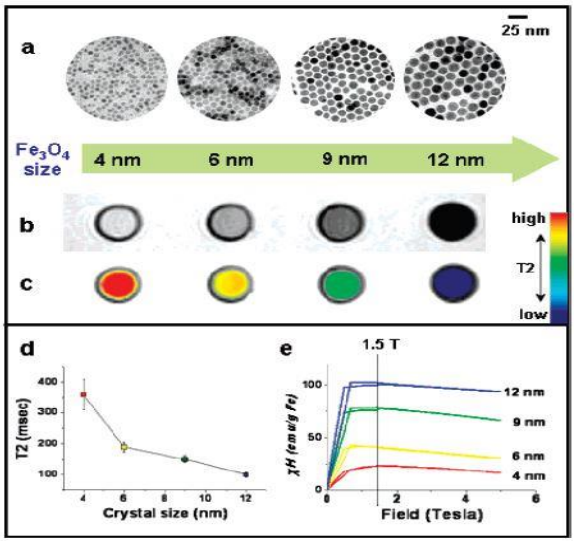

Figure 1.13: a) TEM images of the size increment of magnetic nanoparticles b) size dependent T_2 weighted MR images of the nanoparticles in water at 1.5 T. c) color coded version of the same nanoparticles in b. d) T_2 values versus size increment graph. e) magnetization measurement of nanoparticles based on super conducting quantum interference device (SQUID). (Reprinted with permission from ref. 62. Copyright 2005 American Chemical Society.)

Magnetism can be regarded as the intrinsic property of the super paramagnetic iron oxide nanoparticles. However, there are parameters that can effect magnetization of these particles which is related with the relaxivity of these particles in MRI imaging. These parameters are clarified as size, shape and dopant by alloys by several reviews.[60, 61]

Water solubility or dispersibility is one of the concern for bioimaging application of SPIONs , on the other hand, the other main concern is the size of these particles not only for cell penetration but also for their magnetic properties (Figure 1.13).[59-63] Cheon and coworkers demonstrate 2,3 dimercaptosuccinic acid (DMSA) coated Fe_3O_4 nanocrystals in different sizes which indicate significant variation in their magnetization (Figure 1.13).[62] Particles of size 4 nm, 6 nm, 9 nm and 12 nm exhibit magnetization values of 25, 43, 80 and 102 emu/(g Fe) respectively.[62] DMSA coating is remarkable water solubilizing reagent as providing carboxylic chelate on magnetic particle and thiol groups on

the surface for further modification such as antibody or peptide sequences for cancer diagnosis.[62] Formula 1, which explains the relation between saturation magnetization value (m_s) and size (r); [60, 63]

$$m_s = M_s[(r-d)/r]^3 \quad \mathbf{1}$$

Where d is the thickness of disordered surface layer and M_s is the saturation magnetization of the bulk materials.[60, 63] It is observed that size of the particles, which is less than 5 nm, has much more effect on m_s due to the probability of the disorder in the cation vacancies of the magnetic unit cells which can induce canting effect on the surface or internally.[63]

Doping of the iron oxide nanoparticles with other metals of +2 cation which are Mn, Co, Fe and Ni in order to enhance magnetization property of these particles by creating higher magnetic moment.[64] These metals electronic configurations consist of lone pairs which can induce magnetic field in the presence of the external magnetic moment. $MnFe_2O_4$, $FeFe_2O_4$, $CoFe_2O_4$ and $NiFe_2O_4$ engineered magnetic particles are prepared and their magnetization values are recorded as 110, 101, 99 and 85 (emu/mass of magnetic atoms) respectively.[64] Highest mass magnetization value of the $MnFe_2O_4$ is attributable with the cubic lattice structure of its crystallinity, since it has mixed spinel structure which leads to the different alignment of the spins in tetrahedral and octahedral lattices.[64]

Water Soluble SPIONs Generation

Carboxylate end group poly(amidoamine) dendrimer is prepared to perform water soluble magnetic nanoparticles formation under mild conditions (pH 8.5, Temperature 65 ^{o} C).[54] It gives stability to the magnetic nanoparticles by preventing their aggregation in aqueous media. Additionally, it gives high relaxivity both T_1 and T_2 interestingly. Fe(II) is oxidized in situ in the presence of the oxidizing agent Me_3NO and nanoparticles are formed immediately by surrounding with dendrimer. Size is optimized with respect to addition rate of the oxidizing reagent and reported as 20-30 nm with size exclusion chromatography.[54] Stem cell transplants tracking with magnetodendrimer species is exemplified by Bulte and coworkers and preserve their stability at least as long as six weeks *in vivo*.[55]

Micelle formation is one of the widely used techniques in biomedical applications in order to generate water dispersible drugs which are generally coated with biocompatible and biodegradable moieties.[53, 56, 57] First micelle formation by using magnetic iron oxide nanoparticles performed with amphiphilic diblock copolymer of poly(ε-capro-lactone)-b-(poly-ethylene-glycol) (PCL-b-PEG) with the size of 110 ±9 nm encapsulated 16 nm SPIO inside. In contrast with the lipid containing micelle and amphiphilic polymer coated micelle, results indicated that newly generated PCL-b-PEG covered micelle has much larger capacity in SPIO loading (lipid micelle % 12.4 , polymer micelle % 19.5 for 4 nm SPIOs).[56] This implies the reason of the enhance T_2 relaxivity comparing lipid and polymer formed micelles. Another micelle formation is represented by Hennick *et al.* differently using lactate end groups which can be hydrolyzed under physiological conditions.[57] Oleic acid coated magnetic nanoparticles are demonstrated as one of the efficient methods to obtain monodisperse iron oxide nanoparticles with the size ~ 10 nm owing to strong interactions between carboxylic groups of the oleic acid and iron oxide particles.[58] However, this idea still needed to be improved since, ~10 nm is too small for blood circulation time and these nanoparticles are not water soluble.[58] Another improvement is to increase the SPIONs loading capacity to %40 containing 5-10 nm oleic acid covered SPIONs micelles resulted in ~200 nm particles.[57]

Targeting with SPIONs

Cheon et al. demonstrate multifunctional iron oxide nanoparticles in cancer detection by conjugating Herceptin antibody on the surface of the particles coated with DMSA.[67] Herceptin has specific binding affinity as an antibody against the HER2/neu receptor which is overexpressed in breast cancer cells.[67] 9 nm prepared water soluble iron oxide nanoparticles are reported as ~30 nm after substitution with Herceptin. *In vivo* studies with mice revealed decrease in the T_2 relaxation time (%10 in 5 min and %20 at 4h) which means Herceptin-SPIONs reached the targeted tumor side and this observation is proved with the color change in the images (Figure 1.14).[67]

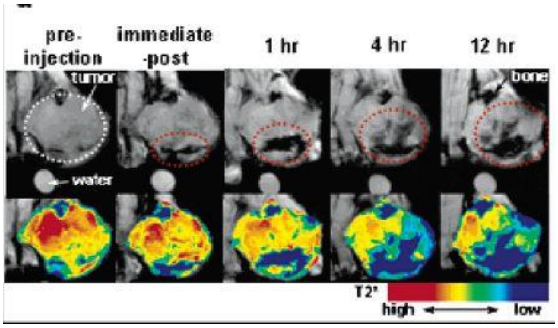

Figure 1.14: In vivo imaging with Herceptin conjugated SPIONs and their drop in relaxation time due to the targeted tumor tissues. (color change from red to green-blue). (Reprinted with permission from ref. 67. Copyright 2005 American Chemical Society.)

Dextran coated SPIONs attaching protein Annexin V, which can target arterial lesion, is another illustration of the modified SPIONs with proteins for enhance detection in vivo imaging.[68] Negative contrast is observed in the abdominal aorta of the hyperlipidemic rabbits after 15 min of the SPIONs injection.[68] SPIONs can be represented as a way of efficient MRI imaging contrast agent by allowing easy surface modification.

Potential gene delivery application by tracking with MRI in the presence of SPIONs loaded with si-RNA is demonstrated by Moore and co-workers.[69] Aminated dextran coated magnetic nanoparticles are modified with si-RNA as therapeutic agent, peptide for cell penetration and with a fluorescent dye for dual imaging.[69] While the relaxivity on muscle tissues remain the same, relaxivity on tumor tissues dropped after injection.[69] T-cell gene delivery is another potential usage of the polymer coated SPIONs in gene therapy.[70] In Figure 1.15, PEG based polymer chain modified with the amine end groups and SPION complexation with antibody conjugation via sulfur moieties are displayed.[70] Active groups on the surface of the SPIONs such as amines, antibody and water miscible PEG groups make these magnetic nanoparticles for multiple biomedical purposes like targeting, tracking and imaging.

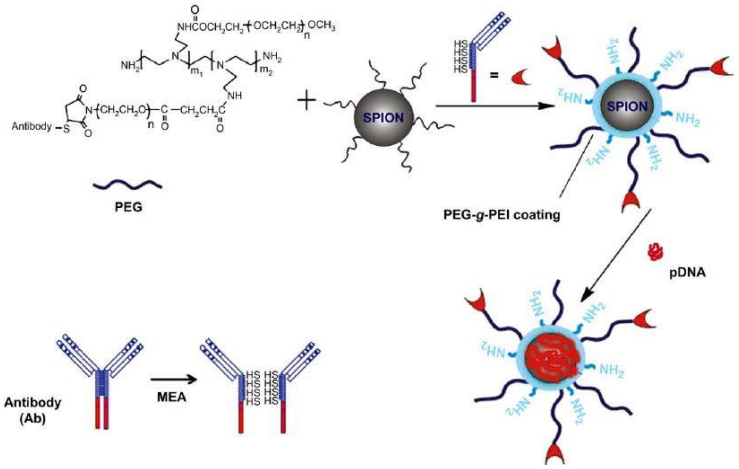

Figure 1.15: Schematic demonstration of complex formation between polymer coating, antibody and DNA. (Reprinted with permission from ref. 70. Copyright 2010 American Chemical Society.)

1.3 SPIONs Containing Conjugated Polymer Nanoparticles

Dual imaging (in vivo and in vitro) examined by using SPIONs micelles with phospholipids coating and hydrophobic conjugated polymer chains (PPE, PFPV, PFBT and MEH-PPV see Figure 6 for structures of polymers) by Green and coworkers.[71] MRI studies upon these hybrid material exhibit decrease in relaxation time T_2 and successful cell encapsulation with no toxic effect on cell growth.[71] As it is shown in TEM image (Figure 1.16), micelle formation occurs in wide range of size. That is the reason why big spherical red nanoparticles of MEH-PPV SPIONs micelle cannot be encapsulated by the cells. MRI study in the third image explains the relation between concentration of the magnetite and enhanced relaxivity owing to the micelle high loading capacity with magnetic nanoparticles.[71]

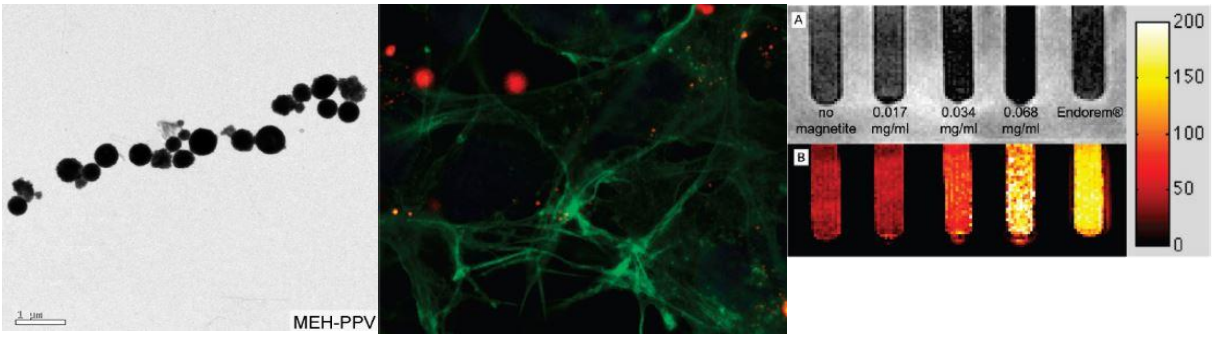

Figure 1.16: From left to right: 1) TEM images of the magnetic-fluorescence SPIONs micelle conjugated with polymer MEH-PPV. 2) Fluorescence Confocal Image of the micelles SH-SY5Y cells. Green part is actin, blue is nuclei and red fluorescence is attributable with MEH-PPV conjugated SPIONs micelles. Scale bar is 25 μm, bigger red spherical particles are about 1 μm. 3) A:T_2 weighted negative contrast images of the different concentration of magnetite containing MEH-PPV SPIONs, Endorem ® contains the same concentration of magnetite with MEH-PPV SPIONs micelle (0.0675 mg/ml). B: Quantitative analysis of images, color change is due to the R_2 (relaxation rate = $1/T_2$). (Reprinted with permission from ref. 71. Copyright 2010 American Chemical Society.)

Liu et al. developed one step further dual imaging nanoprobe by using biodegradable, biocompatible PLGA-PEG (poly(lactic-co-glycolic-acid)-poly(ethylene-glycol)) polymer substituted with folate moiety in order to target MCF-7 breast cancer cells (Figure 1.17).[72] Previously reported dual imaging nanoprobe[71], quantum dots[73] and nanocomposite[74] complexation with SPIONs result in low quantum yield of these fluorescent nanoparticles. Non-emissive absorption of the SPIONs can lead to energy lost on the exciton formed polymer aggregates in aqueous medium.[72] Therefore, this newly designed dual therapy nanoprobe contains PLGA-PEG residues within the magnetic-fluorescence nanoparticles to prevent the interaction between lipid coated iron oxide and conjugated polymer chains.[72]

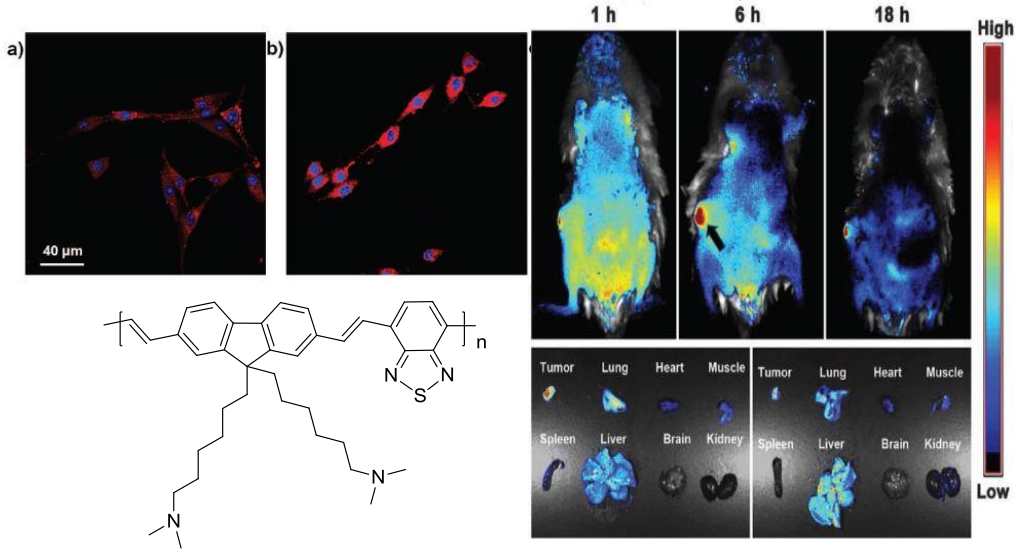

Figure 1.17: From left to right: 1) structure of the far-red/near infrared emissive conjugated polymer. 2) a) non-folate designed magnetic-fluorescent SPIONs nanoparticles in vitro imaging with MCF-7 breast cancer cells b) folate conjugate magnetic-fluorescent SPIONs nanoparticles in vitro imaging with MCF-7 breast cancer cells. 3) in vivo imaging with MRI, signal versus time. Organs 12 h later than injection; left side is treated with folate containing nanoparticles treated mice organs. Right side is without folate nanoparticles. (Reprinted with permission from ref. 72. Copyright 2012 Wiley-VCH Verlag GmbH & Co. KGaA.)

1.4 AIM OF THE PROJECT

This project aims to develop water dispersible hybrid nanoparticles in which super paramagnetic iron oxide nanoparticles (SPIONs) are coated with conjugated polymers for dual imaging. While the presence of SPIONs will be providing magnetic resonance imaging (MRI) capability, the conjugated polymers will act as a matrix holding SPIONs and will allow for optical imaging due to their inherent fluorescent properties. In this way, the resulting nanoparticles will be able to perform dual imaging.

Easy synthesis of their nanoparticles, their brightness and low toxicity make conjugated polymers [75] promising for hybrid material formation with SPIONs.

Conjugated polymers utilized in this work are emitting in the region of blue, green and red and carry allyl pendant groups. Shape persistent, stable

nanoparticles will be obtained by cross-linking of allyl groups through [2+2]-cycloaddition reaction under UV light. Cross-linking will not only confer stability to these hybrid nanoparticles but it will also help preventing the early leakage of SPIONs from the polymer matrix in the biological media. Scheme 1 illustrates the overall view of the project.

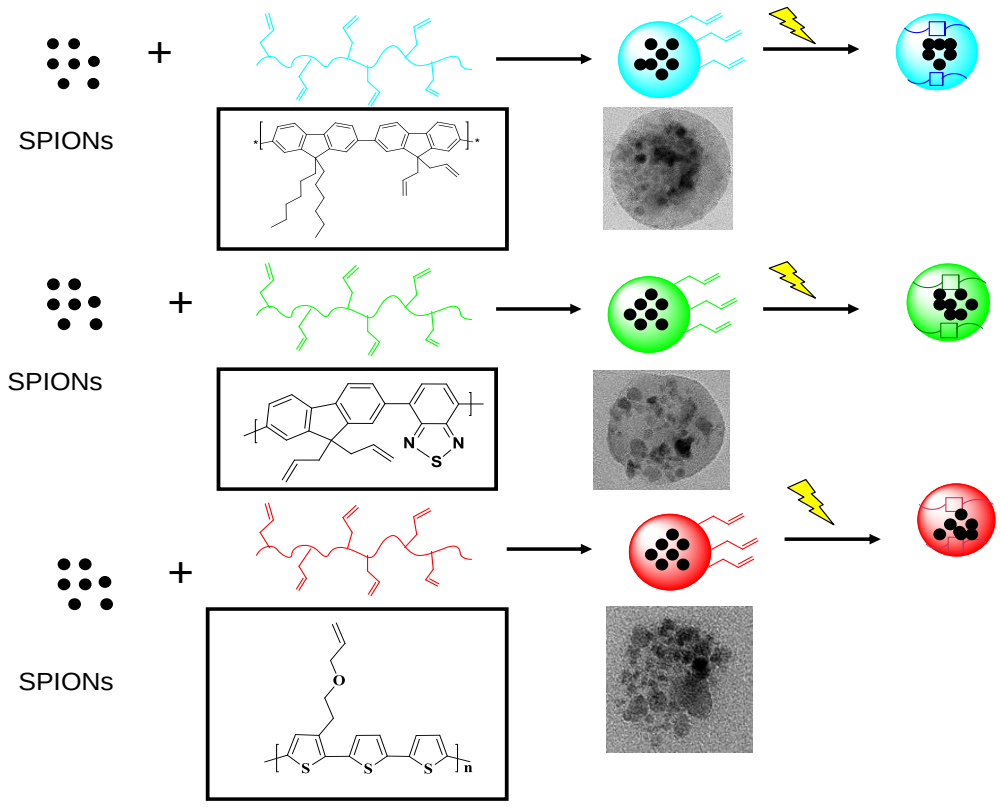

Scheme 1: General scheme of this work.

Chapter 2

Results and Discussion

Introduction

First section discusses the synthesis and characterization of monomers and polymers utilized in this work. Second section deals with the preparation and characterization of conjugated polymer nanoparticles, hybrid SPIONs-conjugated polymer nanoparticles and cross-linking studies of these nanoparticles.

2.1 Synthesis and Characterization of Monomers and Polymers

The synthesis and the characterization of the blue and green emitting polymers were previously reported in the literature by our group.[25, 78] Briefly, as shown in Scheme 2.1, fluorene based monomer having allyl pendant groups and boronic esters of fluorene or benzothiodiazole were polymerized through Suzuki coupling in the presence of palladium catalyst to generate, respectively, blue and green emitting polymers.

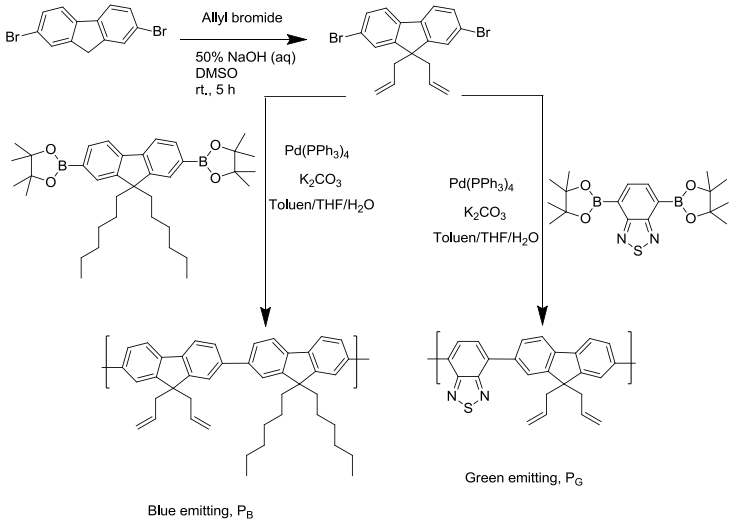

Scheme 2.1: Synthesis route for blue and green emitting polymers

As indicated in Scheme 2.1, blue emitting and green emitting polymers were prepared with allyl functional groups which will enable 2+2 cycloaddition reaction under UV irradiation to obtain shape persistent and stable nanoparticles.

2.1.1 Synthesis and Characterization of 2-(2,5-dibromothiophen-3-yl)ethanol (M1)

2-(2,5-dibromothiophen-3-yl)ethanol was synthesized from 2-(thiophene-3-yl)ethanol in the presence of N-bromosuccinimide (NBS) in ethyl acetate as shown in Scheme 2.2. 2,5 (α- positions) of 3-thiophene ethanol was brominated with electrophilic substitution reaction of NBS. Extraction with water and chloroform renders M1 in organic layer with 60% yield. Characterizations of M1 were done with ^{1}H-NMR and ^{13}C–NMR spectroscopy.

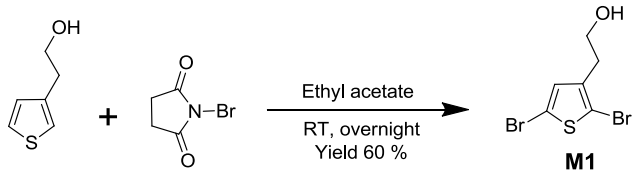

Scheme 2.2: Synthesis scheme of monomer 2-(2,5-dibromothiophen-3-yl)ethanol (M1).

The peak at 6.88 ppm is attributable to thiophene proton of **M1** in the ^{1}H-NMR spectrum in figure 2.1a. Other two triplets at 3.80 and 2.80 are due to the protons of methylene groups of alkyl chain, labeled as b and a, respectively. Hydrogen of the hydroxyl group can usually be observed as broad peak around 2 ppm but OH-hydrogen is not visible in this ^{1}H-NMR spectrum. Probably it disappeared due to H-bonding as the sample is quite concentrated.

Aromatic carbons labelled as a, b, c and d in ^{13}C –NMR spectrum appear between 110-140 ppm as expected in figure 2.1b. Other two peaks belong to methylene carbon of the pendant group at 62 ppm (f) and 32 ppm (e).

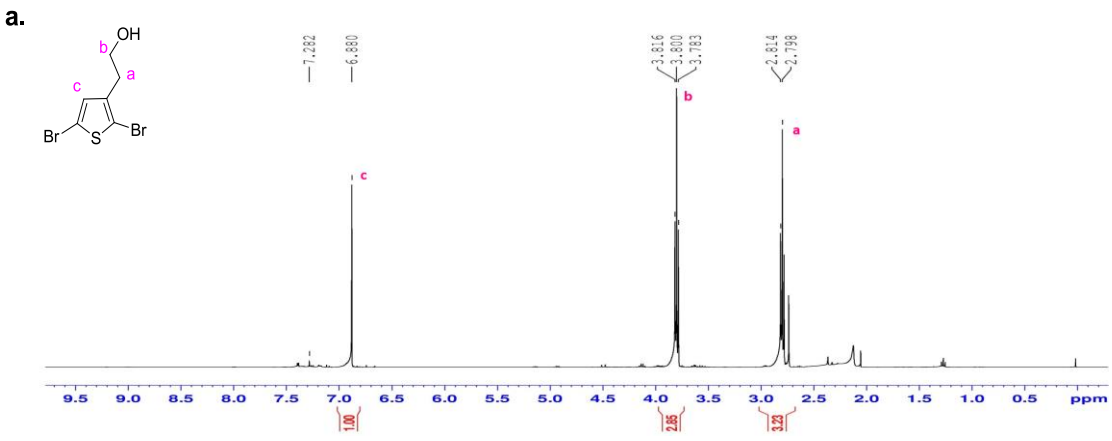

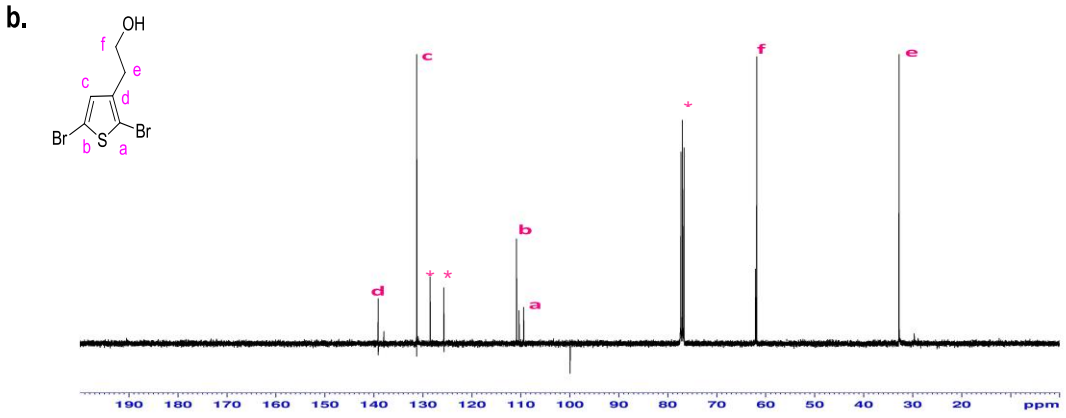

Figure 2.1: a. ^{1}H-NMR (400 MHz, $CDCl_3$, 25 °C) and **b.**^{13}C-NMR spectra (100 MHz, $CDCl_3$, 25 °C) of 2-(2,5-dibromothiophen-3-yl)ethanol (M1). (*Denotes solvent or other impurities coming from solvent)

2.1.2 Synthesis and Characterization of 2-(2,5-dibromothiophen-3-yl)ethyl acetate (M2) from 2-(2,5-dibromothiophen-3-yl)ethanol (M1)

Acetylation of 2-(2,5-dibromothiophen-3-yl)ethanol was performed with acetic anhydride and pyridine as described in Scheme 2.3. Acetic anhydride was utilized as both solvent and reactant. Excess pyridine was acting as catalyst. Nucleophilic attack of the oxygen in M1 was attracted by amide complexation of the pyridine and acetic anhydride. First acetic acid was eliminated from acetic anhydride as a result of pyridine complexation. Then, pyridine was eliminated by nucleophilic attack of M1 through the amide intermediate. Acetic acid and pyridine were generated after the reaction completion. Work-up process consisted of water extraction in order to get rid of pyridine and stirring with methanol to convert acetic acid to low boiling point methyl acetate. Evaporation of solvents under reduced pressure revealed viscous liquid M2 with 98% yield. Characterizations were done via ^{1}H-NMR spectrum and liquid chromatography mass spectrometry time-of-flight (LC/MS- TOF).

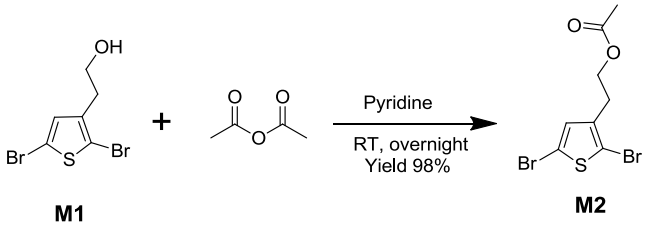

Scheme 2.3: Synthesis scheme of 2-(2,5-dibromothiophen-3-yl)ethyl acetate (M2) from 2-(2,5-dibromothiophen-3-yl)ethanol (M1).

Figure 2.2 shows ^{1}H-NMR spectrum of M2. The most characteristic singlet peak is the methyl hydrogens of the acetyl moiety in the pendant group (labeled as *d*) at 2.07 ppm. A singlet peak at 6.88 ppm is appeared due to the aromatic proton *a* and a triplet at 2.87 ppm is due to the hydrogens of methylene labeled as *c*.

LC/MS-TOF (liquid chromatography mass spectrometry time-of-flight) is based on the ion's mass to charge ratio measurements in terms of time. Accelerated ions with the same electric field travel same distance with varying time range with respect to their mass to charge ratio. TOF-MS spectrum in Figure 2.3 indicates substitution of the two bromine with its unique isotopic pattern as three lines. The starting peak, which is 362.80 m/z, is attributable to the two hydrogen loss of the negatively ionized monomer and potassium cation as counter ion ($[M_2+K-2H]^-$). TOF-MS spectrum confirms structure of M2 in terms of its mass.

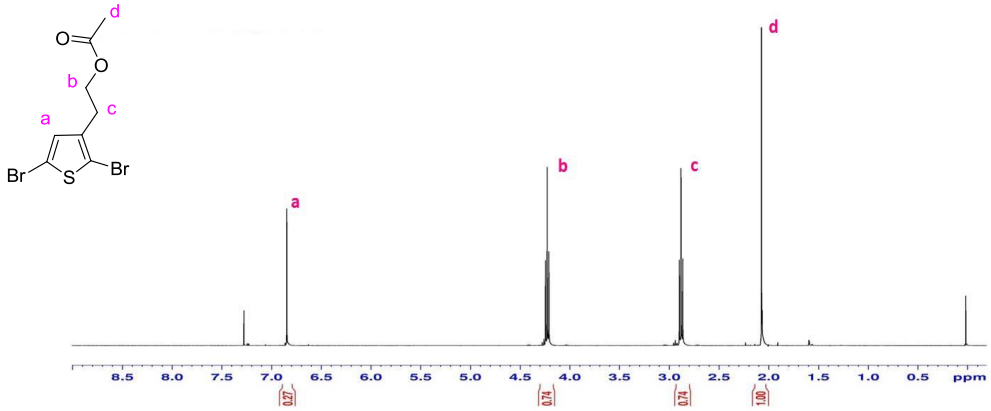

Figure 2.2: ^{1}H-NMR (400 MHz, $CDCl_3$, 25^{o} C) spectrum of 2-(2,5-dibromothiophen-3-yl)ethyl acetate (M2)

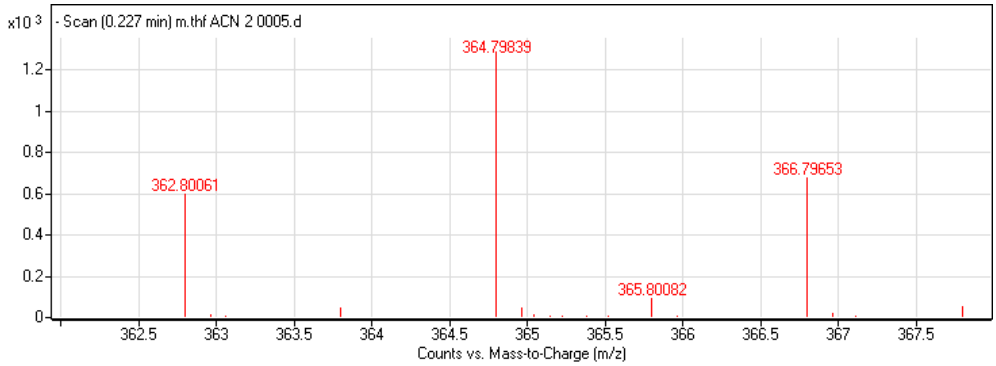

Figure 2.3: LC/MS-TOF spectrum of 2-(2,5-dibromothiophen-3-yl)ethyl acetate (M2)

2.1.3 Synthesis and Characterization of poly[2-{ethyl acetate}(thiophene-2,5-diyl)-co-(5,5'-{2,2'}-bithiophene)] (P1) from 2-(2,5-dibromothiophen-3-yl)ethyl acetate (M2)

Polymerization of acetylated thiophene monomer (M2) is based on Pd^{o} catalyzed cross coupling reaction which is also called Stille Coupling reaction defined in Figure 1.3. 2-(2,5-dibromothiophen-3-yl)ethyl acetate underwent Stille Coupling reaction as alkyl halide and 5,5'-Bis(tributylstannyl)-2,2'-bithiophene as organotin compound in the presence of catalyst $Pd(Ph_3P)_4$ under inert atmosphere. Reaction was kept for 3 days to generate high molecular weight polymer, since low molecular weight polythiophene is obtained as viscous liquid material which makes it difficult to isolate and process. Isolation of pure product was done by washing solid residue with water and methanol to dissolve the oligomeric residues and catalyst. The product was obtained as dark red solid powder with the yield as 60%. Structural characterizations were done with ^{1}H-NMR, ^{13}C-NMR, FT-IR spectra. Optical properties were determined by UV-Vis and fluorescence spectroscopies.

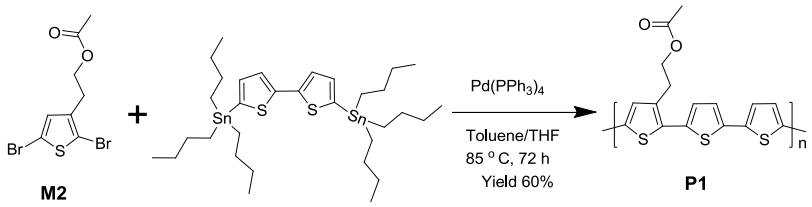

Scheme 2.4: Synthesis scheme of poly[2-{ethyl acetate}(thiophene-2,5-diyl)-co-(5,5'-{2,2'}-bithiophene)] (P1) from M2 .

^{1}H-NMR spectrum of P1 shown in Figure 2.4a, resembles the ^{1}H-NMR spectrum of the M2 in terms of chemical shifting. However, it can be clearly seen that the peaks of P1 are broader, which can be explained with the rigid structure of the long polymer chains and their effect on the mobility of the molecule. Aromatic protons appeared at 7.11 ppm as multiplet, aliphatic protons *b*, *c* and *d* are observed at 4.34 ppm, 3.12 ppm and 2.07 ppm respectively. Other small peaks around 1 ppm and around 7.5 ppm are due to the end groups of the polymer chains. Bithiophene contains tributyltin moieties and some of them stay as end group of the polymer chains. Integration path is consistent with the ratio of the protons.

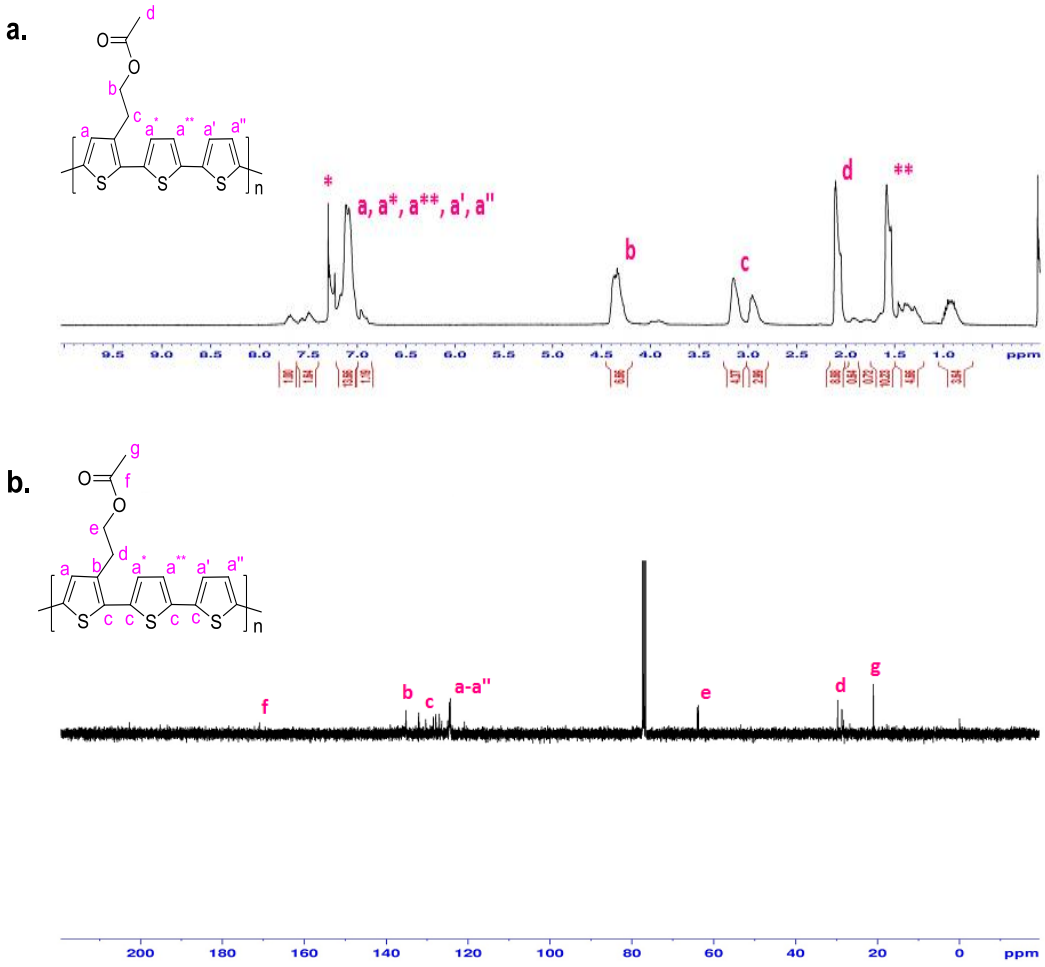

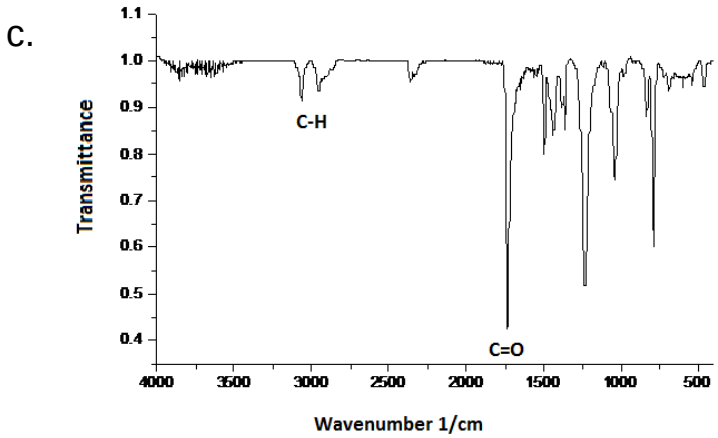

Figure 2.4: a. ^{1}H-NMR (400 MHz, $CDCl_3$, 25^{o} C), **b.** ^{13}C–NMR (400 MHz, $CDCl_3$, 25^{o} C) and **c.** FT-IR (solid state, KBr pellet) spectra of poly[2-{ethyl acetate}(thiophene-2,5-diyl)-co-(5,5'-{2,2'}-bithiophene)] (P1), (*Denotes solvent or other impurities coming from solvent)

^{13}C-NMR spectrum gives the expected peaks of polymer in aromatic region and aliphatic as well indicated in figure 2.4b. Peaks between 120-140 ppm are due to the aromatic carbons and aliphatic moiety appears at 63.2 ppm, 27.4 ppm and 20.7 ppm as *e*, *d* and g respectively. Carbonyl carbon *f* is labeled at 170.2.

FT-IR spectrum gives three types of characteristic peaks for P1 as highlighted in figure 2.4c. First one is intense carbonyl peak at 1750 cm^{-1}. The other ones are labeled as C-H peaks which refers to the aliphatic and aromatic stretchings at 2850 and 3100 cm^{-1} respectively. Characteristic C=O stretching band combining with C-H ones confirms the structure of the P1 polymer.

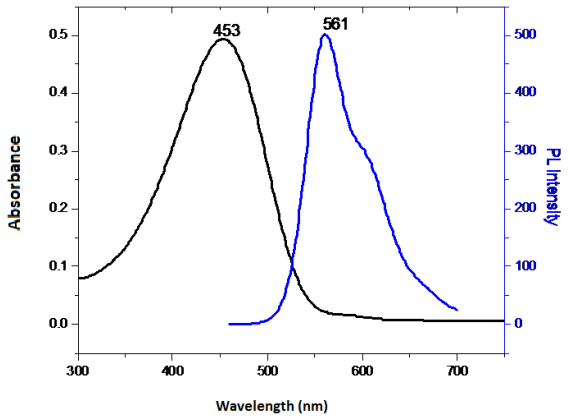

Figure 2.5: Optical characterization of P1, UV-Vis and fluorescence spectra of poly[2-{ethyl acetate}(thiophene-2,5-diyl)-co-(5,5'-{2,2'}-bithiophene)] (P1), (λ_{excit}= 453 nm)

As introduced before, polythiophene is one of the widely studied red emitting conjugated polymers. This red polymer absorption peak maximum is at 453 nm and this excitation leads to the emission at 561 nm as shown in Figure 2.5.

2.1.4 Synthesis and Characterization of ploy[3-{(allyloxy)ethyl}(thiophene 2,5-diyl)-co-(5,5'-{2,2'}-bithiophene)] (P2) from poly[2-{ethyl acetate}(thiophene-2,5-diyl)-co-(5,5'-{2,2'}-bithiophene)] (P1).

Deacetylation of P1 was performed in the presence of strong base potassium hydroxide and followed by the alkylation with allyl bromide as described in Scheme 2.5. Base catalyzed deacetylation of P1 led to the primary alcohol generation in pendant group. Excess potassium hydroxide in reaction mixture formed alkoxide. This reaction mechanism resulted in the nucleophilic substitution of allyl bromide and salts of KBr as side product. Isolation of pure product was done by chloroform and water extraction to get rid of salts and evaporating allyl bromide residues under reduced pressure. Characterizations of P2 were done via ^{1}H-NMR and FT-IR spectrometry. Optical characterization was performed by UV-Vis and Fluorescence spectra.

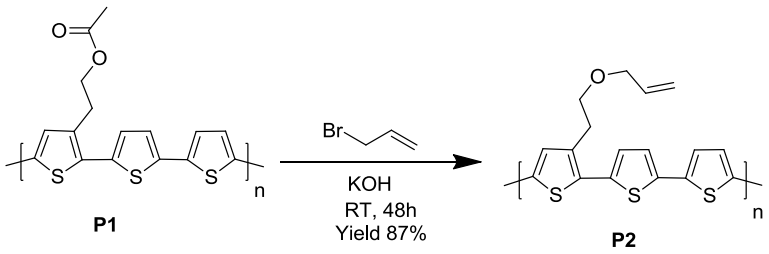

Scheme 2.5: Synthesis scheme of poly[3-{(allyloxy)ethyl}(thiophene 2,5-diyl)-co-(5,5'-{2,2'}-bithiophene)] (P2) from P1.

^{1}H-NMR spectrum of P2 (Figure 2.6) represents aromatic peaks at 7.1 ppm and terminal allyl moiety peaks at about 6 ppm (f) and 5.1-5.3 ppm (e). Integrations of these peaks are consistent with the expected values. The most significant change is observed in the peak labeled as b (4.3 ppm) in the ^{1}H-NMR spectrum of P1 in figure 2.4-a. It is shifted to upfield region indicated as peak c (3.7 ppm) in the ^{1}H-NMR spectrum of P2 in figure 2.6. This shifting occurs due to the shielding effect of the allyl group and it is mostly effective on the adjacent hydrogens. However, hydrogens closer to the polymer chain (b) do not exhibit a considerable shifting.

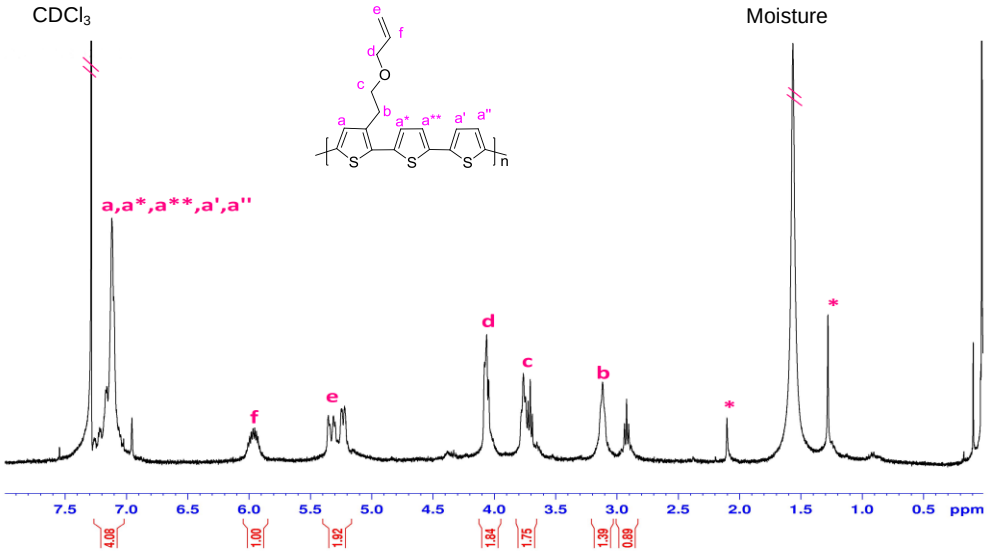

Figure 2.6: ^{1}H-NMR (400 MHz, $CDCl_3$, 25^{o} C) spectra of poly[3-{(allyloxy)ethyl}(thiophene 2,5-diyl)-co-(5,5'-{2,2'}-bithiophene)] (P2), (*Denotes impurities coming from solvent)

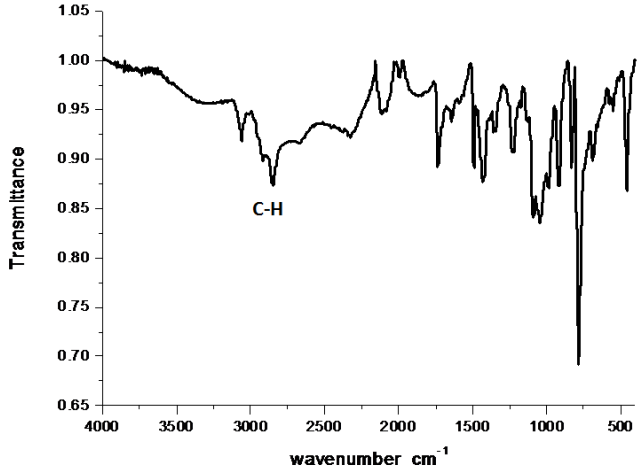

Figure 2.7: FT-IR (solid state, KBr pellet) spectrum of poly[3-{(allyloxy)ethyl}(thiophene 2,5-diyl)-co-(5,5'-{2,2'}-bithiophene)] (P2)

FT-IR spectrum of P2 (figure 2.7) confirms the deacetylation of the P1 with decreased intensity of C=O stretching at 1750 cm^{-1} and increase in the aliphatic stretchings as labeled in the spectrum between 2850-3000 cm^{-1}. At 3100 cm^{-1}, aromatic C=C stretchings of thiophene backbone is appeared as strong stretching band.

Optical properties of P2 resemble that of P1 and their absorption maxima appears at 453 nm (Figure 2.8). When P2 is excited with this value, 559 nm is recorded as fluorescence maxima which shows 2 nm blueshift compare to P1. In conjugated polymers, electron withdrawing or electron releasing character is quite important in pendant group, since it can affect their band gaps. However, substitution of the acyl group with the allyl didn't lead to any significant changes. This can be attributed to the fact that acyl is weakly electron withdrawing and allyl is also weakly electron withdrawing moieties.

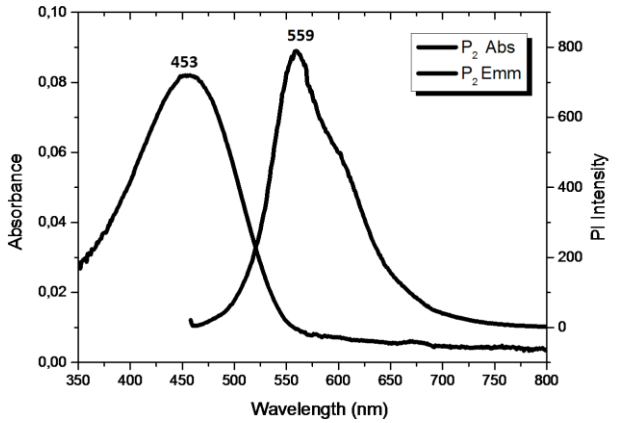

Figure 2.8: UV-Vis and Fluorescence Spectra of poly[3-{(allyloxy)ethyl}(thiophene 2,5-diyl)-co-(5,5'-{2,2'}-bithiophene)] (P2) in THF (λ_{excit} = 453 nm)

2.2 Synthesis and Characterization of Polymer Nanoparticles

Synthesis of water dispersible conjugated polymer nanoparticles was achieved by reprecipitation method after the synthesis of three polymers emitting in the region of blue (PB), green (PG) and red (P2). This method was utilized by dissolving polymer in water miscible solvent THF and filtration of this solution with syringe filter. Filtrated stock solutions of polymers were injected into excess of water immediately while sonicating. The driving force of the reprecipitation method is the packing of the chains as spherical nanoparticles owing to the hydrophobic effect of polymer chains. After removal of the organic solvent, stable water dispersible nanoparticles were obtained.

As it is stated before, obtaining small nanoparticles (<100 nm) with uniform distribution is requirement for biomedical applications.[76, 77] Size of the nanoparticles can be tuned by using polymer concentration and solvent amount as the two significant parameters. Polydispersity index (PDI), which indicates the distribution of the nanoparticles, is related to the nature of the polymer. Therefore, optimizations were performed to obtain evenly distributed nanoparticles under 100 nm.

Characterizations were done by Dynamic Light Scattering (DLS) for size measurements, Scanning Electron Microscope (SEM) and Transmission Electron Microscope (TEM) for morphology studies. Optical Characterizations were carried out with UV-Vis spectrometer and Fluorescence spectrometer.

2.2.1 Synthesis and Characterization of poly[(9,9-bis {3-dihexyl}fluorenyl-2,7-diyl)-co-(9,9-bis {3-diallyl)fluorenyl-2,7-diyl)] (PB) Nanoparticles

Blue polymer (PB) nanoparticles were prepared as indicated in Scheme 2.6. 1 mg of PB was determined as soluble in 1 ml of dry THF. Filtrated 1 ml of PB solution with syringe filter is dropped into 50 ml of water. After sonication of this mixture for 1 h, THF was evaporated under reduced pressure. Characterizations of PB nanoparticles were done with DLS, SEM and TEM for size and shape studies. Optical characterizations were performed with absorbance and UV-Vis spectroscopy.

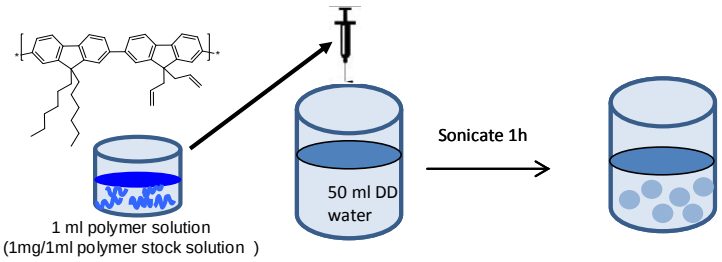

Scheme 2.6: PB nanoparticle preparation scheme

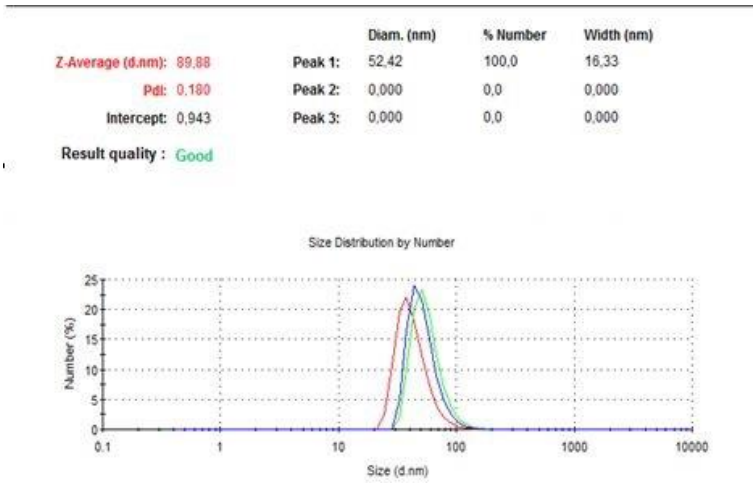

Figure 2.9: Size distribution of PB nanoparticles by number

Dynamic Light Scattering (DLS) measures the time dependent fluctuations of light which is scattered by the particles in solution. In order to form a reliable data, three measurements are taken and their average value is recorded. Peak 1 indicates the size of the most abundant PB nanoparticles which is 52.42 nm in figure 2.9. Polydispersity index (PDI) is 0.180 which denotes dispersion range of the particles. It can be concluded that the particles are uniform, their PDI range and size are acceptable. In order to state that these nanoparticles are reproducible, three synthesis were utilized and standard deviation was calculated as 3.89 for size and 0.019 for PDI measurements.

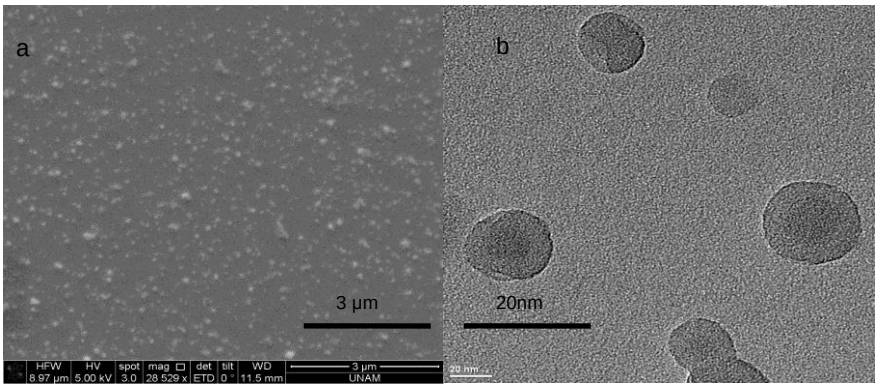

Figure 2.10: a. SEM image of the PB nanoparticles, b. TEM image of the PB nanoparticles.

Scanning electron microscope (SEM) is a technique to visualize the morphology of the nanoparticles synthesized. SEM detects secondary electrons on the surface of the silicon substrate and generates the images about the surface morphology of the samples. Spherical form of the nanoparticles can be observed with their dispersion in figure 2.10-a. The biggest particles are recorded as around 100 nm, abundant small particles are in the range of 45-55 nm as expected from DLS measurements. There is no sign for aggregation.

Transmission electron microscope (TEM) has higher resolution comparing to SEM, since electrons are transmitted through the specimen. As it shown in figure 2.10b, 20 nm scale available and its morphology and size distribution is match with the data obtained from SEM and DLS measurements.

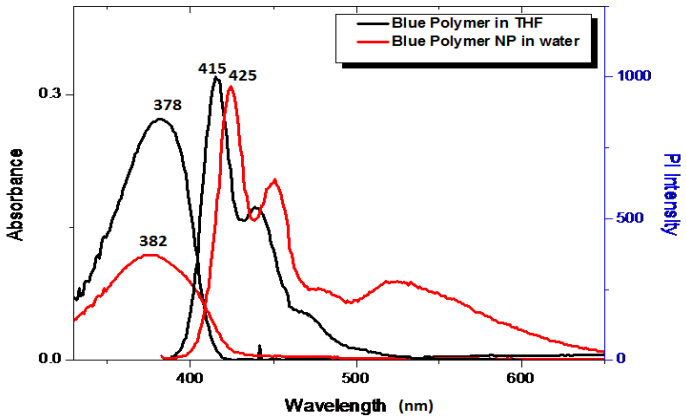

Figure 2.11: UV-Vis and Fluorescence spectra of Blue Polymer (PB) in THF and in water. (λ_{excit}= 378 nm for THF and λ_{excit} = 382 nm for water) * slit width is 5 for water and 2.5 for THF solution in fluorescence spectrums.

PB absorption maximum is determined as 378 nm in water and 382 nm in THF (Figure 2.11). Their fluorescence is observed in blue region with these excitations as 415 nm and 425 nm in THF and in water respectively. This red shift around 10 nm, is observed as general trend in CPN formation and related with the increased interchain interactions such as π-π stacking.

2.2.2 Synthesis and Characterization of Poly [(9,9-bis ({3-diallyl}fluorenyl-2,7-diyl)-co-(benzothiadiazole)] (PG) Nanoparticles

PG nanoparticles were synthesized with the same method as reprecipitation by dissolving 2 mg polymer in 5 ml dry THF and dropping it into 50 ml water immediately as shown in Scheme 2.7. The concentration of the polymer was determined with respect to the literature published by our group[25]. Green polymer nanoparticles were characterized with DLS, SEM, TEM and its optical characterizations were done with UV-Vis and fluorescence spectroscopy.

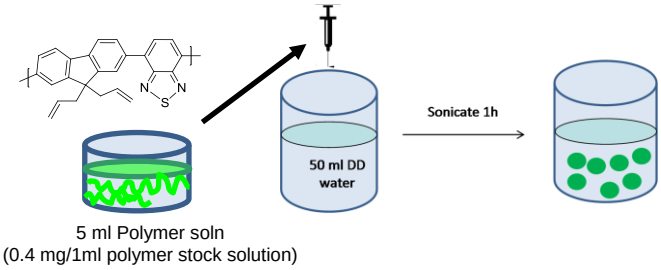

Scheme 2.7: PG nanoparticle preparation scheme

DLS result represents that peak one is 44. 63 nm and PDI is 0.243 (Figure 2.12). This result clarifies that some bigger or smaller particles were produced, but the size of the most abundant nanoparticles were ~45 nm. Reproducibility of these nanoparticles were tested with at least three different syntheses with the same method and standard deviations for size and PDI were found as 6.30 nm and 0.089, respectively.

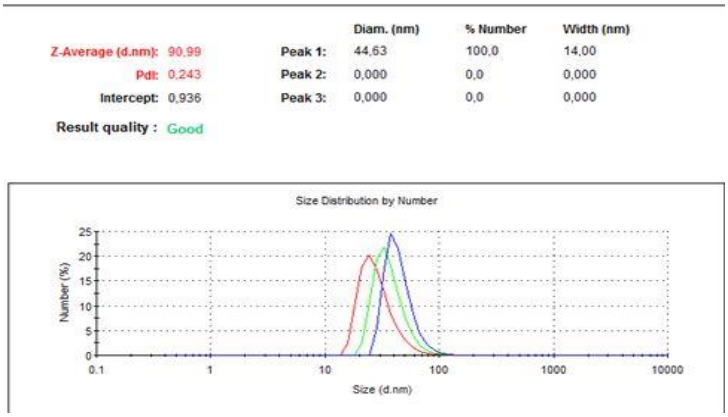

Figure 2.12: Size distribution of PG nanoparticles by number

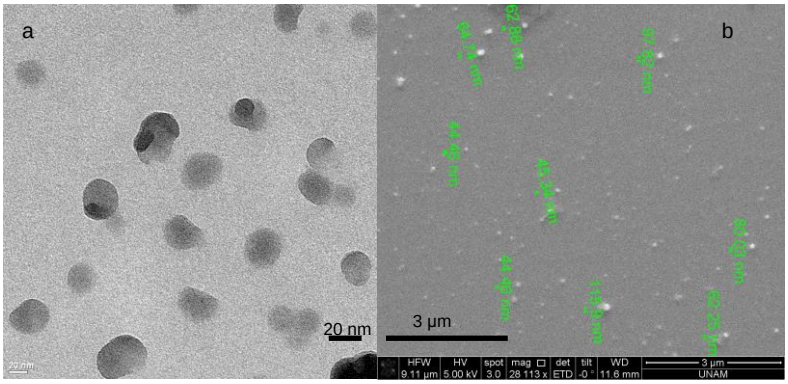

Figure 2.13: a. TEM image of PG nanoparticles b. SEM image of PG nanoparticles.

Morphology of PG nanoparticles were investigated via SEM and TEM microscopy (Figure 2.13a-b). From TEM, their average size was determined as ~45-50 nm and they are spherical particles. From SEM studies, it can be concluded that their size is around ~45 nm. Bigger particles are observed as expected from a PDI of 0.243 but there is no sign for aggregation.

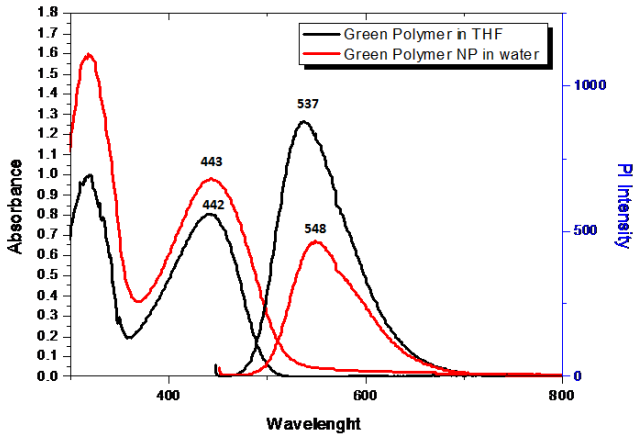

Figure 2.14: UV-Vis and Fluorescence spectra of Green Polymer (PG) in THF and in water. (λ_{excit}= 442 nm for THF and λ_{excit} = 443 nm for water) * Green Polymer absorption in THF is normalized.

Green polymer PG and its nanoparticles are in green-yellow range as their emission is found as 537 nm in THF and 548 nm in water (figure 2.14).

2.2.3 Synthesis and Characterizations of poly[3-{(allyloxy)ethyl}(thiophene 2,5-diyl)-co-(5,5'-{2,2'}-bithiophene)] P2 Nanoparticles

P2 nanoparticles were prepared with the same reprecipitation method by dissolving it in dry THF and adding into excess of distilled water in one shot as indicated in Scheme 2.8. Concentration of P2 was determined as 0.25 mg in 1 ml of THF. The characterization of the resulting nanoparticles were done with the same methods as previously described; DLS, SEM, TEM and UV-Vis, fluorescence spectrometry.

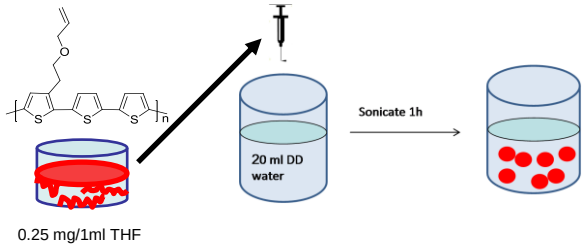

Scheme 2.8: P2 (Red Polymer) nanoparticles preparation scheme

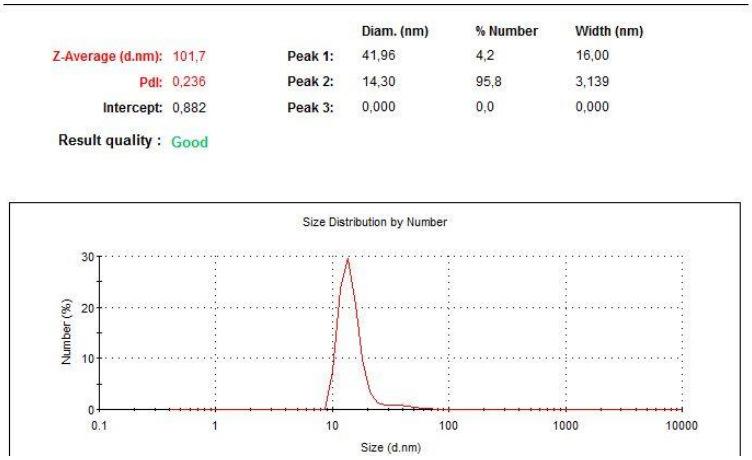

Figure 2.15: Size distribution of P2 nanoparticles by number

The size of the particles is recorded as 41.96 nm from their DLS result. PDI is recorded as 0.236 with no indication for aggregation in figure 2.15.

In figure 2.16, the SEM and TEM data agrees with the DLS results in terms of size of the particles. Most of them are in the range of 40-50 nm, however, some big particles are observed in minor amount. Their morphology was examined and revealed the spherical shape nanoparticles with a dispersion that is consistent with the DLS data.

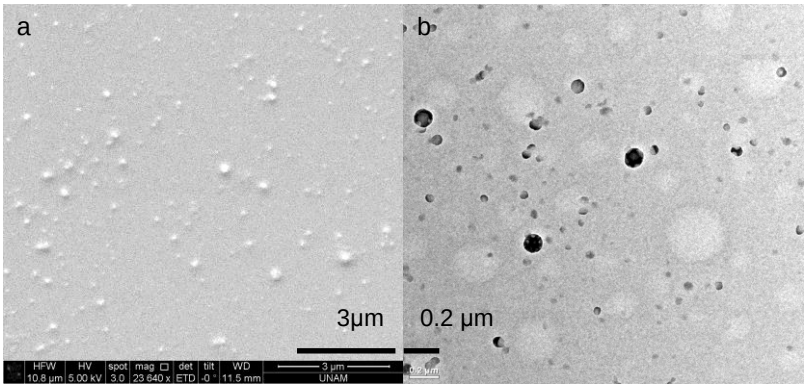

Figure 2.16: a. SEM image of P2 nanoparticles b. TEM image of P2 nanoparticles

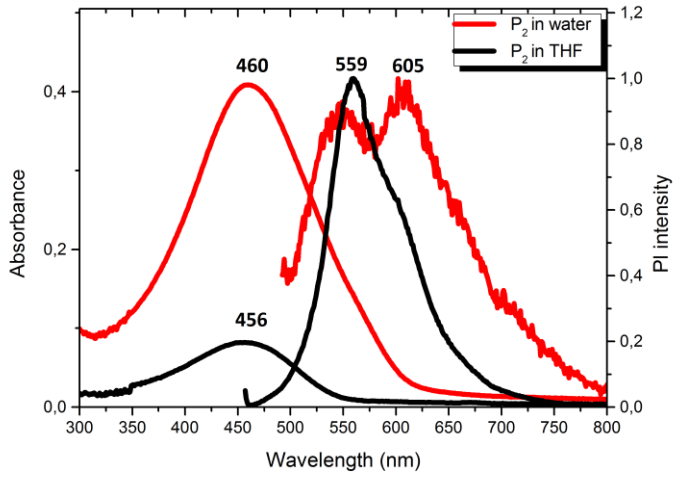

Figure 2.17: Optical data of P2 and P2 nanoparticles (λ_{excit}= 460 nm in water and λ_{excit} = 456 nm in THF. *Fluorescence data is normalized and slit width is increased to 10 from 5 for emission measurements in water)

P2 absorbs and emits the light in the red region as it is stated before and represented in Figure 2.17. The dramatic change is observed in their emission pathway as P2 nanoparticles exhibit 46 nm red shift from 559 nm to 605 nm. Additionally, Pl intensity decreased in water owing to the nanoparticle formation. This fact is related to the more π interaction between the polymer chains in water. It leads to both red shift and loss in emission intensity.

2.3 Synthesis and Characterization of Hybrid Nanoparticles with Conjugated polymers and SPIONs

Nanoparticles of blue polymer (PB), green polymer (PG) and red polymer (P2), which were utilized in hybrid nanoparticle synthesis with SPIONs, were examined. Blank nanoparticles of the polymers and the SPIONs containing polymer nanoparticles were synthesized with the same polymer concentrations. Polymer coated SPIONs were investigated in terms of their size, morphology and optical properties same as blank polymer nanoparticles. Moreover, cross-linking studies of those hybrid nanoparticles were achieved under 273 nm UV light in order to form 2+2 cycloaddition between allyl groups. Changes in these nanoparticles

owing to the cross-linking are characterized by DLS, SEM, TEM and optical properties are performed with UV-Vis and fluorescence spectroscopies.

2.3.1 Synthesis and Characterization of Blue Polymer (PB) SPIONs Nanoparticles (SPB)

Hybrid material of SPIONs and PB (Blue polymer) nanoparticles synthesis was performed in situ by dissolving them in THF and mixing them together as described in Scheme 2.9. SPIONs solution was kept in toluene solution. Therefore, first toluene solution of 250 µl SPIONs was evaporated under reduced pressure and then it was dissolved in 1 ml of THF. Then, reprecipitation method was utilized by adding polymer and SPIONs THF solution mixture into the 50 ml of distilled water. THF was evaporated after 1 hour of sonication and nanoparticles (SPB) were obtained. Their characterizations were performed via DLS, SEM, TEM and their optical characterizations were done with UV-Vis and fluorescence spectrometers.

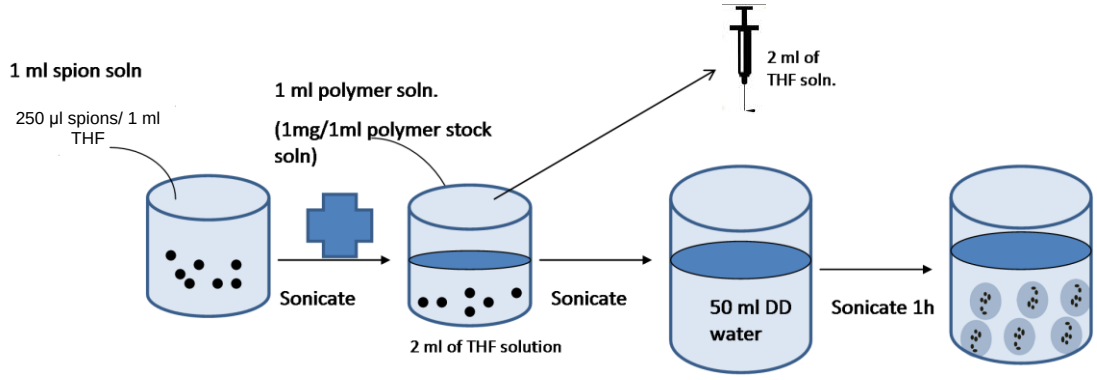

Scheme 2.9: Preparation scheme of SPB nanoparticles

DLS data of the SPB nanoparticles indicate that most of them are around 60.30 nm and PDI is 0.116 implying narrow size range for the nanoparticles. Average diameter is 95.48 nm which is considerable size for nanoparticles in biomedical applications. Standard deviations calculation which points the reproducibility of these SPB nanoparticles results as 7.05 for size and 0.011 for PDI.

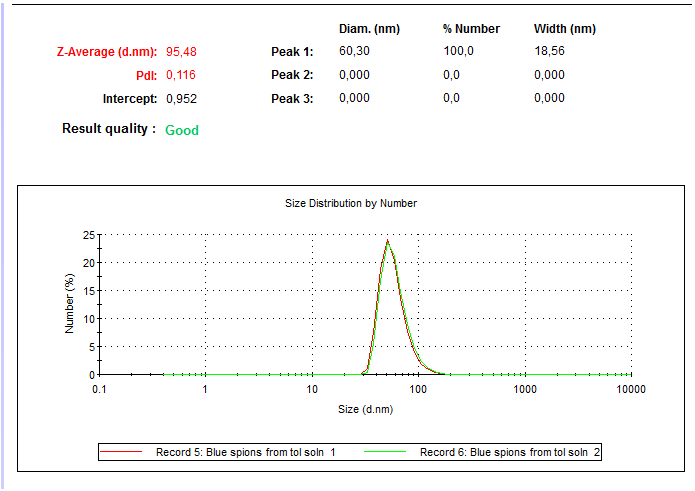

Figure 2.18: Size distribution of SPB nanoparticles by number

Spherical shape of these nanoparticles can be observed in SEM and TEM images in figure 2.19. Additionally, their size and polydispersity data match with the DLS data. Their uniform dispersity is confirmed with TEM and SEM images that majority of the nanoparticles are in the range of 55-60 nm with well-defined spherical form.

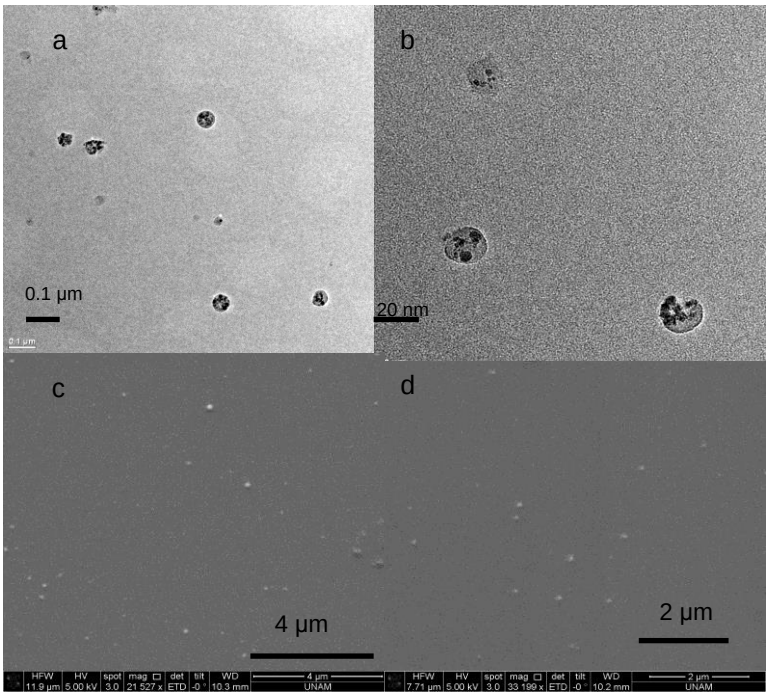

Figure 2.19: a and b are the TEM images of SPB nanoparticles, c and d are SEM images of SPB nanoparticles

Cross-linking studies of SPB Nanoparticles

Cross-linking study aims to obtain 2+2 cycloaddition under UV irradiation within the allyl groups of the single nanoparticles which leads to confinement of the SPIONs inside of the SPB nanoparticles. In order to accomplish cross linking, short wavelength (273 nm) was applied on the diluted SPB solution for 2 hours. This dilution was done by adding 10 ml of water on the 2 ml of the SPB mother liquor. The reason of this was to prevent cross linking between the nanoparticles which can result in aggregation of the SPB nanoparticles.

Indications of cross-linking were examined with DLS, SEM, TEM and optical studies.

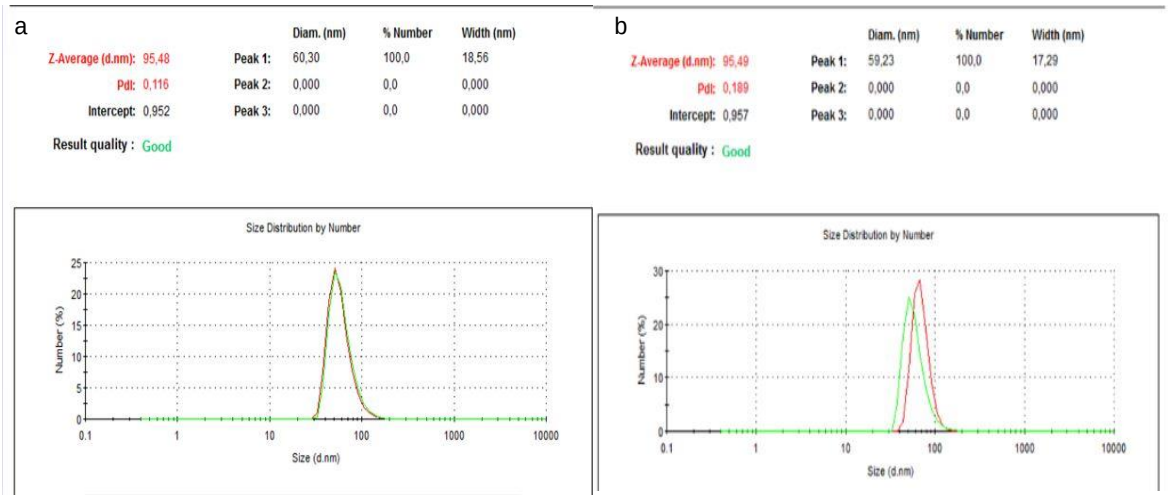

Figure 2.20: DLS data of SPB nanoparticles, a. before cross-link; b. after cross-link

DLS data before cross-linking and after cross-linking of these SPB nanoparticles shows decrease in size of about 1 nm-from 60.30 nm to 59.23 nm as shown in figure 2.20. This minor change is due to the formation of the cyclobutane from allyl moieties. It can be attributed to the more compact shape of these nanoparticles. However, PDI is increased from 0.116 to 0.189. The reason for this drastic change can be due to the different cross-linking density of these nanoparticles. Moreover, some of them can cross-link with the other particles,

even if they are prepared as diluted solutions. Average diameter is recorded as about 95 nm for each sample as indication of their reasonable size distribution. Standard deviation study for cross-linked SPB nanoparticles results to 5.50 for size and 0.033 for PDI which indicates the reproducibility of these particles.

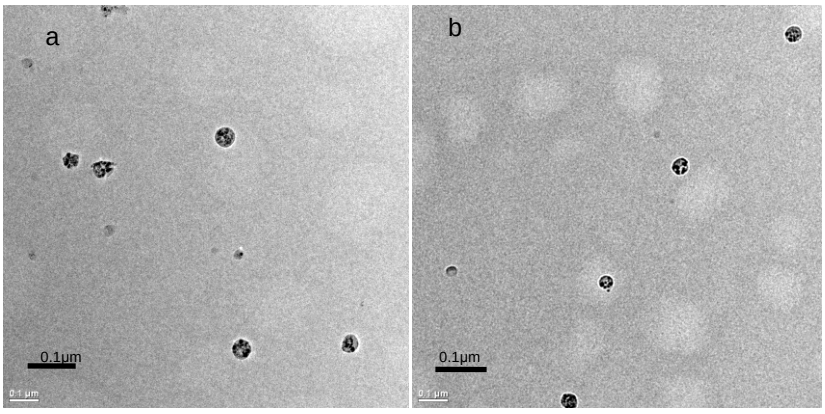

Figure 2.21: TEM data of SPB nanoparticles at 0.1 µm scale. a. before cross link, b after cross link.

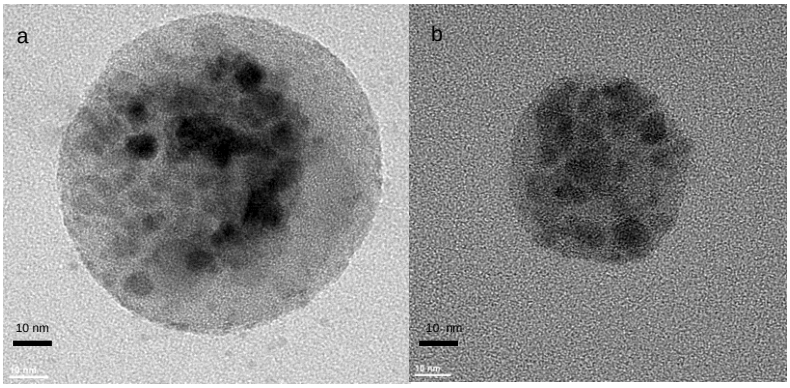

Figure 2.22: TEM data of SPB nanoparticles at 10 nm scale. a. before cross link, b. after cross link.

TEM analyses of SPB nanoparticles clearly showed that 2+2 cycloaddition leads to the more compact nanoparticles. Most of them tend to become smaller in their size as described in Figure 2.21 and 4.22.

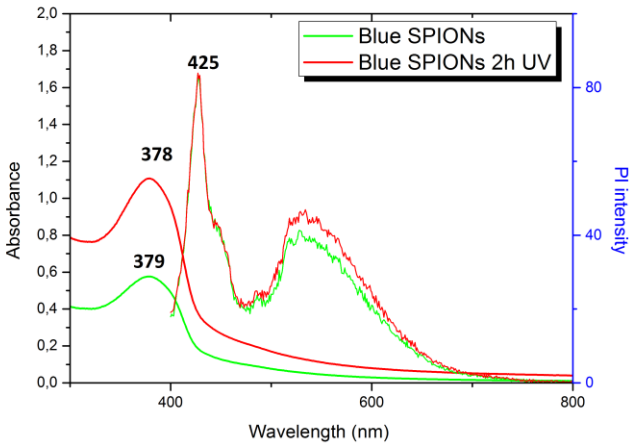

Figure 2.23: Optical data of the before cross-link and after cross-link SPB nanoparticles, λ_{excit}= 379 nm for SPB before cross-link, λ_{excit}= 378 nm for after cross-link

Absorption (378 and 379 nm) and fluorescence (425 nm) maxima of SPB nanoparticles are not changed after and before cross-linking studies as shown in figure 2.23. Another significant issue is quenching or photobleaching of the UV exposed SPIONs nanoparticles. Even if, loss in intensity is recorded after cross-linking, stability is preserved.

Figure 2.24 indicates the optical stability of cross-linked SPB nanoparticles are not affected by quenching or precipitation after leaving at room temperature for a month.

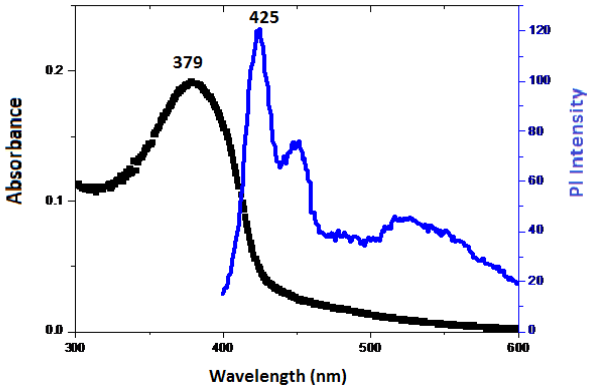

Figure 2.24: Absorbance and emission spectra of cross-linked SPB nanoparticles 30 days later (λ_{excit} = 379 nm).

2.3.2. Synthesis and Characterizations of Green Polymer (PG) SPIONs nanoparticles (SPG)

Hybridization of PG was performed with same concentration as the green polymer nanoparticles in that 2 mg of polymer was dissolved in 4 ml of THF, sonicated with 1 ml of SPIONs solution in THF and dropping into water led to synthesis of green SPIONs (SPG) nanoparticles as described in Scheme 2.10.

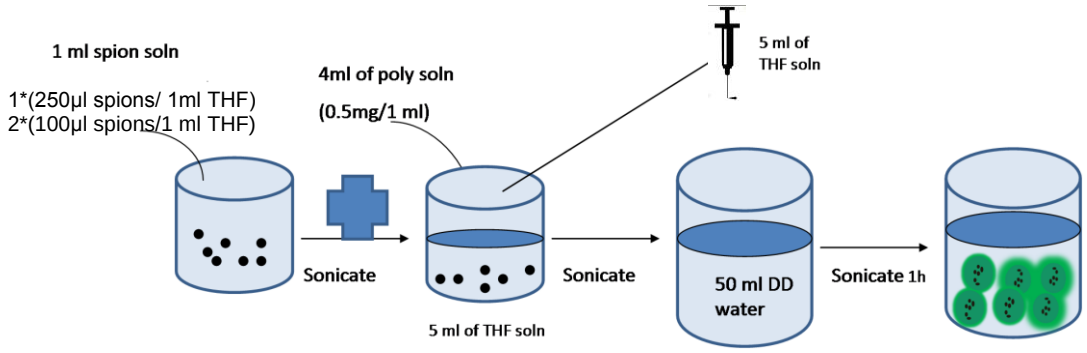

Scheme 2.10: Synthesis scheme of Green SPIONs (SPG)

Table 1 includes the polymer concentration optimizations study in terms of their size. Even though, increase in polymer concentration leads to increase in size of the particles, the smallest SPG nanoparticles were obtained from highest polymer concentration which is 0.4 mg/ml THF solution. The reason would be the interaction of PG with SPIONs. Coating ability of SPIONs is directly related to the size and PDI of these hybrid nanoparticles. Therefore, it can be concluded that best size characterizations results are obtained with 0.4 mg/ml polymer containing batch.

First syntheses of these SPG nanoparticles were prepared using 250 µl SPIONs stock solution and diluted with 1 ml of THF as in SPB preparation. However, PG differentiates from PB with its hexyl chains substituted with flourene unit. This fact decreases the hydrophobicity of PG, since it carries unsubstituted benzothiodiazole moiety. Decrease in hydrophobicity implies decrease in holding capacity of PG as a SPIONs matrix. Therefore, second preparation is carried out with 100 µl SPIONs stock solution and its effect was observed in terms of their size and morphology in Table 1 and Figure 2.25. SPG nanoparticles synthesized with 250 µl SPIONs (Figure 2.25a) tend to gather, also, their morphology and

surrounding ability by green polymer was less than 100 µl SPIONs containing SPG nanoparticles (Figure 2.25b). Additionally, DLS results introduced in table 2 approves the effect of SPIONs concentration on size that smaller particles are obtained from 100 µl SPIONs involved synthesis.

Table 1. Polymer concentration optimization

250µl SPIONs/ 1ml THF	Size	PDI
0.5 mg PG / 5 ml THF	86.14	0.154
1 mg PG / 5 ml THF	148.6	0.239
2 mg PG / 5 ml THF	73.67	0.101

Table 2. SPIONs concentration optimization

	250 µl SPIONs solution	100 µl SPIONs solution
SPG Nanoparticles Size	73.67	46.97

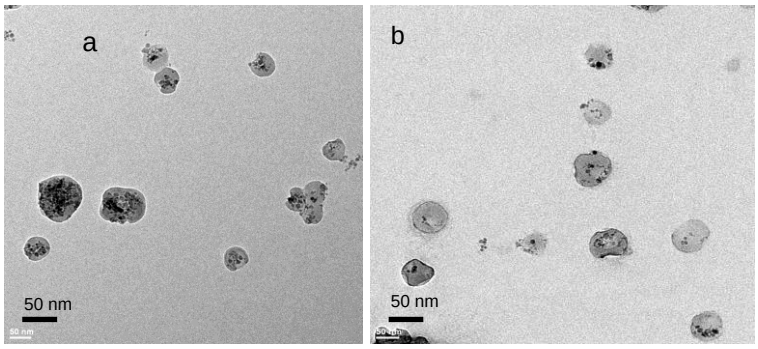

Figure 2.25: TEM image of a. 250 µl SPIONs containing SPG nanoparticles, b. 100 µl SPIONs containing SPG nanoparticles.

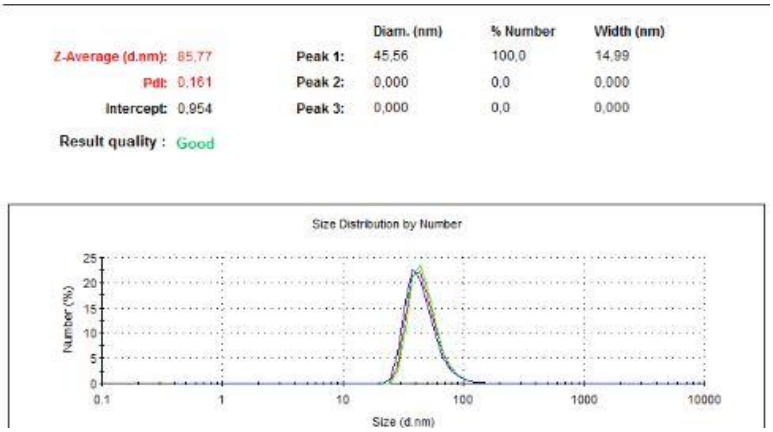

Figure 2.26: Size distribution of the SPG nanoparticles by number

Figure 2.26 is DLS data belong to the SPG nanoparticles containing 2 mg PG and 100 µl SPIONs solution. Size is 45.56 and PDI is 0.161 which are consistent with the expectation as monodisperse and small in their size.

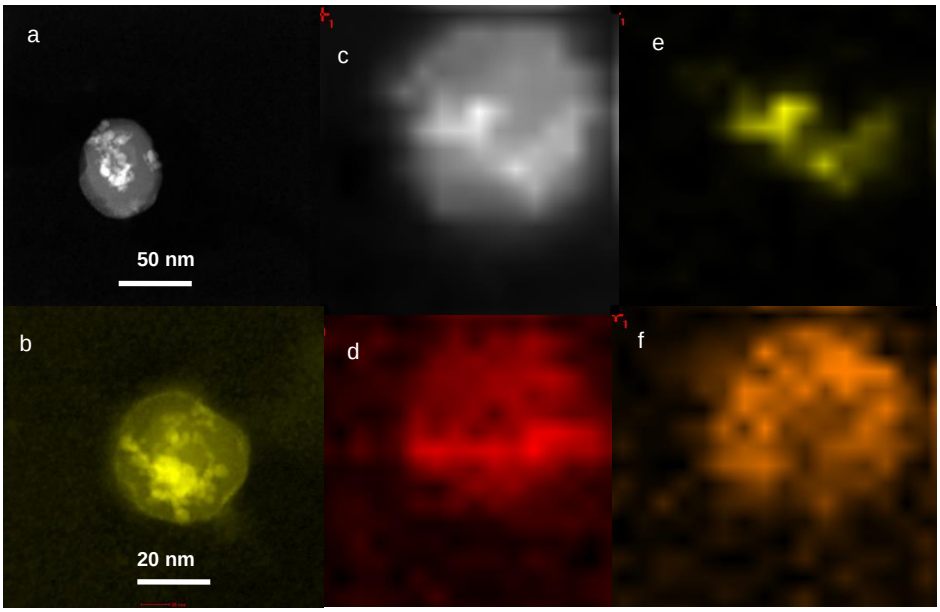

Figure 2.27: EDAX map of SPG nanoparticles, a: STEM (50 nm) , b: yellow contrast (20 nm), c: zoom in image , d: Nitrogen labeled, e: Iron labeled, f: Sulfur labeled.

Energy dispersive X-Ray analysis (EDAX or EDX) corresponds to the elemental analysis in TEM or SEM imaging studies. This analysis indicates the presence of PG and iron inside of polymer nanoparticles. In figure 2.27, EDAX map and scanning transmission electron microscope (STEM) images are given. From STEM images (figure 2.27a and b), iron contrast is visible inside of these nanoparticles. Figure 2.27; c-f, are related to the mapping of the nanoparticles, d and f denotes elements which are sulfur and nitrogen spilled all over the polymer nanoparticle. Image e is iron labeling merely exhibited in the middle of this nanoparticle.

Cross-linking Study of SPG Nanoparticles

2 ml SPG nanoparticles solution was diluted with 10 ml of distilled water and left for 4 h under UV-light to achieve [2+2]-cycloaddition. SPG nanoparticles are left 2 h UV light (273 nm) same as SPB nanoparticles, however it was found that they dissolved in THF and lost their shape and morphology. Differences in the nature of the polymers such as their structural properties are effective on cross-linking density of these nanoparticles.

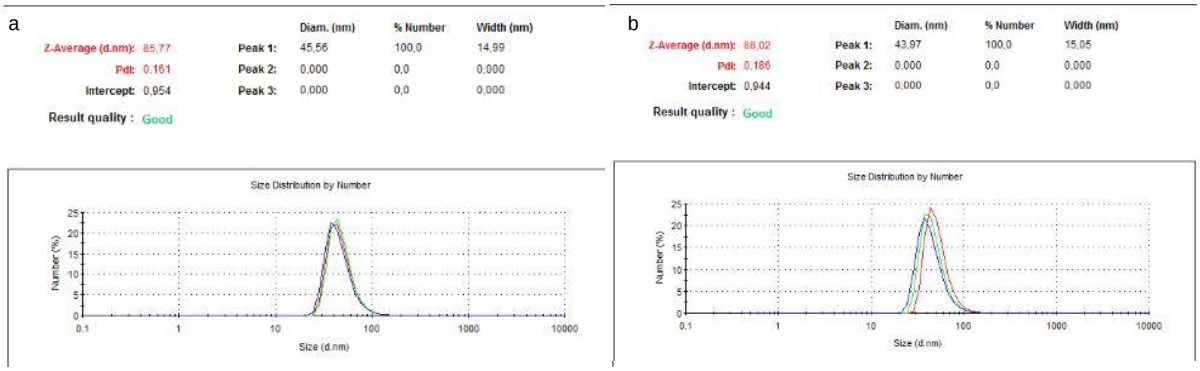

Figure 2.28: DLS results for SPG nanoparticles a. before cross-link, b. after cross-link

DLS data supports the cross-linking which leads to decrease in the size of SPG nanoparticles from 45.56 nm to 43.97 nm as shown in figure 2.28. Moreover, PDI value increases from 0.161 to 0.186. This small change is attributable to the variable cross-linking density of the nanoparticles. Additionally, some particles can result in inter-particle cross-linking rather than intra-particle cross-linking. However, 0.025 change in PDI is reasonable for cross-linking studies. Standard deviation calculations, which are done out of three synthesis, are recorded as 4.10 for size and 0.015 for PDI measurements. These results indicate the reproducibility of cross-linked SPG nanoparticles.

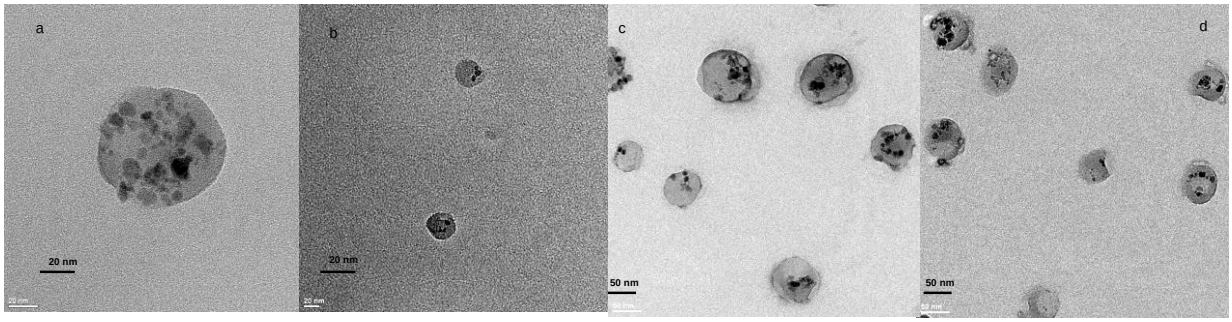

Figure 2.29: TEM image of the SPG nanoparticles; a and c. before cross-link, b and d. after cross-link

TEM study before and after cross-linking of SPG nanoparticles are performed in order to observe change in their morphology. Decrease in their size about couple of nanometers was confirmed by DLS results. TEM implies that before cross-linking, nanoparticles were about 50 nm and afterwards it decreases to about 40-45 nm in general as described in figure 2.29. More compact morphology of the cross-linked material is confirmed by TEM analysis as well.

The most significant indication of the cross-linking of nanoparticles is the preservation of their shape in organic solvent as well. SPG nanoparticles are left 2 hours more than SPB nanoparticles in order to accomplish high cross-linking density. Since, it is observed that 2 hours cross-linked SPG nanoparticles have a tendency to destroy their shape in THF as it is observed in Figure 2.30a,b.

THF dispersed cross-linked (4h UV irradiation) blank nanoparticles of PG were also studied as control experiments. They were prepared with the same method as SPG cross-linked nanoparticles. 2.5 ml of PG nanoparticle aqueous solution was diluted with 10 ml of distilled water and left for 4 hour UV (273 nm) irradiation. Water was evaporated under reduced pressure and resulting PG nanoparticles were redispersed in THF. Their TEM images were provided in appendix, Figure A.2. Results of THF dispersed PG nanoparticles showed that cross-linked nanoparticles preserve their morphology in organic solvent as well.

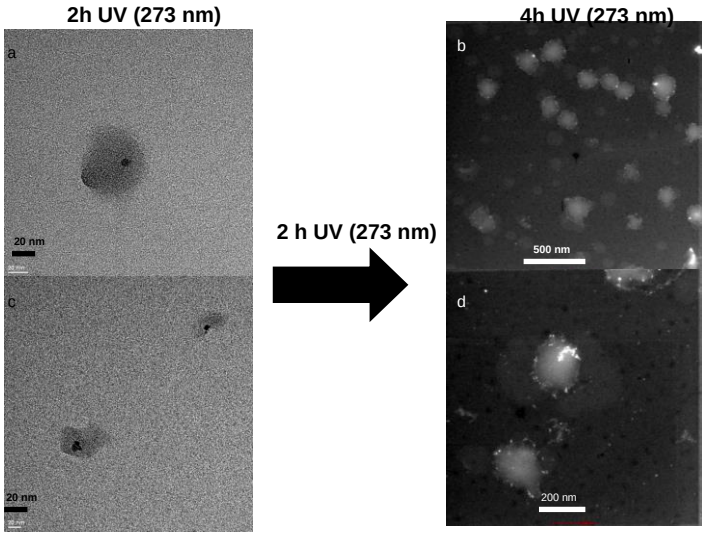

Figure 2.30: TEM image of the THF dispersed cross-linked SPG nanoparticles, a and c; 2 h UV exposed and THF dispersed SPG nanoparticles, b and d; 4 h UV exposed and THF dispersed SPG nanoparticles (STEM images).

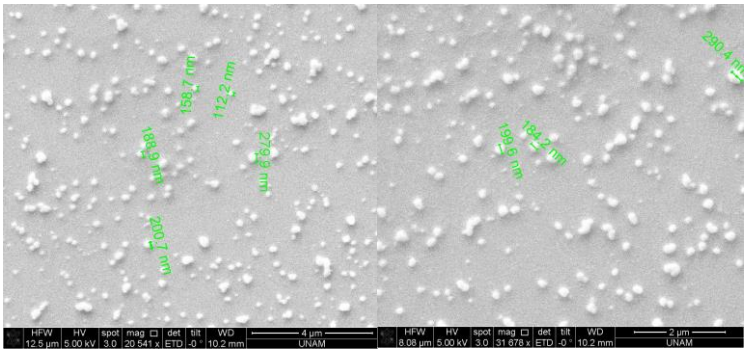

Figure 2.31: SEM image of cross-linked SPG nanoparticles dispersed in THF.

SEM image of THF dispersed SPG nanoparticles highlights the size of these particles and their morphology in detail (figure 2.31). Silicon substrates utilized in SEM imaging are more resistant to organic solvents than TEM grid. Therefore, it is easier to obtain better image for THF dispersed particles in SEM. THF can dissolve organic residues on TEM grid and prevent successful imaging. In SEM, abundance of the nanoparticles are in the range of 100-200 nanometers which are considerable results for an organic solvent. It is expected to swell and extend their size. The target is not to dissolve completely and lead to no aggregation or no film formation on the substrates.

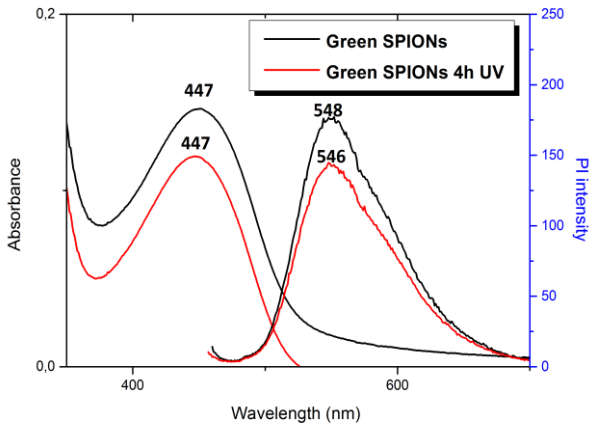

Figure 2.32: Absorbance and fluorescence spectra of SPG (Green SPIONs) before and after cross-linked. (λ_{excit}= 447 nm).

Green emitting SPG nanoparticles absorption maxima is determined as 447 nm and excitation with this wavelength emits at around 546 nm and 548 nm for after cross-linked and before cross-linked nanoparticles respectively (Figure 2.32). Intensities of before and after cross-link SPG nanoparticles are close to each other which means 4 hours high energy UV radiation exposure does not lead to any quenching in these nanoparticles. They maintain their optical properties.

SPG nanoparticles optical properties were investigated after 1 month in order to check their stability in terms of any photobleaching. In Figure 2.33, it is clearly seen that nanoparticles still emits light in the same region and intensity. Moreover, these nanoparticles were kept at room temperature for 1 month and no precipitation occurred after this time period.

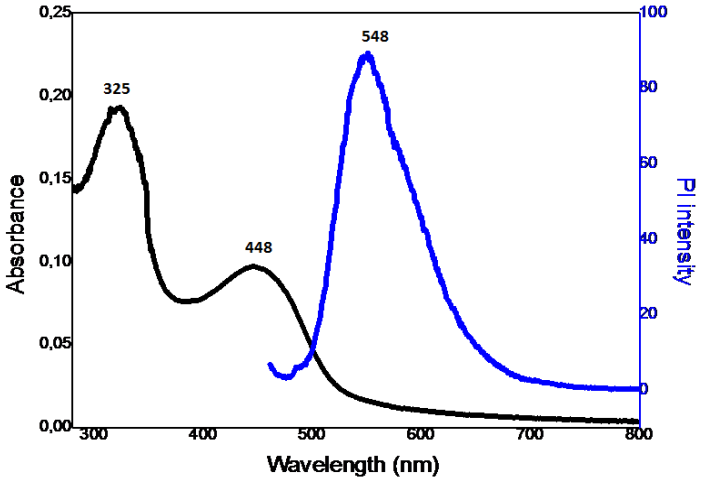

Figure 2.33: Absorbance and fluorescence spectra of cross-linked SPG 30 days later (λ_{excit} = 448 nm)

2.3.3. Synthesis and Characterizations of Red Polymer (P2) and SPIONs nanoparticles (SP2)

Hybridization of SPIONs with P2 polymer was carried out with the same methods as previously explained as reprecipitation method in Scheme 2.11. Owing to the hydrophobic polymer chains (P2), nanoparticles were generated as SP2. 0.25 mg of P2 was dissolved in 1 ml of THF and Sonicated with SPIONs dissolved in 1 ml of THF. This mixture was added at once in 20 ml of distilled water with a syringe. Formation of these nanoparticles was characterized with DLS and TEM. Their optical characterizations were done via UV-Vis and fluorescence spectroscopy.

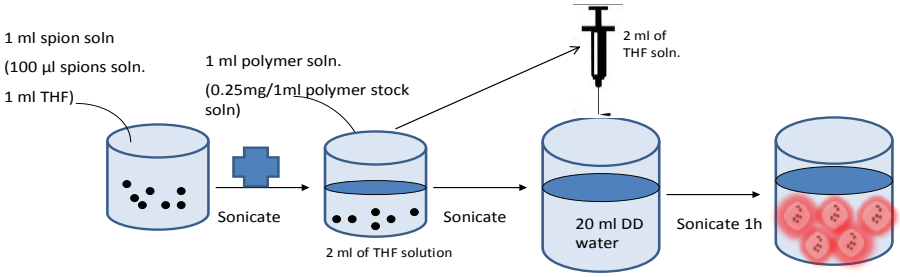

Scheme 2.11: Preparation scheme of SP2 nanoparticles

DLS data of SP2 nanoparticles reveals that the size is 56.31 nm and PDI is 0.211. Especially, hybrid synthesized nanoparticles tends to have larger size[72]. In our

case less than 100 nm (56.31) was synthesized with reprecipitation method. Standard deviations calculations were done out of three measurements and obtained as 2.23 for size and 0.028 for PDI which indicate that results are quite reproducible.

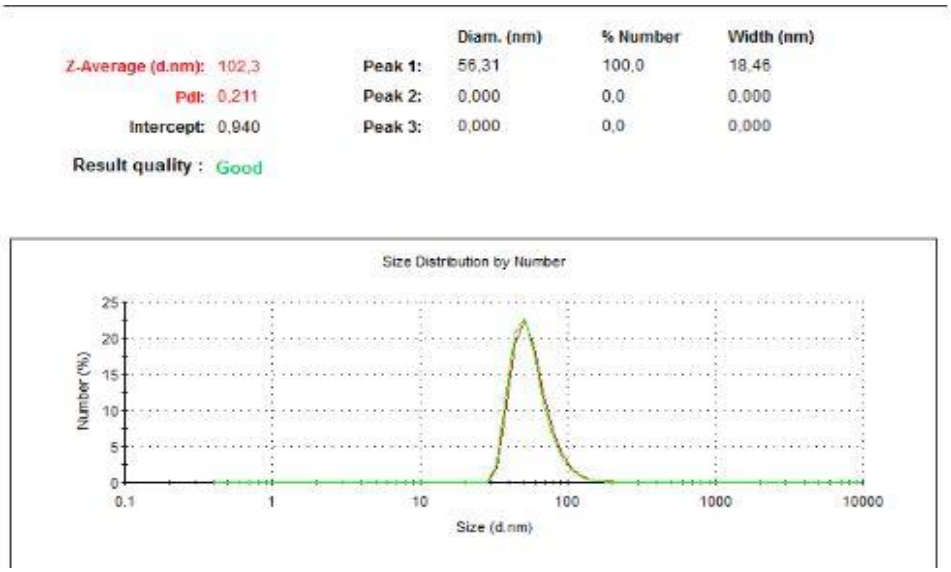

Figure 2.34: Size distribution of SP2 nanoparticles by number

TEM images of SP2 are consistent with the DLS data of these nanoparticles that they both point out the size of these nanoparticles to be about 50 nm. Furthermore, SPIONs were capped by P2 polymer chains and no free SPIONs were observed on the grid, even if 0.25 mg polymer was utilized for these synthesis. However, these syntheses can be optimized with less SPIONs usage for each batch in order to provide better encapsulations of SPIONs.

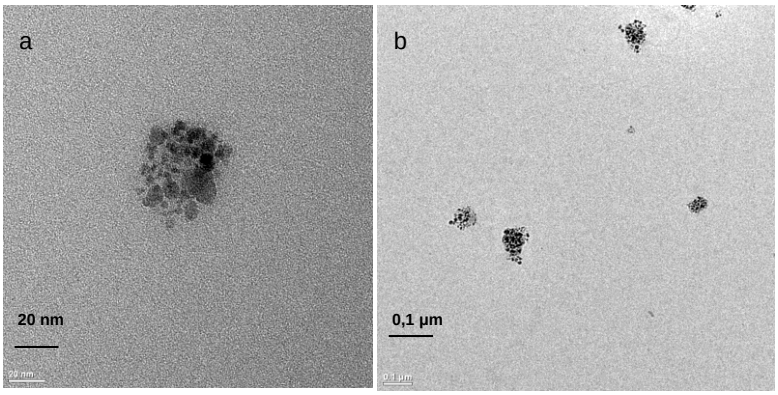

Figure 2.35: TEM data of SP2 nanoparticles, a; 20 nm scale, b; 0,1 µm scale bars.

Cross-linking Study of SP2 Nanoparticles

Cross-linking of SP2 nanoparticles were accomplished with 2 hours UV light (273 nm) by diluting 2.5 ml of stock solution with 10 ml of distilled water. One of the most important indications was decrease in their size after UV exposure.

DLS data exhibited in Figure 2.36 supports this assumption as dramatic decrease in size from 56.31 to 49.11 nm was ascertained. PDI increase was expected due to the differences in cross-linking density in each particle. In this case, PDI increased from 0.211 to 0.241.

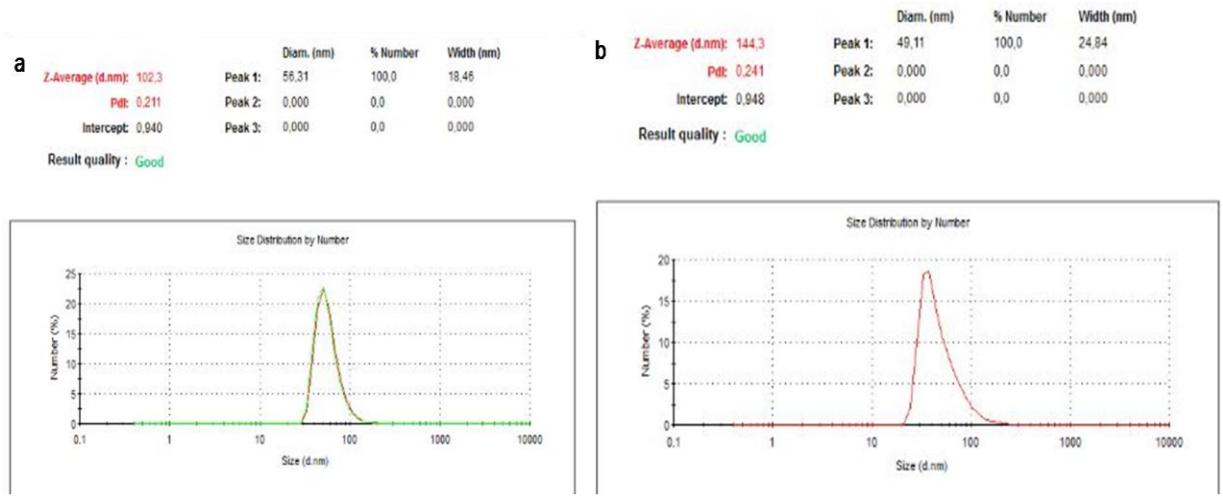

Figure 2.36: Size distribution of SP2 nanoparticles by number, a; before cross-link, b; after cross-link

When TEM images of the before and after cross-linked nanoparticles are compared, shrinkage of the cross-linked nanoparticles can be observed easily (Figure 2.37ab). Other morphological change was the more compact structure of the nanoparticles as shown in Figure 2.37. This is attributable to the UV assisted [2+2]-cycloaddition. Another general trend was the generation of the layer by layer polymer surrounding in these hybrid nanoparticle after cross-linking.

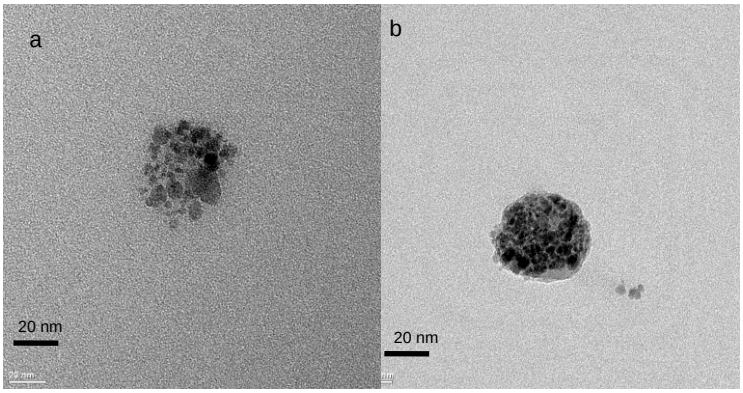

Figure 2.37: TEM image of SP2 nanoparticles, a; before cross-link, b; after cross-link

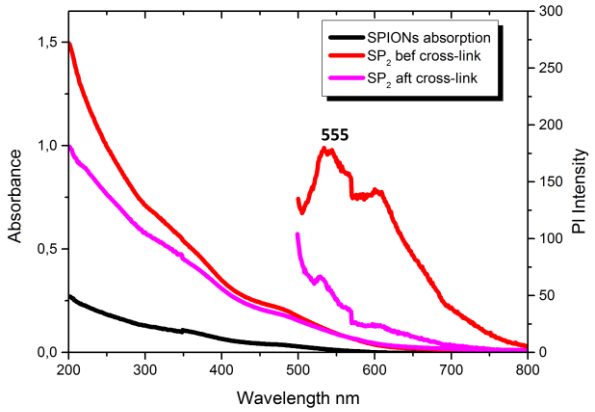

Figure 2.38: Optical data of SP2 nanoparticles, (λ_{excit}= 450 nm for both after and before cross-link SP2 nanoparticles).

Figure 2.38 indicates that SP2 nanoparticles loss their optical property mostly after hybridization with SPIONs. Their absorbance data is overlapping with the SPIONs absorption itself. In other words, SPIONs are dominating SP2 nanoparticles absorption. In order to determine excitation wavelength, the absorption maxima of P2 nanoparticles is evaluated. Decrease in the polymer amount for SP2 hybrid nanoparticles can prevent optical quenching or decrease the interaction of SPIONs with polymer by coating with another layer[72] such as PEG, which can enhance the optical properties of these nanoparticles.

2.4 Characterizations of Super-paramagnetic Iron Oxide Nanoparticles (SPIONs)

SPIONs were obtained as coated with lauric acid in the form of nanoparticles by our collaborator, Koç University. SPIONs have magnetic property due to its nature. Therefore, they can easily agglomerate. In order to overcome this obstacle, SPIONs were coated with lauric acid. The size of SPIONs was characterized with DLS. Lauric acid content of the SPIONs was determined with Thermal Gravimetric Analysis (TGA) studies. Moreover, Fe^{+3} amount is examined for relaxivity experiments and were done with Inductively Coupled Plasma Mass Spectrometry (ICP-MS).

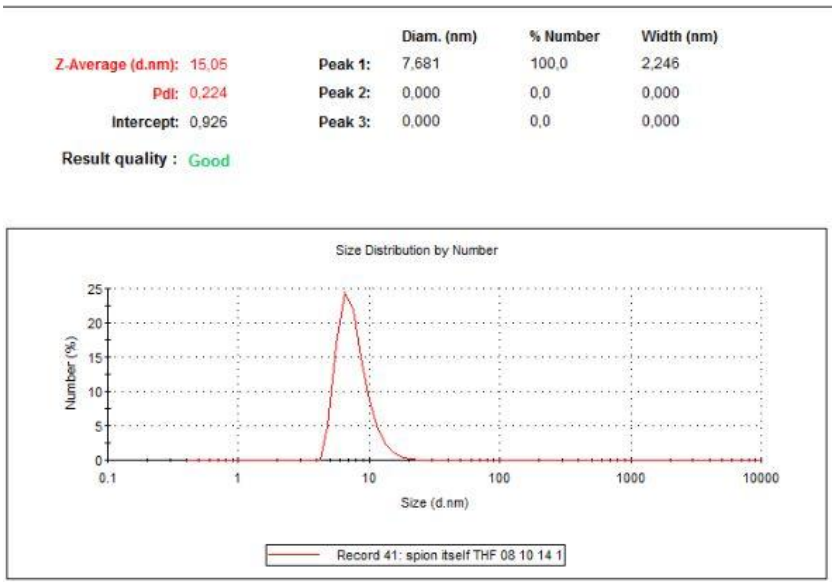

Figure 2.39 : Size distribution of SPIONs by number

It was shown that the size of the SPIONs is about 8 nm. Average size was acceptable and recorded as 15 nm. SPIONs solution was kept in toluene, but DLS results were taken in THF.

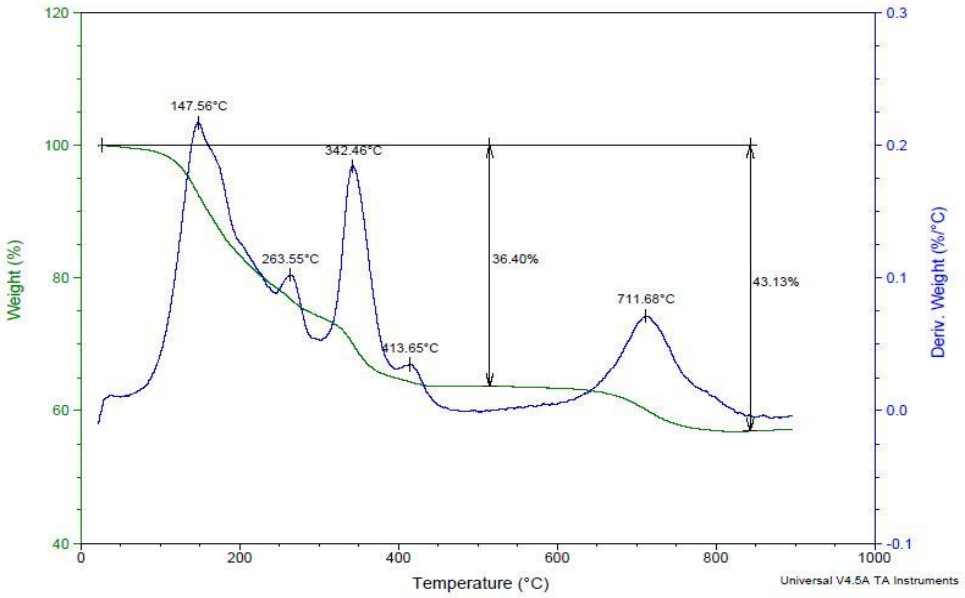

Figure 2.40 : Thermal Gravimetric Analysis of SPIONs

	Green SPIONs (SPG)	Green SPIONs After Cross-link	Blue SPIONs (SPB)	Blue SPIONs After Cross-link
Fe_3O_4 concentration	0.01 mg/ 1 ml	0.002 mg/1 ml	0.025 mg/1 ml	0.005 mg/1 ml

Table 3: Iron-oxide concentration in hybrid nanoparticles

Thermal Gravimetric Analysis (TGA) is based on the thermal decomposition of the material. Complex samples can be deduced in terms of their weight loss because of increasing temperature. Lauric acid percentage was determined due to the weight loss of the sample up to 800 ° C. As it is labeled in Figure 2.40, % 43.13 weight loss indicates the lauric acid content of the sample. In the light of TGA data, table 3 is generated. Fe_3O_4 content of each hybrid material is given by table 3.

ICP-MS results, which were done by Koç University, revealed that raw SPIONs solution contains 5.4 mg Fe^{3+} per 1 ml.

2.5 Relaxivity Results of Nanoparticles

SPIONs are negative contrast agents which mean that they are shortening T_2 (transverse) relaxation time of the neighboring protons. T_2 relaxation time defines the relaxation of the nuclei to its low energy state due to the dephasing of the

spins [40]. Mainly, SPIONs are utilized to generate darkening in iron oxide loaded tissues. The studies about the efficiency of the SPIONs are attributable with the relaxation time of them at certain concentration, since high concentrations of the SPIONs can result in agglomeration in the blood. In order to prevent toxicity, dose reduction in the injected magnetite amount is requirement. Therefore, the aim is to be able to obtain signal at lowest concentrations as possible.

Lauric acid coated SPIONs were hybridized with conjugated polymers (PG, PB, P2) to provide them dual imaging opportunities and water solubility. Besides, solubility and mutifunctionality, coating with conjugated polymers can affect the MRI contrast capability of the SPIONs. One of the signs indicating enhancement in MRI contrast is the relaxivity of the SPIONs before and after hybridization with conjugated polymers. It is reported that three parameters should be referred for engineered iron oxide nanoparticles with polymer scaffolds: their composition, surface and size properties [79].

Conjugated polymers utilized in this work caries same functional group, but different repeating units in their backbone (scheme 2.1). Therefore, it is considered that chemical structure of these polymers can change the surface and the size of the nanoparticles. Hybrid nanoparticles generated in our work consist of multi-core SPIONs, not a single core. However, Discussions on the relation between size of the SPIONs and relaxivity mainly evaluates the single core SPIONs [79]. In the light of these explanations, primary effect of the usage of different conjugated polymers on relaxivity would be the change on the surface of the nanoparticles.

Relaxivities of raw SPIONs and Hybrid nanoparticles (SPB, SPG before and after cross-link) were examined UMRAM, Dr. Sarıtas and Utkur. Transverse relaxation rate (T_2) measurements were done with Siemens MAGNETOM Trio System under 3 Tesla [81].

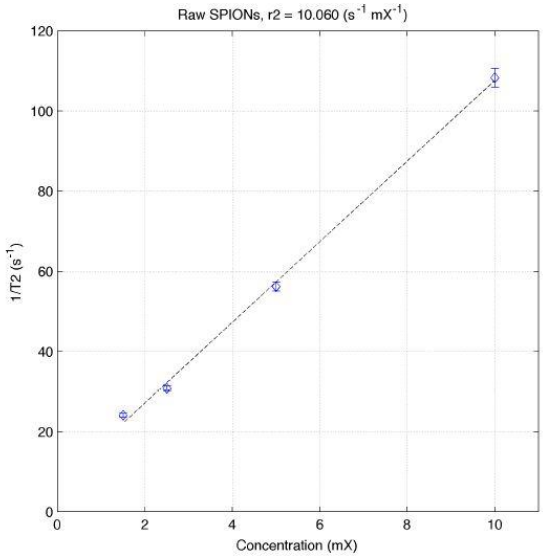

Figure 2.41: Relaxivity of non hybridized SPIONs

Raw SPIONs, which are merely coated with lauric acid, is diluted as 1000 fold and donated as 1 mX. T_2 relaxation time is expressed with r_2 value which defines the transverse relaxivity with respect to the concentration of Fe^{3+}. r_2 value is the slope of the $1/T_2$ versus concentration graph (Figure 2.41). Fe^{3+} concentration of SPIONs coated with lauric acid was found as 5.4 mg/ml (0.096 M) from ICP results. When r_2 (s^{-1} mX^{-1}) was divided by 0.096 M, r_2 was calculated as 103.41 s^{-1} mM^{-1} .

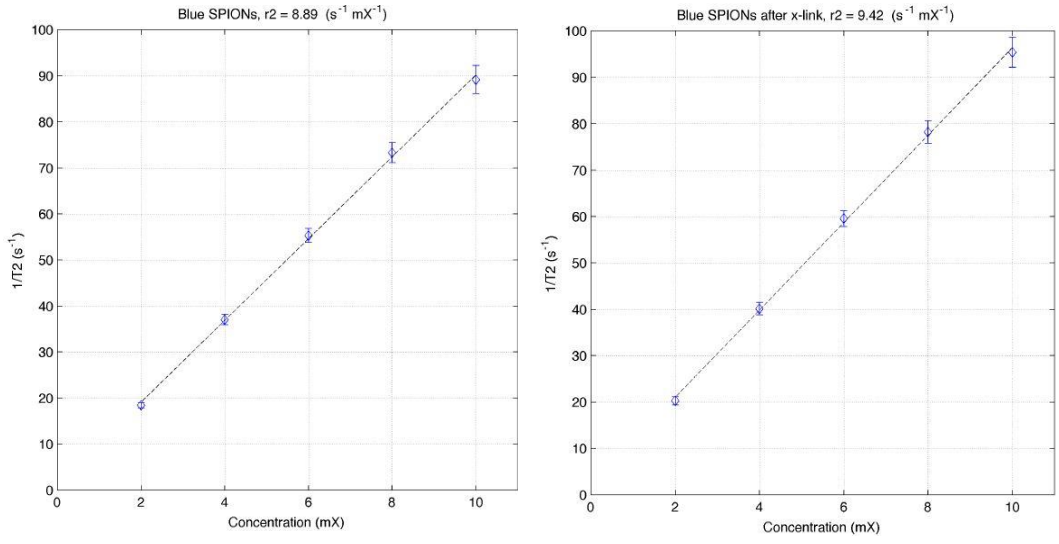

Figure 2.42: Relaxivity of Blue SPIONs (SPB), relaxivity of Blue SPIONs (SPB) after cross-link (from left to right)

In figure 2.42, r_2 values were measured as 8.89 and 9.42 s^{-1} mX^{-1} for Blue SPIONs and Blue SPIONs after cross-link, respectively. Their concentrations were calculated due to the starting raw SPIONs solution. Since, hybrid nanoparticle synthesis with Blue polymer (SPB) was carried out with the certain SPIONs amount (Scheme 2.9). 0.25 ml from raw SPIONs solution was taken and injected into the 50 ml of Milli-Q water. 5 fold dilutions from original concentration were prepared and decrease in relaxation time (T_2) was observed due to the increase in magnetite concentration (Figure 2.42). r_2 values calculations were done with dividing it by raw SPIONs molarity and found as 91.93 s^{-1} mM^{-1} for Blue SPIONs and 97.41 s^{-1} mM^{-1} for Blue SPIONs after cross-link samples. It indicates that relaxivity was decreased by 12 s^{-1} mX^{-1} for Blue SPIONs comparing with raw SPIONs. It can be concluded that encapsulated SPIONs by Blue Polymer preserves their MRI contrast efficiency. Cross-linked nanoparticles indicates ~ 6% enhancement which means their relaxivity did not expose to significant change by this UV-irradiated reaction.

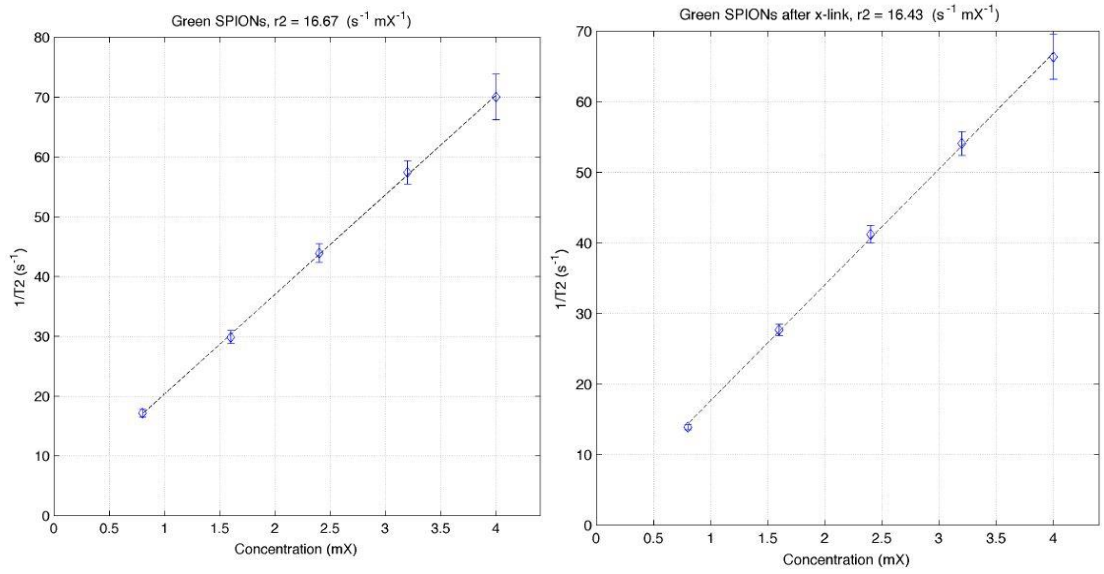

Figure 2.43: Relaxivity of Green SPIONs (SPG), relaxivity of Green SPIONs (SPG) after cross-link (from left to right)

SPG nanoparticles before and after cross-link r_2 values were consistent with each other with the values 16.67 and 16.43 s^{-1} mX^{-1}, respectively. When these values

were divided by 0.096 M (original raw SPIONs iron (III) concentration), it was found that r_2 values were 173.64 s^{-1} mM^{-1} for Green SPIONs (SPG) and 169.90 64 s^{-1} mM^{-1} for Green SPIONs (SPG) after cross-link. When raw SPIONs and Blue SPIONs relativities are taken into consideration, significant enhancement can be easily noticed in Green SPIONs. The reason of this enhancement can be regarded as the benzothiadiazole moiety in Green Polymer (PG). Since, surface of the nanoparticles was composed of different polymers; one is only flourene and the other is flourene and benzothiadiazole. Sulfur and nitrogen atoms in Green polymer (PG) can effect the interaction between residing water molecules and iron oxide nanoparticles.

Chapter 3

Experimental

3.1 General

Reagents used in the synthesis of monomers and polymers were purchased from Sigma Aldrich Chemical Co. and utilized directly. Column chromatography performed in Synthesis of 2-(2,5-dibromothiophen-3-yl)ethanol was packed with silica gel (Kiegesel 60, 0.063-0.200 nm). Monomer was monitored with TLC (Thin Layer Chromatography, Kieselgel 60 F254, 1mm) which was silica gel plates. Monomer 2-(2,5-dibromothiophen-3-yl)ethyl acetate was characterized in terms of its mass with TOF LC/MS (time of flight liquid chromatography mass spectroscopy, Agilent 1200/6210). Structural characterizations of monomer and polymers were done via NMR (nuclear magnetic resonance, Bruker Avance III 400 MHz spectrometer) and FT-IR (Fourier Transform Infrared Spectroscopy, Bruker Tensor 27). The solvent used in NMR was $CDCl_3$ –d. KBr pallets were prepared for FT-IR measurements. The data was scanned 64 times and collected at 25^oC by adjusting the range as 4000 cm^{-1}- 400 cm^{-1} with the resolution set as 4 cm^{-1} . Optical characterizations were carried out with UV-Vis spectrophotometer and Fluorescence spectrophotometer with the software run as Cary UV-Vis and Cary Eclipse respectively. The sizes of nanoparticles were detected with DLS measurements (dynamic light scattering, Zetasizer Nano-ZS) has the monochromatic light source, laser, at 663 nm. In order to produce reliable data, DLS measurements were repeated for three times and average data was taken. SEM (scanning electron microscope, Quanta 200 FEG) and TEM (transmission electron microscope, FEI Tecnai G2 F30) were devices that identify morphological characterizations of these nanoparticles.

3.2. Synthesis of Monomers and Polymers

3.2.1. Synthesis of 2-(2,5-dibromothiophen-3-yl)ethanol (M1)

N-Bromosuccinimide (NBS) (4.35 g, 0.0244 mol) was dissolved in 40 ml of degassed ethyl acetate, which was bubbled with nitrogen for 15 minutes, by sonicating it for 10 minutes. It was expected not to observe any white precipitate in the flask. Freeze-pump-thaw was utilized as two cycles to this mixture. 2-(thiophene-3-yl)ethanol (1.161 g, 9.070 mmol) was added under nitrogen. The mixture was left at room temperature stirring overnight by covering the surface of the flask with aluminum foil. Work-up was performed by washing resulting yellowish-brownish reaction mixture with brine solution (30 ml) and Milli-Q water (30 ml) following. Ethyl acetate was evaporated under reduced pressure. Viscous yellowish liquid was obtained in the flask. Silica packed column chromatography was run with cyclohexane as an eluent. Product was dried under vacuum and overall yield was 60%. ^{1}H-NMR (400 MHz, $CDCl_3$, 25^{o} C) δ ppm: 6.88 (s, 2H), 3.80 (t, 2H), 2.80 (t, 2H) .^{13}C-NMR (400 MHz, $CDCl_3$, 25^{o} C) δ ppm: 139.1, 131.2, 111.5, 109.1, 62.3, 33.7

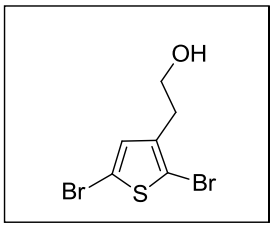

Scheme 3.1: 2-(2,5-dibromothiophen-3-yl)ethanol (M_1)

3.2.2. Synthesis of 2-(2,5-dibromothiophen-3-yl)ethyl acetate (M2)

2-(2,5-dibromothiophen-3-yl)ethanol (0.5 g, 1.8 mmol) was mixed with pyridine (180 µl, 2.30 mol) and acetic anhydride (5 ml). Reaction mixture was left at room temperature overnight stirring. In order to carry out extraction process, reaction mixture was diluted with DCM (25 ml). Then, extraction was done with (2x40 ml) water. Silica filtration was applied to obtain colorless solution. Resulting organic solution was concentrated under reduced pressure (10 ml) and stirred with methanol for 2 hours. Solvent was evaporated under reduced pressure and viscous

light green liquid was dried under vacuum and obtained with 98% yield. ^{1}H-NMR (400 MHz, $CDCl_3$, 25^{o} C) δ ppm: 6.88 (s, 2H), 4.21 (t, 2H), 2.87 (t, 2H), 2.07 (s, 3H) .TOF-MS: $[M+K^{+}]^{-2}$ m/z: 364.79839

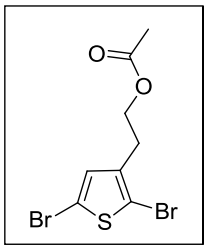

Scheme 3.2: 2-(2,5-dibromothiophen-3-yl)ethyl acetate (M2)

3.2.3. Synthesis of Poly[2-{ethyl acetate}(thiophene-2,5-diyl)-co-(5,5'-{2,2'}-bithiophene)] (P1)

2-(2,5-dibromothiophen-3-yl)ethyl acetate (0.836 g, 2.54 mmol) (M1) and 5,5'bwas(tributylstannyl)-2,2'-bithiophene (1.90 g, 2.54 mmol) were mixed in a round bottom flask and dried under vacuum. Solvents -degassed with nitrogen- (20 ml) THF and (20 ml) toluene were added and stirred under nitrogen. 2 cycle freeze-pump-thaw technique was applied in order to get rid of free oxygen. Catalyst, $Pd(PPh_3)_4$ (tetrakis triphenylphosphine palladium) was added as (0.146 g, 0.13 mmol) by dissolving in degassed THF under nitrogen. Reaction was left stirring at 85 ^{o}C for two days and 55 ^{o}C for two more days. Yellowish reaction mixture was obtained as dark brown-red viscous liquid at the end of four days. Solvent was evaporated under reduced pressure and washed with water, n-hexane and methanol, respectively in order to get rid of oligomeric species and catalyst. Dark red solid residue was dried under vacuum and the yield was 60 % . ^{1}H-NMR (400 MHz, $CDCl_3$, 25^{o} C), δ ppm: 7.11 (m, 5H), 4.34 (m, 2H), 3.12 (M, 2H), 2.07 (s, 3H) .^{13}C-NMR (100 MHz, $CDCl_3$, 25^{o} C) δ ppm: 170.2, 137.2, 131.3, 124.2, 124.5, 123.6, 121.7, 63.2, 27.4, 20.7 .FT-IR (KBr, pellet, $\nu_{max}(cm^{-1})$): 1750 (C=O,s) , 2950 (C-H, m), 3100 (C-H, s)

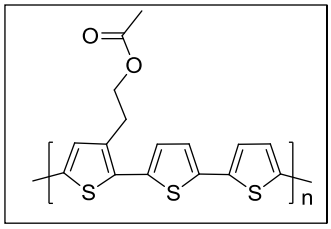

Scheme 3.3: Poly[2-{ethyl acetate}(thiophene-2,5-diyl)-co-(5,5'-{2,2'}-bithiophene)]

3.2.4. Synthesis of Ploy[3-{(allyloxy)ethyl}(thiophene 2,5-diyl)-co-(5,5'-{2,2'}-bithiophene)] (P2)

0.150 g P_1 was mixed with 4 ml of allyl bromide (in excess) and 0.5 g KOH (in excess). They were left for overnight stirring at room temperature by adding catalytic amount tetrabutyl ammonium iodide (TBAI) which is a phase transfer catalyst. Work-up procedure starts with diluting the reaction mixture with chloroform, then, extraction with water to purify it from excess KOH. Organic layer was evaporated under reduced pressure to evaporate allyl bromide and chloroform. After washing with methanol, it was dried under vacuum. Yield was 87 %. ^{1}H-NMR (400 MHz, $CDCl_3$, 25^o C) δ ppm: 7.11 (m, 5H), 5.95 (s, 1H), 5.34 (d, 1H), 5.21 (d, 1H), 4.05 (m, 2H), 3.71 (m, 2H), 3.10 (m, 2H) .FT-IR (KBr, pellet, ν(cm^{-1})) : 2950 (C-H, m), 3100 (C-H, s)

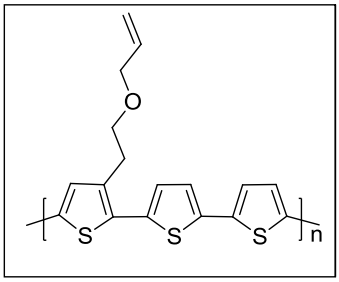

Scheme 3.4: Poly[3-{(allyloxy)ethyl}(thiophene 2,5-diyl)-co-(5,5'-{2,2'}-bithiophene)] (P_2)

Other Attempts for Synthesis of Poly[3-{(allyloxy)ethyl}(thiophene 2,5-diyl)-co-(5,5'-{2,2'}-bithiophene)] (P2)

Route 1

This route was based on the synthesis of M3 and polymerization of M3 under Stille Coupling reaction.

Synthesis of 3-(2-(allyloxy)ethyl)-2,5-dibromothiophene (M3)

It was synthesized from (0.7 g ,2.44 mmol) M1 mixing with (0.824 ml ,9.76 mmol) allyl bromide and (0.275 g ,4.88 mmol) of KOH. Reagents was left for stirring by adding catalytic amount of phase transfer catalyst tetrabutyl ammonium iodide (TBAI) 5 hours at room temperature. Reaction was monitored with Thin Layer Chromatography (TLC). R_f values were 0.88 and 0.42 for M3 and M1 respectively in a solvent system 5 ml ethyl acetate and 5 ml cyclohexane. Reaction mixture was purified with water chloroform extraction and evaporation of allyl bromide with solvents under reduced pressure. Yield was 55 %. ^{1}H-NMR (400 MHz, $CDCl_3$, 25^o C) δ ppm: 6.91 (s, 1H), 5.89 (m, 1H), 5.41 (d, 1H), 5.21 (d, 1H), 4.05 (m, 2H), 3.65 (m, 2H), 2.86 (m, 2H) .^{13}C-NMR (400 MHz, $CDCl_3$, 25^o C) δ ppm: 140.8, 134.5, 131.2, 126.9, 109.1, 72.1, 68.2, 30.3

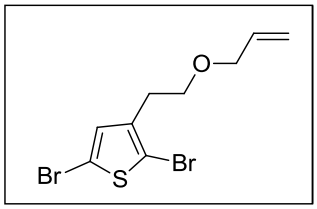

Scheme 3.5: 3-(2-(allyloxy)ethyl)-2,5-dibromothiophene (M_3)

Synthesis of Ploy[3-{(allyloxy)ethyl}(thiophene 2,5-diyl)-co-(5,5'-{2,2'}-bithiophene)] (P2)

Polymerization reaction of (0.3 g ,0.92 mmol) 3-(2-(allyloxy)ethyl)-2,5-dibromothiophene and (0.69 g, 0.92 mmol) 5,5'bwas(tributylstannyl)-2,2'-bithiophene was carried out in the presence of catalyst (0.053g ,0.046 mmol) $Pd(PPh_3)_4$ and solvents THF (10 ml) and toluene (10 ml). Solvents and reagents were mixed and 2 cycle freeze-thaw was utilized. Then, catalyst was added under

nitrogen and left for 4 days at 85ºC for 2 days and 55ºC for last 2 days. Work-up was performed by washing with water, N-hexane and methanol respectively. It was dried under vacuum. Yield was not calculated, since ^{1}H-NMR indicated that peaks were interfering with the oligomeric species and washing with methanol constantly reveal very low yield. ^{1}H-NMR (400 MHz, $CDCl_3$, 25º C) δ ppm: 7.08 (m, 5H), 6.42, 6.01, 5.48, 5.38, 5.21, 4.82, 4. 47, 4.22, 3.91, 3.75, 3.14, 2.61, 2.01

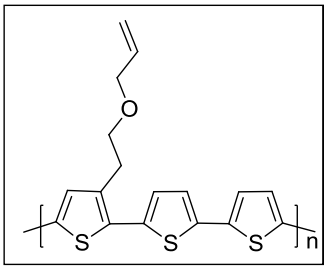

Scheme 3.6: Poly[3-{(allyloxy)ethyl}(thiophene 2,5-diyl)-co-(5,5'-{2,2'}-bithiophene)] (P_2)

Route 2

This route was based on the hydrolysis of P1 resulting the synthesis of P3 and substitution of P3 with allyl bromide.

Synthesis of Poly[2-{ethanol}(thiophene-2,5-diyl)-co-(5,5'-{2,2'}-bithiophene)] (P3)

0.607 g (1.825 mmol/1 equiv) P_1 and 0.205 (3.65 mmol/2 equiv) g KOH were dispersed in THF-water solvent mixture. They left for 2 days stirring at 55ºC. Work-up procedure was based on to get rid of excess KOH and acetic acid salts. First solvents were evaporated under reduced pressure. Then, it was washed with excess of water (300 ml). ^{1}H-NMR (400 MHz, $CDCl_3$, 25º C) δ ppm: 7.31 (m, 5H), 3.69 (m, 2H), 2.92 (m, 2H) .FT-IR (KBr, pellet, νmax(cm^{-1})) : 3300 (O-H ;s ,b), 3050 (C-H, s), 2850 (C-H, m)

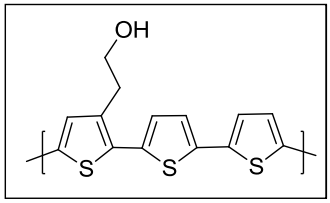

Scheme 3.7: Poly[2-{ethanol}(thiophene-2,5-diyl)-co-(5,5'-{2,2'}-bithiophene)]

Synthesis of Poly[3-{(allyloxy)ethyl}(thiophene 2,5-diyl)-co-(5,5'-{2,2'}-bithiophene)] (P2)

P3 (60 mg, $1.87x10^{-4}$ mol) was dissolved in 20 ml of dry THF. THF is degassed with freeze-thaw method before adding P3. NaH (0.2 g, excess) and P3 were left for 4 hours stirring. Allyl bromide (0.2 ml, excess) was added at 0 ^{o}C and left for 48 hours stirring. Work-up procedure was consisting of quenching of NaH with methanol and washing with water in order to get rid of salts. Solubility problems in organic solvent and NMR studies indicated that no functionalization occurred.

3.3. Synthesis and Characterization of Poly[(9,9-bis {3-dihexyl}fluorenyl-2,7-diyl)-co-(9,9-bis {3-diallyl)fluorenyl-2,7-diyl)] (PB) Nanoparticles

PB (1mg, $1.72x10^{-3}$ mmol) was dissolved in 1 ml of THF and eluted through a filter prepared with cotton filled Pasteur pipette. This polymer solution was injected to 50 ml of Milli-Q water rapidly and Sonicated for 1 hour. THF was evaporated under reduced pressure at 40^{o}C to obtain nanoparticles. Characterizations of nanoparticles were done by UV-Vis spectroscopy, Florescence spectroscopy, DLS (Zeta sizer), SEM and TEM. All results provided confirmation about the stable nanoparticles.

3.4. Synthesis and Characterization of Poly[(9,9-bis ({3-diallyl}fluorenyl-2,7-diyl)-co-(benzothiadiazole)] PG Nanoparticles

PG (2 mg, $5.28x10^{-3}$ mmol) was dissolved in 5 ml of dry THF and filtrated through 0.45 μM syringe filter. This polymer solution was dropped into 50 ml of Milli-Q water in one shot and left for 1 hour sonication. THF was evaporated under reduced pressure at 40^{o}C. Characterizations of nanoparticles were done by UV-Vis spectroscopy, Florescence spectroscopy, DLS (Zeta sizer), SEM and TEM.

3.5. Synthesis Characterization of Poly[3-{(allyloxy)ethyl}(thiophene 2,5-diyl)-co-(5,5'-{2,2'}-bithiophene)] (P2) Nanoparticles

0.25 mg P2 was dissolved in 1 ml of dry THF and the solution was filtrated through 0.45 μM syringe filter. Solution of P2 was injected into 20 ml of Milli-Q water rapidly. It was left for 1 hour sonication in order to obtain nanoparticles and THF was evaporated under reduced pressure at 40 ^{o}C. Characterizations of nanoparticles were done by UV-Vis spectroscopy, Florescence spectroscopy, DLS (Zeta sizer), SEM and TEM.

3.6. Synthesis and Characterization of Hybrid Nanoparticles of Poly[(9,9-dihexylflourene)-co-(9,9-bis (3-diallylflourene)] PB and SPIONs (SPB)

250 μl SPIONs from stock solution was taken and toluene was evaporated in rotary evaporator under reduced pressure and dispersed in 1 ml of THF. PB solution was prepared by dissolving 1 mg in 1ml of THF. This PB solution is filtered through 0.45 μM syringe filter. SPIONs and polymer solutions were mixed together and left for sonication for 30 minutes. They were syringed to 50 ml of Milli-Q water and sonicated for 1 hour. THF was evaporated under reduced pressure at 40 ^{o}C. Cross-linking was utilized by diluting 2.5 ml of mother liquor with 10 ml of Milli-Q water and left under UV light (273 nm) for 2 hours. Characterizations of nanoparticles were done by UV-Vis spectroscopy, Florescence spectroscopy, DLS (Zeta sizer), SEM and TEM.

3.7 Synthesis and Characterization of Hybrid Nanoparticles of Poly[(9,9-bis ({3-diallyl}flourene)-co-(benzothiodiazole)] PG and SPIONs (SPG)

Two different way of synthesis of SPG was carried out in terms of SPIONs concentration. First one was consist of 250 μl SPIONs were taken from toluene stock solution. After evaporation of toluene, it was dispersed in 1 ml of THF. 2 mg PG is dissolved in 4 ml of THF and filtrated through 0.45 μM syringe filter. Then, 4 ml of PG solution and 1 ml of SPIONs solution in THF are mixed. They were left for 30 minutes sonication. Mixture of SPIONs and PG was injected into the 50 ml of Milli-Q water. THF was evaporated under reduced pressure to obtain nanoparticles of SPG.

Second Synthesis method was almost same except SPIONs concentration. 100 µl SPIONs were taken and redispersed in 1 ml of THF. SPIONs solution was sonicated with 2 mg PG containing 4 ml THF solution for 30 minutes. Mixture of SPIONs and PG were injected into the 50 ml of Milli-Q water. THF was evaporated under reduced pressure. Evaluations of the results implied that second way of preparation is more effective on the synthesis of stable nanoparticles. Cross-linking experiments were carried out with 100 µl SPIONs containing batch (second synthesis method).

Cross-linking experiments were performed by diluting 2.5 ml of mother liqueur of SPG nanoparticles with 10 ml of Milli-Q water and left under UV light (273 nm) for 4 hours.

Characterizations of nanoparticles were done by UV-Vis spectroscopy, Florescence spectroscopy, DLS (Zeta sizer), SEM and TEM.

3.8 Synthesis and Characterization of Hybrid Nanoparticles of Poly[3-{(allyloxy)ethyl}(thiophene 2,5-diyl)-co-(5,5'-{2,2'}-bithiophene)] (P2) and SPIONs (SP2)

100 µl of SPIONs was taken from toluene stock solution and redispersed in 1 ml of THF. 0.25 mg of SP2 was dissolved in 1 ml of THF and filtrated with 0.45 µM syringe filter. SP2 solution was mixed with 1 ml of SPIONs solution. Mixture of them was left for 30 minutes sonicating. 2 ml of THF solution is injected into the 20 ml of Milli-Q water in one shut while sonicating. It was left for 1 hour sonicating. THF was evaporated under reduced pressure at 40^{o} C. Cross-linking was performed by diluting 2.5 ml of SP2 nanoparticles aqueous solution with 10 ml of Milli-Q distilled water. 12.5 ml solution is left under UV irradiation (273 nm) for 2 hours.

Characterizations of nanoparticles were done by UV-Vis spectroscopy, Florescence spectroscopy, DLS (Zeta sizer), SEM and TEM.

3.9 Synthesis of Nanoparticles Lauric Acid-Coated Magnetic Iron Oxide (Fe_3O_4-LA) NPs.[80]

Synthesis of SPIONs coated with iron oxide (raw SPIONs) was done by Dr. Funda Acar Yağcı lab., Koç University [80]. Iron salts $FeCl_3 .6H_2O$ (2.365 g, 8.75

mmol), and $FeCl_2.4H_2O$ (0.870 g, 4.37 mmol) and 1.64 mL of LA were dissolved in 46 mL of deoxygenated water in a three-neck round-bottomed flask fitted with N_2 inlet/outlet and a reflux condenser. This solution was purged with nitrogen for at least 30 min and then heated to 85 °C in an oil bath. NH_4OH (12.06 mL, 26%) was injected rapidly to the hot solution under vigorous stirring which caused immediate formation of dark brown-black color indicating formation of Fe_3O_4. After 30 min reaction allowed for crystal growth, this solution was cooled to room temperature and placed on top of a magnet for one day. Any precipitate was removed with magnetic decantation. Magnetic NPs were washed with fresh DI water using the Amicon Ultra centrifugal filter (10kDa cutoff) with deionized water. These particles are coated with LA bilayer. LA monolayer coated Fe_3O_4 NPs were prepared as follows: 10 mL of the aqueous colloidal solution of LA bilayer coated Fe_3O_4 NPs was shaken vigorously with 20 mL of toluene and 3 mL of isopropyl alcohol for 15 min, and was transferred into a separatory funnel. The organic phase, containing the LA monolayer coated Fe_3O_4 was separated from the aqueous solution in a separatory funnel. This extraction procedure transfers all iron oxides into the organic phase.

Chapter 4

Conclusion

In this work, water dispersible SPIONs hybrid nanoparticles were prepared with conjugated polymers in order to provide them dual imaging opportunity. Polymers functionalized with allyl groups utilized to yield a cross-linkable scaffold for these nanoparticles. Shape persistent and stable nanoparticle generation is aimed for potential bioimaging applications under physiological conditions.

Size, shape and optical characterizations of these nanoparticles were done by DLS, SEM, TEM, UV-Vis and Fluorescence spectrometers. Encapsulation of SPIONs by conjugated polymers and generation of spherical nanoparticles were approved with morphological studies, TEM and SEM. Uniform distributions of Hybridized and non-hybridized (only polymer nanoparticles) conjugated polymer nanoparticles were supported with their optimal size assays (less than 100 nm). It is recorded that SPB and SPG nanoparticles resemble the optical properties of their PB and PG nanoparticles, respectively.

MRI contrast agent enhancement of conjugated polymer-SPIONs hybridized nanoparticles as was carried out with relaxivity studies. Relaxation time versus concentration of iron(III) was measured and represented with graphs. r_2 values were interpreted from the slope of these graphs as 103.41 s^{-1} mM^{-1} for raw SPIONs, 91.93 s^{-1} mM^{-1} for Blue SPIONs (SPB), 97.41 s^{-1} mM^{-1} for Blue SPIONs (SPB) after cross-link samples, 173.64 s^{-1} mM^{-1} for Green SPIONs (SPG) and 169.90 64 s^{-1} mM^{-1} for Green SPIONs (SPG) after cross-link ones. To the best of our knowledge, relaxivity reported up to now for hybrid nanoparticles with conjugated polymer is ~ 53 s^{-1} mM^{-1} with 180 nm size.

It can be concluded that stable water dispersible conjugated polymer nanoparticle generation were done for potential dual imaging applications. Relaxivity studies

indicated that coating SPIONs with fluorescence polymers did not change their MRI contrast agent capability, even they can provide enhancement to SPG nanoparticles.

Bibliography

[1] Feng, L., Zhu, C., Yuan, H., Liu, L., Lv, F., Wang, S., 'Conjugated polymer nanoparticles: preparation, properties, functionalization and biological Applications' *Chem. Soc. Rev.*, vol. 42, pp. 6620, 2013

[2] Ronclai, J., 'Molecular Engineering of the Band Gap of p-Conjugated Systems: Facing Technological Applications', *Macromol. Rapid Commun.*, vol. 28, pp. 1761-1775, 2007

[3] Diaz, A.F., Logan, J.A., 'Electroactive Polyaniline Films', *j. Electroanal. Chem.*, vol. 111, pp. 111-114, 1980

[4] http://www.nobelprize.org/nobel_prizes/chemistry/laureates/2000/

[5] Tuncel, D., Demir, H. V., 'Conugated Polymer Nanoparticles', *Nanoscale*, vol. 2, pp. 484-494, 2010

[6] Wu, C., Chui, D. T., 'Highly Fluorescent Semiconducting Polymer Dots for Biology and Medicine', *Angew. Chem. Int. Ed.*, vol. 52, pp. 3086-3109, 2013

[7] Wu, C., Szymanski, C., McNeill, J., 'Preparation and Encapsulation of Highly Fluorescent Conjugated Polymer Nanoparticles ', *Langmuir*, vol. 22, pp. 2956-2960, 2006

[8] Li, K., Pan, J., Feng, S., Wu, A., Pu, K., Liu, Y. and Liu, B., 'Generic Strategy of Preparing Fluorescent Conjugated-Polymer-Loaded Poly(DL-lactide- co -Glycolide) Nanoparticles for Targeted Cell Imaging.' *Advanced Functional Materials*, vol.19, pp.3535-3542, 2009

[9] a) Suzuki, A., Miyaura, N., 'Palladium-Catalyzed Cross-Coupling Reactions of Organoboron Compounds', *Chem. Rev.*, vol. 95, pp. 2457-2483, 1995

b) Suzuki, A., 'Cross-Coupling Reactions Of Organoboranes: An Easy Way To Construct C_C Bonds (Nobel Lecture)', *Angew. Chem. Int. Ed.*, vol. 50, pp. 6723-6737, 2011

c) Danishefsky, J. S., Trauner, D., Chembler, S. R., 'The B-Alkyl Suzuki ± Miyaura Cross-Coupling Reaction: Development, Mechanistic Study, and Applications in Natural Product Synthesis ', *Angew. Chem. Int. Ed.*, vol. 40, pp. 4544-4568, 2001

d) Stille K. J., 'The Palladium-Catalyzed Cross-Coupling Reactions of Organotin Reagents with Organic Electrophiles', *Angew. Chem. Int. Ed. Engl.*, vol. 25, pp. 508-524, 1986

[10] http://www.nobelprize.org/nobel_prizes/chemistry/laureates/1963/

[11] Grubbs, R. H., Tumas, W., 'Polymer Synthesis and Organotransition Metal Chemistry', *Science* , vol. 243, pp. 907-915, 1989

[12] Chen, Y.-X. E., Marks, T. J., 'Cocatalysts for Metal-Catalyzed Olefin Polymerization: Activators, Activation Processes, and Structure-Activity Relationships ', *Chem. Rev.*, vol. 100, pp. 1391-1434, 2000

[13] McCullough, R. D., 'The Chemistry of Conducting Polythiophenes ', *Adv. Mat.*, vol. 10, pp. 93-116, 1998

[14] a) Rocali, J., 'Conjugated Poly(thiophenes): Synthesis, Functionalization, and Applications', *Chem. Rev.*, vol. 92, pp. 711-738, 1992

b) Lecrerc, M., Rondeau, D., Ranger, M., ‘New Well-Defined Poly(2,7-fluorene) Derivatives: Photoluminescence and Base Doping’, *Macromolecules,* vol. 30, pp. 7686-7691, 1997
c) Cho, N.-S., Hwang, D.-H., Jung, J.-B., Lim, E., Lee, J., Shim, H.-K., ‘Synthesis, Characterization, and Electroluminescence of New Conjugated Polyfluorene Derivatives Containing Various Dyes as Comonomers ‘, *Macromolecules,* vol. 37, pp. 5265-5273, 2004

[15] Fukuda, M., Sawada, K., Yoshino, K., ‘Synthesis of Fusible and Soluble Conducting Polyfluorene Derivatives and Their Characteristics ‘, *j. Polymer Science, Part A: Polymer Chemistry*, vol. 31, pp. 2466-2471, 1993

[16] Waltman, J. R., Borgani, J., ‘ The Electropolymerization of Polycyclic Hydrocarbons: substituent effects and reactivity/structure correlaitons ‘, *j. Electroanal., Chem.*, vol. 194, pp. 42-62, 1985

[17] Pecher, J., Mecking, S., ‘Nanoparticles of Conjugated Polymers’, *Chem., Rev.*, vol. 110, pp. 6260-6279, 2010

[18] Feng, X., Tang, Y., Duan, X., Liu, L., Wang, S., ‘Lipid-modified conjugated polymer nanoparticles for cell imaging and transfection’, *J. Mater. Chem.*, vol. 20, pp. 1312-1316, 2010

[19] Tang, H., Xing, C., Liu, L., Yang, Q., Wang, S., ‘Synthesis of Amphiphilic Polythiophene for Cell Imaging and Monitoring the Cellular Distribution of a Cisplatin Anticancer Drug’, *small,* vol. 7, pp. 1464-1470, 2011

[20] Xing, C., Liu, L., Tang, H., Feng, X., Yang, Q., Wang, S., Bazen, G. C., ‘Design Guidelines For Conjugated Polymers With Light- Activated Anticancer Activity’, *Adv. Func.Mat.,* vol. 21, pp. 4058-4067, 2011

[21] Qu, Y., Zhang, X., Wu, Y., Li, F., Hua, J., 'Fluorescent conjugated polymers based on thiocarbonyl quinacridone for sensing mercury ion and bioimaging', *Polym. Chem.*, vol. 5, pp. 3396, 2014

[22] Feng, X., Lv, F., Liu, L., Tang, H., Xing, C., Yang, Q., Wang, S., 'Conjugated Polymer Nanoparticles for Drug Delivery and Imaging', *Appl. Mater.. & Interfaces*, vol. 2, pp. 2429-2435, 2010

[23] Pennakalathil, J., Jahja, E., Özdemir, E., Konu, Ö. and Tuncel, D. 'Red Emitting, Cucurbituril-Capped, pH-Responsive Conjugated Oligomer-Based Nanoparticles for Drug Delivery and Cellular Imaging'. *Biomacromolecules*, vol. 15, pp.3366-3374., 2014

[24] Pennakalathil, J., Özgün, A., Durmaz, I., Cetin-Atalay, R. and Tuncel, D. 'pH-responsive near-infrared emitting conjugated polymer nanoparticles for cellular imaging and controlled-drug delivery'. *Journal of Polymer Science Part A: Polymer Chemistry*, vol. 53, pp.114-122., 2014

[25] Gezici, Ö., Durmaz, İ., Bilget Güven, E., Ünal, Ö., Özgün, A., Cetin-Atalay, R. and Tuncel, D.' Dual functionality of conjugated polymer nanoparticles as an anticancer drug carrier and a fluorescent probe for cell imaging' *RSC Adv.*, vol. 4, pp.1302-1309., 2014

[26] Wu, C., Hansen, S., Hou, Q., Yu, J., Zeigler, M., Jin, Y., Burnham, D., McNeill, J., Olson, J. and Chiu, D. 'Design of Highly Emissive Polymer Dot Bioconjugates for In Vivo Tumor Targeting'. *Angew. Chem.*, vol. 123, pp.3492-3496., 2011

[27] Pei, Q., Yang, Y., 'Efficient Photoluminescence and Electroluminescence from a Soluble Polyfluorene' *J. Am. Chem. Soc.*, vol. 118, pp.7416-7417., 2011

[28] Feng, X., Yang, G., Liu, L., Lv, F., Yang, Q., Wang, S. and Zhu, D. 'A Convenient Preparation of Multi-Spectral Microparticles by Bacteria-Mediated Assemblies of Conjugated Polymer Nanoparticles for Cell Imaging and Barcoding' *Adv. Mater.*, vol. 24, pp.637-641., 2011

[29] Wang, S., Bazan, G., 'Solvent-dependent aggregation of a water-soluble poly(fluorene) controls energy transfer to chromophore-labeled DNA.' *Chem. Commun.*, vol. 21, p.2508., 2004

[30] Peng, L., He, M., Chen, B., Wu, Q., Zhang, Z., Pang, D., Zhu, Y., Hu, B., 'Cellular uptake, elimination and toxicity of CdSe/ZnS quantum dots in HepG2 cells.' *Biomaterials*, vol. 34, pp.9545-9558., 2013

[31] Tang, Y., Han, S., Liu, H., Chen, X., Huang, L., Li, X., Zhang, J.,' The role of surface chemistry in determining in vivo biodistribution and toxicity of CdSe/ZnS core–shell quantum dots.' *Biomaterials*, vol. 34, pp.8741-8755., 2013

[32] Shiohara, A., Hoshino, A., Hanaki, K., Suzuki, K., Yamamoto, K.,' On the Cyto-Toxicity Caused by Quantum Dots.' *Microbiology and Immunology*, vol. 48, pp.669-675., 2004

[33] Howes, P., Thorogate, R., Green, M., Jickells, S., Daniel, B., ' Synthesis, characterisation and intracellular imaging of PEG capped BEHP-PPV nanospheres.' *Chem. Commun.*, vol. 18, p.2490., 2009

[34] Schwartz B. J., 'Conjugated Polymers as molecular materials: How Chain Conformation and Film Morphology Influence Energy Transfer and Interchain Interactions ', *Annu. Rev. Phys.Chem.*, vol.54, pp. 54-141, 2003

[35] Moon, J., Mendez, E., Kim, Y., Kaur, A.,'Conjugated polymer nanoparticles for small interfering RNA delivery.' *Chem. Commun.*, vol. 47, p.8370. , 2011

[36] Li, Y., Liu, J., Liu, B., Tomczak, N., 'Highly emissive PEG-encapsulated conjugated polymer nanoparticles.', *Nanoscale*, vol. 4, p.5694., 2012

[37] Wu, C., Jin, Y., Schneider, T., Burnham, D., Smith, P., Chiu, D., ' Ultrabright and Bioorthogonal Labeling of Cellular Targets Using Semiconducting Polymer Dots and Click Chemistry.' *Angew. Chem.*, vol. 122, pp.9626-9630., 2010

[38] Wu, C., Bull, B., Szymanski, C., Christensen, K., McNeill, J., 'Multicolor Conjugated Polymer Dots for Biological Fluorescence Imaging.' *ACS Nano*, vol. 2, pp.2415-2423., 2008

[39] Smith, F., 'Magnetic resonance imaging: Basic principles.' *Magnetic Resonance Imaging*, vol. 7, p.118, 1989

[40] Na, H., Song, I., Hyeon, T., 'Inorganic Nanoparticles for MRI Contrast Agents.', *Adv. Mater.*, vol. 21, pp.2133-2148., 2009

[41] Caravan, P., Ellison, J., McMurry, T., Lauffer, R., 'Gadolinium(III) Chelates as MRI Contrast Agents: Structure, Dynamics, and Applications.' *Chem. Rev.*, vol. 99, pp.2293-2352., 1999

[42] Laurent, S., Forge, D., Port, M., Roch, A., Robic, C., Vander, Elst, L., Muller, R., 'Magnetic Iron Oxide Nanoparticles: Synthesis, Stabilization, Vectorization, Physicochemical Characterizations, and Biological Applications.' *Chem. Rev.*, vol. 110, pp.2574-2574., 2010

[43] Mendonca Dias M. H., Lauterbur P. C., ' Ferromagnetic particles as contrast agents for magnetic resonance imaging of liver and spleen', *Mag. Res. Med.*, vol. 3, pp. 328-330, 1986

[44] Bulte, J., Kraitchman, D., 'Iron oxide MR contrast agents for molecular and cellular imaging.', *NMR in Biomedicine*, vol. 17, pp.484-499., 2004

[45] Mailänder, V., Landfester, K., 'Interaction of Nanoparticles with Cells.' *Biomacromolecules*, vol. 10, pp.2379-2400., 2009

[46] Turner, J., Pan, D., Plummer, R., Chen, Z., Whittaker A., Wooley, K., 'Synthesis of Gadolinium-Labeled Shell-Crosslinked Nanoparticles for Magnetic Resonance Imaging Applications.' *Advanced Functional Materials*, vol. 15, pp.1248-1254., 2005

[47] Vuu, K., Xie, J., McDonald, M., Bernardo, M., Hunter, F., Zhang, Y., Li, K., Bednarski, M., Gccione, S.,'Gadolinium-Rhodamine Nanoparticles for Cell Labeling and Tracking via Magnetic Resonance and Optical Imaging.' *Bioconjugate Chem.*, vol. 16, pp.995-999., 2005

[48] Reynolds, C., Annan, N., Beshah, K., Huber, J., Shaber, S., Lenkinski, R., Wortman, J., 'Gadolinium-Loaded Nanoparticles: New Contrast Agents for Magnetic Resonance Imaging.' *J. Am. Chem. Soc.*, vol.122, pp.8940-8945., 2000

[49] Aime, S., Frullano, L., Geninatti, Crich, S., 'Compartmentalization of a Gadolinium Complex in the Apoferritin Cavity: A Route To Obtain High Relaxivity Contrast Agents for Magnetic Resonance Imaging.' *Angew. Chem.*, vol.114, pp.1059-1061., 2002

[50] Kuo, P., Kanal, E., Abu-Alfa, A. and Cowper, S., 'Gadolinium-based MR Contrast Agents and Nephrogenic Systemic Fibrosis 1.' *Radiology*, 242(3), pp.647-649, 2007

[51] Semelka, R. C., Helmberger, T. K. G., 'Contrast Agents for MR Imaging of the Liver.' *Radiology*, vol. 218, p.27., 2001

[52] Jordan, A., Scholz, R., Wust, P., Schirra, H., Thomas, S., Schmidt, H., Felix, R., 'Endocytosis of dextran and silan-coated magnetite nanoparticles and the effect of intracellular hyperthermia on human mammary carcinoma cells in vitro.' *Journal of Magnetism and Magnetic Materials*, vol.194, pp.185-196., 1999

[53] Reddy, L., Arias, J., Nicolas, J., Couvreur, P., 'Magnetic Nanoparticles: Design and Characterization, Toxicity and Biocompatibility, Pharmaceutical and Biomedical Applications.' *Chem. Rev.*, vol.112, pp.5818-5878., 2012

[54] Strable E., Bulte J., Moskowitz B., Vivekanandan K., Allen M., Douglas, T. ' Synthesis and Characterization of Soluble Iron Oxide−Dendrimer Composites.' *Chem. Mater.*, vol.13, pp.2201-2209., 2001

[55] Bulte J., Douglas T., Witwer B., Zhang S., Strable E., Lewis B., Zywicke H., Miller B., van Gelderen P., Moskowitz B., Duncan I., Frank, J. 'Magnetodendrimers allow endosomal magnetic labeling and in vivo tracking of stem cells.' *Nat. Biotechnol.*, vol.19, pp.1141-1147., 2001

[56] Ai, H., Flask, C., Weinberg, B., Shuai, X., Pagel, M., Farrell, D., Duerk, J. and Gao, J., 'Magnetite-Loaded Polymeric Micelles as Ultrasensitive Magnetic-Resonance Probes.' *Adv. Mater.*, vol.17, pp.1949-1952., 2005

[57] Talelli, M., Rijcken, C., Lammers, T., Seevinck, P., Storm, G., van Nostrum, C. and Hennink, W. 'Superparamagnetic Iron Oxide Nanoparticles Encapsulated in Biodegradable Thermosensitive Polymeric Micelles: Toward a Targeted Nanomedicine Suitable for Image-Guided Drug Delivery.' *Langmuir*, vol.25, pp.2060-2067., 2009

[58] Zhang, L., He, R. and Gu, H., 'Oleic acid coating on the monodisperse magnetite nanoparticles.' *Applied Surface Science*, vol.253, pp.2611-2617., 2006

[59] Guardia, P., Batlle-Brugal, B., Roca, A., Iglesias, O., Morales, M., Serna, C., Labarta, A., Batlle, X., 'Surfactant effects in magnetite nanoparticles of controlled size.' *Journal of Magnetism and Magnetic Materials*, 316(2), pp.e756-e759., 2007

[60] Jun, Y., Seo, J., Cheon, J., 'Nanoscaling Laws of Magnetic Nanoparticles and Their Applicabilities in Biomedical Sciences.' *Acc. Chem. Res.*, vol.41, pp.179-189., 2008

[61] Jun, Y., Lee, J., Cheon, J., 'Chemical Design of Nanoparticle Probes for High‐Performance Magnetic Resonance Imaging.' *Angew. Chem. Int. Ed.*, vol.47, pp.5122-5135., 2008

[62] Jun, Y., Huh, Y., Choi, J., Lee, J., Song, H., Kim, Yoon, S., Kim, K., Shin, J., Suh, J. , Cheon, J., 'Nanoscale Size Effect of Magnetic Nanocrystals and Their Utilization for Cancer Diagnosis via Magnetic Resonance Imaging.' *J. Am. Chem. Soc.*, 127(16), pp.5732-5733., 2005

[63] Morales, M., Veintemillas-Verdaguer, S., Montero, M., Serna, C., Roig, A., Casas, L., Martínez, B., Sandiumenge, F., 'Surface and Internal Spin Canting in γ-Fe_2O_3 Nanoparticles.' *Chem. Mater.*, vol.11, pp.3058-3064., 1999

[64] Lee, J., Huh, Y., Jun, Y., Seo, J., Jang, J., Song, H., Kim, S., Cho, E., Yoon, H., Suh, J., Cheon, J., 'Artificially engineered magnetic nanoparticles for ultra-sensitive molecular imaging.' *Nat Med*, vol.13, pp.95-99., 2007

[65] Farquhar, D., Newman, R., Zuckerman, J., Andersson, B., 'Doxorubicin analogs incorporating chemically reactive substituents.' *Journal of Medicinal Chemistry*, vol.34, pp.561-564., 1991

[66] Schultz, A., 'Camptothecin.' *Chem. Rev.*, vol.73, pp.385-405., 1973

[67] Huh, Y., Jun, Y., Song, H., Kim, S., Choi, J., Lee, J., Yoon, S., Kim, K., Shin, J., Suh, J., Cheon, J., 'In Vivo Magnetic Resonance Detection of Cancer by Using Multifunctional Magnetic Nanocrystals.' *J. Am. Chem. Soc.*, vol.127, pp.12387-12391., 2005

[68] Smith, B., Heverhagen, J., Knopp, M., Schmalbrock, P., Shapiro, J., Shiomi, M., Moldovan, N., Ferrari, M., Lee, S., 'Localization to atherosclerotic plaque and biodistribution of biochemically derivatized superparamagnetic iron oxide nanoparticles (SPIONs) contrast particles for magnetic resonance imaging (MRI).' *Biomedical Microdevices*, vol.10, pp.129-130., 2007

[69] Medarova, Z., Pham, W., Farrar, C., Petkova, V., Moore, A., 'In vivo imaging of siRNA delivery and silencing in tumors.' *Nat Med*, vol.13, pp.372-377., 2007

[70] Chen, G., Chen, W., Wu, Z., Yuan, R., Li, H., Gao, J., Shuai, X., 'MRI-visible polymeric vector bearing CD3 single chain antibody for gene delivery to T cells for immunosuppression.' *Biomaterials*, vol.30, pp.1962-1970., 2009

[71] Howes, P., Green, M., Bowers, A., Parker, D., Varma, G., Kallumadil, M., Hughes, M., Warley, A., Brain, A., Botnar, R., 'Magnetic Conjugated Polymer Nanoparticles as Bimodal Imaging Agents.' *J. Am. Chem. Soc.*, vol.132, pp.9833-9842., 2010

[72] Li, K., Ding, D., Huo, D., Pu, K., Thao, N., Hu, Y., Li, Z. and Liu, B. 'Conjugated Polymer Based Nanoparticles as Dual-Modal Probes for Targeted In Vivo Fluorescence and Magnetic Resonance Imaging.' *Advanced Functional Materials*, vol.22, pp.3107-3115, 2012

[73] Mokari, T., ' Selective Growth of Metal Tips onto Semiconductor Quantum Rods and Tetrapods.' *Science*, vol.304, pp.1787-1790, 2004

[74] Hu, S. and Gao, X., 'Nanocomposites with Spatially Separated Functionalities for Combined Imaging and Magnetolytic Therapy.' *J. Am. Chem. Soc.*, vol. 132, pp.7234-7237, 2010

[75] Feng, X., Liu, L., Wang, S., Zhu, D. 'Water-soluble fluorescent conjugated polymers and their interactions with biomacromolecules for sensitive biosensors.' *Chem. Soc. Rev.*, vol. 39, pp. 2411, 2010

[76] Wang, E. and Wang, A. 'Nanoparticles and their applications in cell and molecular biology'. *Integr. Biol.*, vol.6, pp.9-26., 2014

[77] Albanese, A., Tang, P. and Chan, W. 'The Effect of Nanoparticle Size, Shape, and Surface Chemistry on Biological Systems.' *Annu. Rev. Biomed. Eng.*, 14(1), pp.1-16., 2012

[78] Ibrahimova, V., 'Synthesis and Characterization of Water Dispersible Conjugated Polymer Nanoparticles', *Thesis, Master of Science*, 2011

[79] Huang J., Zhong X., Wang L., Yang L. and Mao H., 'Improving the Magnetic Resonance Imaging Contrast and Detection Methods with Engineered Magnetic Nanoparticles ' , *Theranostics,* 2(1), pp. 86-102, 2012

[80] Funda Acar Yağcı, Rouhollah Khodadust, Yasemin Yar, unpublished results, retrieved July 2015

[81] Emine Ülkü Sarıtaş, Mustafa Ütkür, unpublished results, retrieved June 2015

Appendix A

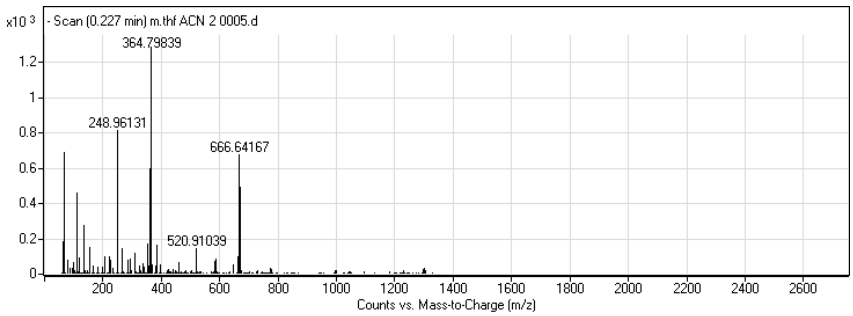

Figure A.1: LC/MS-TOF spectrum of 2-(2,5-dibromothiophen-3-yl)ethyl acetate (M2) ($[M2+K-2H]^-$ = 364)

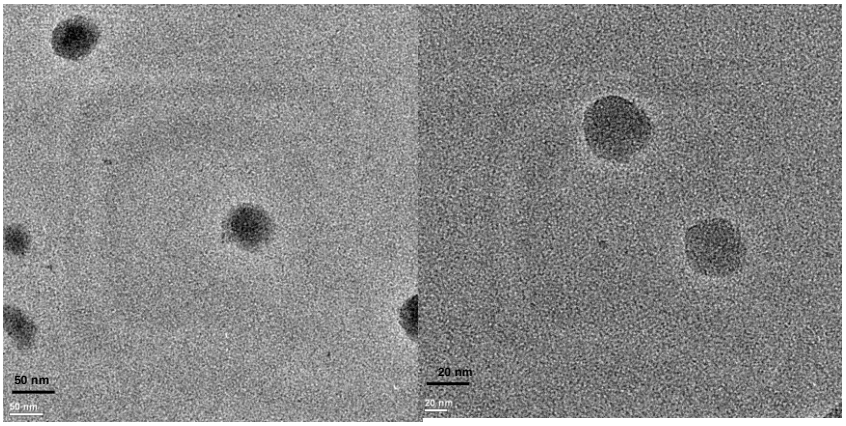

Figure A.2: TEM images of THF dispersed cross-linked (4h UV irradiation) PG nanoparticles